LAND AND WATER
www.csiro.au

Geochemical Response to Reinjection

Henning Prommer, Bhasker Rathi, Mike Donn, Adam Siade, Laura Wendling, Evelien Martens and Bradley Patterson

October 2016

ISBN (print) 978-1-4863-0754-8

ISBN (online) 978-1-4863-0755-5

Citation

Prommer, H., Rathi, B., Donn, M., Siade, A., Wendling, L., Martens, E., Patterson, B. (2016) Geochemical response to reinjection. Final Report. CSIRO, Australia.

Copyright and disclaimer

Important disclaimer

Content

Figures

Tables

Acknowledgments

This report was funded by the Gas Industry Social and Environmental Research Alliance (GISERA). GISERA is a collaborative vehicle established to undertake publicly-reported independent research addressing the socio-economic and environmental impacts of Australia's natural gas industries. The governance structure for GISERA is designed to provide for and protect research independence and transparency of funded research. See www.gisera.org.au for more information about GISERA's governance structure, funded projects, and research findings.

This report would not have been possible without a close collaboration between CSIRO and Origin. All field experiments described in this report were performed by Origin, with major contributions from Ryan Morris, Lauren Helm and Andrew Moser. Catherine Moore (now at GNS New Zealand) has contributed to the calibration of the Reedy Creek trial model. Ilka Wallis and Catherine Moore have performed the bulk of the work for the manuscript "'*Using predictive uncertainty analysis to optimise tracer test design and data acquisition*" by Wallis *et al.* (2014), which was directly motivated by this project. Many constructive discussions on conceptual models of arsenic fate were held with Jing Sun (Columbia University), Benjamin Bostick (Columbia University) and Olivier Atteia (University of Bordeaux). Also, Olivier Atteia deserves special thanks for adopting his GUI ipht3d to pre- and post-process radial flow models.

This report was subject to CSIRO-internal review. We thank our internal reviewers Dirk Mallants and Sreekanth Janardhanan for their constructive feedback.

Executive summary

Background

Over the next two decades coal seam gas production in Australia requires the management of large quantities of production waters that will be extracted from coal seam horizons, with an average of 70GL/year and a maximum of 110 GL/year anticipated for the next 3 years (OGIA 2016). For many sites the most viable and socially most widely accepted option is to treat the water to a high standard via reverse osmosis (RO) or other suitable treatment methods and to inject it into deep aquifers. However, the geochemical dis-equilibrium between the injectant composition and the target aquifer matrix can drive a wide range of water sediment interactions. One of the key concerns for injection into deep aquifers is the risk of metal and/or metalloid mobilization. Previous studies at managed aquifer recharge (MAR) sites showed that such concerns are also still warranted in cases where neither the ambient groundwater nor the injectant contains any elevated concentrations of metals or metalloids. Therefore a detailed understanding of the geochemical background conditions and of geochemical mechanisms is required to predict and manage future water quality changes and risks for the receiving aquifers at both the local and regional scale. The present report describes the most important steps that contributed to the understanding and predictions of the potential geochemical impacts of large-scale CSG product water reinjection. Key information for this research was obtained by a series of injection trials that were performed within the Precipice Sandstone aquifer, which showed to have the greatest promise as reinjection target aquifer. The first injection trial was performed at the Reedy Creek site at a depth between 1285 and 1376 mBGL. During the injection bromide was amended to assist with the characterisation of the flow and solute transport process behaviour. Reactive transport modelling was subsequently used to interpret the data collected from this trial. A second set of injection trials was performed at the Condabri site (i) to verify the process understanding that was developed from the Reedy Creek trial results and (ii) to investigate the impact of different types of injectant pre-treatment. The Condabri injection trial consisted of three separate push-pull tests (PPT1-PPT3). The first two tests were performed to investigate whether acid amendment to the injectant could effectively reduce arsenic mobilisation while the third test was performed to test the necessity of deoxygenating the injectant.

- The geochemical response to the injection of CSG product water was investigated
- Data from two injection trials in the Precipice Sandstone aquifer were analysed through reactive transport modelling
- The reactivity of the Precipice Sandstone was generally low
- Arsenic was mobilised during both trials with concentrations reaching up to 24ppm when the injectant was deoxygenated and up to 180ppm without deoxygenation of the injectant
- Predictive modelling was used to determine the large-scale impacts of reinjection, demonstrating that arsenic levels will remain low with appropriate pre-treatment of the injectant

Key results

REEDY CREEK INJECTION TRIAL

The injection trial at Reedy Creek was performed over a period of 65 days, including a storage period of 64 days and a recovery phase spanning 65 days. The water quality analysis of the recovered water suggested a generally low reactivity of the Precipice Sandstone, with the water composition of the recovered water closely resembling that of the injectant. However, the most relevant difference was found to be the increase of arsenic concentrations from below detection limit in the injectant to up to 24ppm in the recovered water. The results of the reactive transport modelling study suggested that the alkaline nature (pH of up to 9.4) of the injectant was the main reason for arsenic release. These results were underpinned by (i) dedicated arsenic sorption experiments that, consistent with the literature, showed a decreasing sorption affinity for arsenic with increasing pH and (ii) laboratory-scale respirometer incubations tests that did not show a link between oxygen addition and arsenic mobilisation. Other mechanisms that could have caused arsenic mobilisation such as competitive desorption by phosphate or bicarbonate were also

investigated but showed not to play a role. The model developed on the basis of the trial results was used for predictive simulations. Assuming that the injectant would be deoxygenated the model predictions showed that an increase in arsenic concentration would remain confined to the aquifer zone adjacent to the injection well. The modelling suggested further that a pre-treatment of the injectant (acid amendment) could reduce dissolved arsenic concentrations further.

CONDABRI INJECTION TRIAL

Push-pull tests PP1-PP3 were successfully completed within the Precipice Sandstone at the Condabri site. Confirming the results of the Reedy Creek injection trial it was found that the reactivity of the aquifer sediments was generally low. However, like at Reedy Creek, levels of dissolved arsenic increased during recovery. The maximum arsenic concentrations during PPT1, which was performed with acid amendment, were 9 µg/L, somewhat lower than the maximum concentrations occurring during the recovery phase of PPT2 (16 µg/L), which involved a higher total injection volume of 48,173 m^3 and no acid amendment. Corresponding with the occurrence of arsenic during the recovery, sulphate concentrations increased above the detection limit. Observed arsenic concentrations were highest in the final test (PPT3, without de-oxygenation) in which concentrations of up to 180 µg/L were observed, again accompanied by increasing sulphate concentrations. In the reactive transport model that was constructed for the Condabri injection trial these observation could be well explained by the occurrence of pyrite oxidation and a stoichiometric release of arsenic (0.04 mol As released per mol FeS_2 oxidised).

GEOCHEMICAL RESPONSE TO LARGE-SCALE INJECTION

Predictive model simulations were performed for both injection trial sites to inspect the long-term response to the injection of treated CSG product water. These simulations showed that predicted arsenic concentrations remain at acceptable levels for all simulated cases that assumed deoxygenation of the injectant. In contrast, elevated arsenic concentrations might need to be anticipated if the injectant is not deoxygenated. Compared to deoxygenation acid amendment had a smaller impact on predicted arsenic concentrations.

Conclusion and recommendations

The results of this study suggest that the injection of large volumes of highly treated CSG product water will cause no foreseeable adverse impacts on groundwater quality with exception of the potential mobilisation of arsenic. However, mobilisation of arsenic can largely be eliminated through a suitable pre-treatment of the injectant, most importantly through deoxygenation. Due to the relatively short time-scale of the injection trials and in the absence of monitoring wells it was not possible to uniquely identify potential attenuation mechanisms. Future investigations might be able to clarify whether, for example, arsenic sorption would be sufficient to eliminate arsenic migration over longer travel distances even in cases where the injectant is not deoxygenated. Based on the current investigations deoxygenation of the injectant is recommended until the occurrence of arsenic attenuation mechanisms is verified.

1 Introduction

1.1 Background

Over the next two decades coal seam gas production in Australia requires the management of large quantities of production waters that will be extracted from coal seam horizons, with an average of 70 GL/year and a maximum of 110 GL/year anticipated for the next 3 years (OGIA 2016). For many sites the most viable and socially most widely accepted option is to treat the water to a high standard via reverse osmosis (RO) or other suitable treatment methods and to inject it into deep aquifers. However, the geochemical dis-equilibrium between the injectant composition and the target aquifer matrix can drive a wide range of water sediment interactions. One of the key concerns for injection into deep aquifers is the risk of metal and/or metalloid mobilization. Previous studies at managed aquifer recharge (MAR) sites showed that such concerns are also still warranted in cases where neither the ambient groundwater nor the injectant contains any elevated concentrations of metals or metalloids. For example, mobilisation of geogenic arsenic during MAR has been reported to occur in a variety of geochemical environments and to be associated with different geochemical mechanisms (see, e.g., Neil *et al.* (2012) for a review). In addition, Wallis *et al.* (2010) described a case in which MAR of an aerobic injectant induced pyrite oxidation and a temporary release of arsenic. Similarly, Jones and Pichler (2007) as well as Wallis *et al.* (2011) linked the initial release of arsenic in the Suwannee Limestone at aquifer storage and recovery (ASR) sites in SW Florida to pyrite oxidation. On the other hand, McNab *et al.* (2009) attributed elevated As concentrations at a MAR site in the Central Valley (California) to the more alkaline character of the recharge water and the displacement of As by OH^- from sorption sites. Also, both Appelo and Vet (2003) and later Vanderzalm *et al.* (2011) discussed cases where phosphate caused As desorption during aquifer recharge. These and other incidences suggest that a detailed understanding of the geochemical mechanisms is required to predict and manage future water quality changes and risks for the receiving aquifers at both the local and regional scale. The present report describes the most important steps that contributed to the understanding and predictions of the potential geochemical impacts of large-scale CSG product water reinjection.

1.2 Overview of investigations

The work performed in this project was initiated in 2010 at a time when very little hydrochemical baseline data were available. Therefore the work plan included a relatively broad geochemical characterisation for a wide range of potential reinjection sites and a range of different target aquifers. However, as the project progressed specific locations and aquifers were selected among the initially investigated sites, mostly for operational reasons in combination with favourable hydraulic performances. The Reedy Creek and Condabri sites (see Figure 1.1) evolved as the main study sites for the present project, with the main focus of the investigations on the planned injection into the Precipice Sandstone aquifer. The results of the trial injection at the Reedy Creek site showed an unexpected and undesired increase in dissolved arsenic concentrations during the recovery phase of the trial, despite the absence of any detectable arsenic in the aquifer prior to injection. Therefore the majority of the research efforts was subsequently focussed on developing an understanding of the processes controlling the fate of arsenic and on understanding how arsenic release could be mitigated during the full-scale implementation of the reinjection scheme(s). To understand the nature of the arsenic mobilisation mechanism the original scope of the project was modified and extended. This involved a series of additional laboratory experiments, including respirometer tests and batch sorption experiments.

Based on the joint interpretation of the field and laboratory data it was concluded that the alkaline nature of the injectant was the most likely cause for arsenic desorption and mobilisation from aquifer material while pyrite oxidation was initially thought not to be responsible for the observed arsenic release. This led to an additional series of field experiments in the Precipice Sandstone in which this hypothesis was tested and the link between injectant pre-treatment and arsenic mobilisation was more closely investigated. These experiments were performed at the Condabri site (see Figure 1.1), also within the Precipice Sandstone.

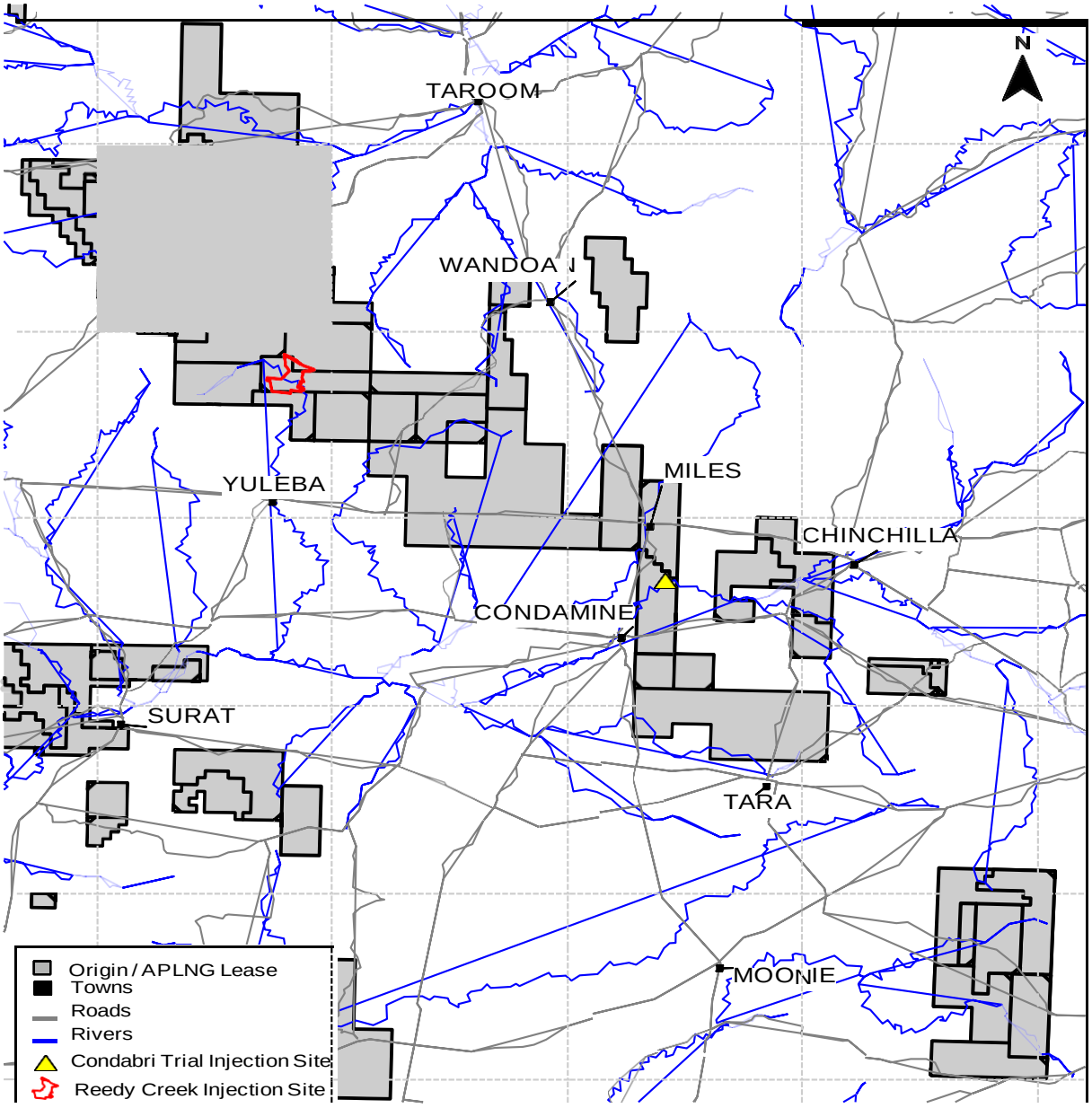

Figure 1.1: Overview map for injection trial site locations

For both sites (Reedy Creek and Condabri) reactive transport modelling was used to integrate and interpret the collected hydrochemical data in conjunction with the pre-trial geochemical and mineralogical characterisation of the Precipice Sandstone and laboratory experiments. This approach allowed the identification and quantification of key hydrogeological and geochemical processes controlling arsenic concentrations.

The models that were established, based on the injection trails, were subsequently adopted to,

- derive quantitative predictions for the long-term fate of arsenic for specific injectant pre-treatment levels.
- determine injectant water treatment requirements for suitably mitigating the undesired increase of the naturally low arsenic concentrations.

The present report provides a description of the experimental and numerical modelling work that was performed to foremost understand the geochemical response at the two specific study sites but also to document and illustrate the developed experimental and modelling approaches to allow their application to other sites with similar geochemical characteristics.

2 Field Injection Experiments Reedy Creek

2.1 Study Site

Reedy Creek is located approximately 30 km north of Yuleba, in southeast Queensland (Figure 1.1). It is situated in the Surat Basin, a sub-basin of the Great Artesian Basin (GAB). The site was one of several sites that was considered by Origin Energy for large-scale aquifer injection and the injection trial into the Precipice Sandstone was a component of a wider program of trials to assess the technical and economic feasibility of aquifer injection as a means of managing treated CSG water. The Precipice Sandstone trial injection bore (RCINJ2-P) is located 150 m south of the Reedy Creek pilot (feed) pond (Figure 2.1). The corehole from which geochemical, mineralogical and other data was obtained (RC-MB3-H) is located approximately 250 m west of RC-INJ2-P. A Precipice Sandstone monitoring bore (RC-INJ4-P) is located approximately 4.5 km northwest of RC-INJ2-P. The closest groundwater bore screening the Precipice Sandstone is the APLNG owned water supply bore Combabula (COM)-WB1-P, located approximately 15 km northeast of the trial site.

Figure 2.1: Reedy Creek site map: Key infrastructure elements, including treatment plant and boreholes.

2.2 Hydrogeology

The local hydrostratigraphy at Reedy Creek, including formation depths and thicknesses encountered during drilling operations is summarised in Figure 2.2. At the formational level, significant aquitards typically separate the main aquifers within the Surat Basin. As a result, the potential for hydraulic interconnection between the main aquifers and underlying and overlying formations is limited. At Reedy Creek the Evergreen Formation aquitard separates the Precipice Sandstone aquifer from the overlying Hutton Sandstone aquifer. The Precipice Sandstone is underlain by the Moolayember Formation, which is also considered to be an aquitard. CSG and associated water at Reedy Creek are produced from the Jurassic age Walloon Coal Measures. These coal measures are separated from the underlying Hutton Sandstone aquifer by the Eurombah Formation regional aquitard. The Precipice Sandstone outcrops approximately 150 km to the north of the trial injection site, from which point it dips to the south. The lowermost portion of the Precipice Sandstone is known as the Braided Stream Facies (BSF). The BSF is considered to be the most permeable zone of the overall formation, comprising relatively coarse-grained material representative of a high energy fluvial depositional environment. Although this sub-formation does not extend across the full lateral extent of the Precipice Sandstone, it is present at Reedy Creek. The BSF varies in thickness across the area, with general thickening eastwards, towards the basin axis. No large regional scale faults have been mapped within the vicinity of Reedy Creek. The Hutton/Wallumbilla fault lies to the west, however was outside of the predicted hydraulic impact

zone for the injection trial (APLNG, 2012a). Although there is offset of the hydrostratigraphic units across the Wallumbilla Fault in the approximate latitude of the trial injection site, the offset does not result in the connection of separate aquifers (Feitz *et al.* 2014). Small scale faulting has been interpreted in both seismic surveys and in drillholes. However, these structures do not appear to be continuous over significant distances, in either the horizontal or vertical sense, from the Precipice Sandstone to any other aquifer.

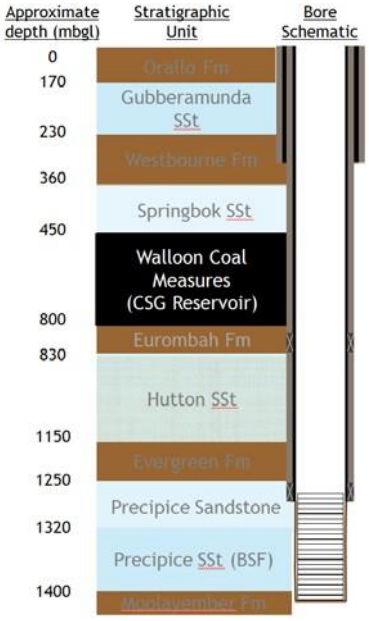

Figure 2.2: Hydrostratigraphy at Reedy Creek. Precipice Sandstone is the target aquifer for injection.

2.3 Geochemistry and Mineralogy

Besides the broader geochemical and mineralogical characterisation (reported in Appendix A), a more specific mineralogical and geochemical characterisation was performed for material from the Precipice Sandstone aquifer at Reedy Creek. Two sub-samples were selected, one from the Sandstone sub-unit (MB3-H 065-A) and one from the Braided Stream Facies (BSF) sub-unit (MB3-H BSF). The mineralogical composition of the samples was determined using quantitative X-ray diffraction (XRD). The major elemental composition of each sample was quantified as element oxide by fusion X-ray fluorescence (XRF) and trace elements by pressed powder XRF analysis. Samples were analysed by the CSIRO Mineralogical and Geochemical Services Centre (Urrbrae, SA). Sample electrical conductivity (EC), pH, acid neutralisation capacity (ANC), acid-digestible metal and total organic carbon (TOC) contents, cation exchange capacity (CEC), and ammonium oxalate-extractable Al, Fe, Mn and Si were determined by the ChemCentre (Perth, WA). Chromium-reducible S analysis was performed for each sediment sample by ALS Group (Perth, WA).

2.3.1 Mineralogy

The mineralogical analysis showed that quartz was the dominant mineral in both selected samples. However, the proportion of quartz was typically greater in the BSF sub-unit compared to the sandstone sub-unit (Figure 2.2, Figure 2.3). For the sandstone sub-unit sample, MB3-H 065-A, the clay minerals kaolinite ($Al_4Si_4O_{10}(OH)_8$) and orthoclase feldspar (microcline, $KAlSi_3O_8$) were found in appreciable quantities of 13% and 16%, respectively. The clay mineral content was lower in the MB3-H BSF sediment sample, with kaolinite and illite ($K_{1.0\text{-}1.5}Al_4(Si,Al)_8O_{20}(OH)_4$) the next most abundant minerals present, 4% and 1% respectively. Minor quantities of illite (1%) were also present in the sandstone sample (MB3-H 065-A) along with minor amounts of siderite ($FeCO_3$). Other crystalline iron minerals such as goethite, hematite, and pyrite were below detection limit. Carbonate minerals were also not detected in either of the two samples (see also Table 2.1). The mineralogical composition of the core material used in the sorption and respirometer experiments was similar to the composition of other samples from the Precipice aquifer (see Appendix A, section A.2.2 (Wendling *et al.* 2013)).

Table 2.1 Mineralogy composition of Reedy Creek MB3-H sub-samples selected for arsenic mobilisation studies

SAMPLE ID		MB3-H 065-A	MB3-H-BSF
Sub-unit		Precipice Sandstone	Precipice Braided Stream Facies
Depth (mBGL)		1302.6 – 1303.4	1332.53-1333.55
Mineral	Formula	Composition (wt%)	
Quartz	SiO_2	70	95
Orthoclase/ Microcline	$KAlSi_3O_8$	13	nd
Kaolinite	$Al_4Si_4O_{10}(OH)_8$	16	4
Illite/ Mica	$K_{1.0\text{-}1.5}Al_4(Si,Al)_8O_{20}(OH)_4$	1	1
Siderite	$FeCO_3$	1	nd
Calcite	$CaCO_3$	nd	nd
Dolomite	$Ca,Mg(CO_3)_2$	nd	nd
Pyrite	FeS_2	nd	nd

nd = not detected

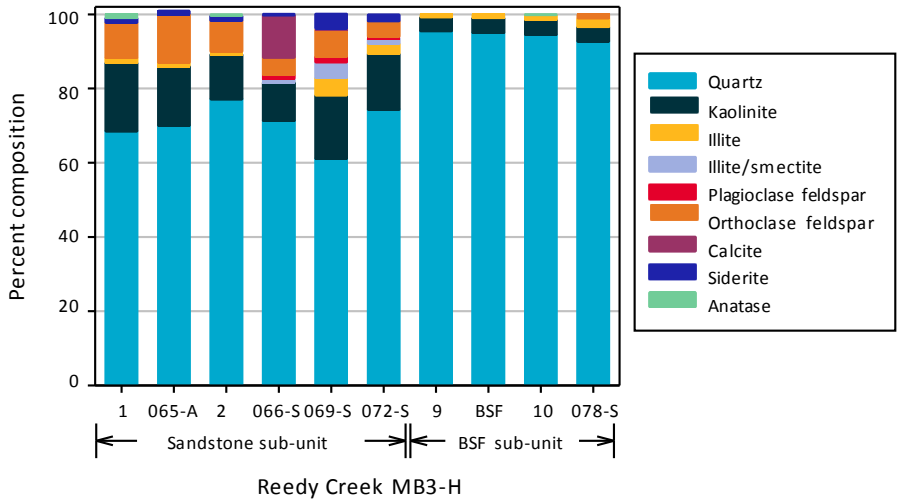

Figure 2.3: Mineralogy of selected sub-samples from the Reedy Creek MB3-H core, 065-A and BSF from current investigation and the remainder from Wendling *et al.* (2013) (Appendix A)

2.3.2 Sediment geochemistry

The major components identified by elemental analysis (XRF) were SiO_2, Al_2O_3 and K_2O (Table 2.2, Figure 2.4). These results reflect the dominance of quartz, clay and feldspar minerals that were simultaneously identified in the mineralogical analysis. Iron as Fe_2O_3 was present in minor quantities with 1.2 wt% and 0.39 wt% in MB3-H 065-A and MB3-H BSF, respectively. The major element geochemistry of MB3-H 065-A was similar to that of other Precipice Sandstone sub-samples (Wendling *et al.* 2013) (069-S and 072-S) from the Reedy Creek MB3-H core (Figure 2.4). Calcium as CaO was generally low (<0.5 wt%) with the exception of MB3-H 066-S (Figure 2.4), which suggests that calcite and other carbonate minerals were only present at trace levels in the sandstone sub-unit. The major element geochemistry of the Reedy Creek MB3-H BSF sample was similar to that of the only other previously analysed BSF sample (078-S, Figure 2.4).

Trace element contents of MB3-H 065-A (0.10 wt%) and MB3-H BSF (0.04 wt%) were found to be low (Figure 2.5) and typical of trace element content of previously analysed core sub-samples (Wendling *et al.* 2013). The majority of the trace element concentrations were similar among the different core sub-samples. However the concentrations of As, Cr, Cu and Zn were lower and Cd, Co and Th were higher in MB3-H 065-A relative to the other sandstone sub-unit samples (066-S, 069-S and 072-S; Figure 2.5). This is important as both As and Cr fall below the ISQG-Low (trigger value;

20 mg/kg As and 80 mg/kg Cr) in the 065-A sub-sample while being above for the remaining sub-samples. The As content of the BSF sample was similar to 065-A. However it is lower than the content measured for the BSF sample MB3-H 078-S and it should be noted that it falls below the ISQG-Low (trigger value) (Figure 2.5) and generally would not raise any concerns.

Table 2.2: Major element composition of the Reedy Creek MB3-H sub-samples selected for arsenic mobilisation studies

SAMPLE ID		MB3-H 065-A	MB3-H-BSF
Sub-unit		Precipice Sandstone	Precipice Braided Stream Facies
Depth (mBGL)		1302.6 – 1303.4	1332.5-1333.6
SiO_2	wt%	85.23	96.45
Al_2O_3	wt%	7.12	1.93
K_2O	wt%	2.14	0.17
Fe_2O_3	wt%	1.17	0.15
CaO	wt%	0.27	0.03
TiO_2	wt%	0.27	0.13
MgO	wt%	0.26	0.06
Na_2O	wt%	0.12	0.07
P_2O_5	wt%	0.05	0.02
MnO	wt%	0.02	0.005
SO_3	wt%	0.01	0.04
Cl	mg/kg	21	207
LOI	wt%	3.33	0.95
Sum %		100	100

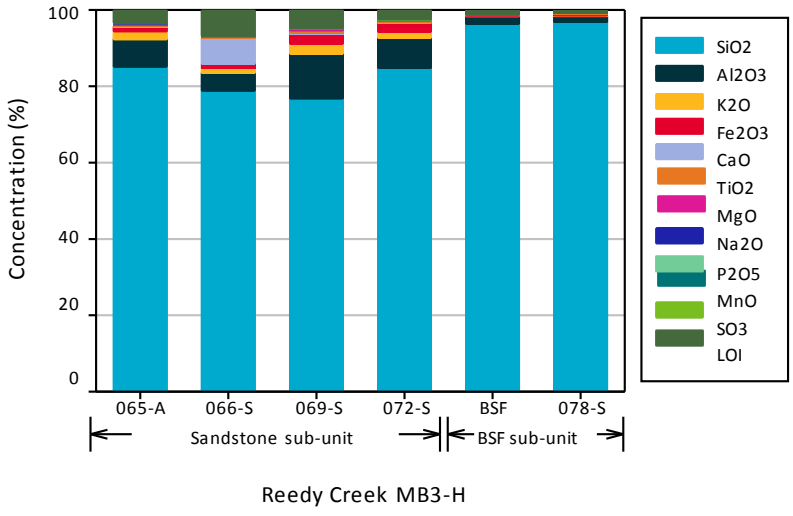

Figure 2.4: Major element composition of selected sub-samples from Reedy Creek MB3-H core, 065-A and BSF from current investigation and the remainder from Wendling *et al.* (2013) (Appendix A)

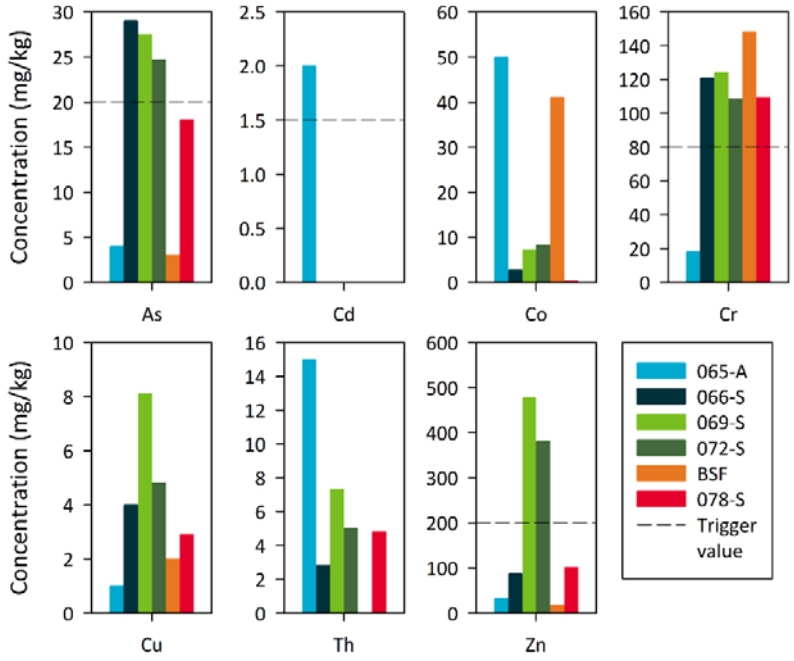

Figure 2.5: Selected trace element composition of selected sub-samples from Reedy Creek MB3-H core, 065-A and BSF from current investigation and the remainder from Wendling *et al.* (2013) (Appendix A)

2.3.3 Potential reductive capacity of the Precipice Sandstone sediments

Estimates of the potential reduction capacity (PRC) allow to determine the overall abundance and (potential) relative importance of various oxygen consuming phases such as pyrite, sediment organic matter and Fe(II)-minerals (Hartog *et al.* 2002; Descourvieres *et al.* 2010a). In the present study the potential reductive capacity of the core material samples was assessed with a particular focus on identifying and quantifying potential contribution of iron sulphides. Under the ambient highly reducing conditions that naturally prevail in the Precipice aquifer, minerals such as iron sulphides and reactive Fe(II) minerals such as siderite are expected to be stable. However, these minerals, along with sedimentary organic carbon may be oxidised if oxygen or other oxidants (e.g., nitrate, chlorine, hydrogen peroxide) are introduced into the aquifer during reinjection. For samples MB3-H 065-A and MB3-H BSF that were used in this study the estimated total PRC was 49.4 µmol(O_2)/g and 24.3 µmol(O_2)/g, respectively (Figure 2.6).

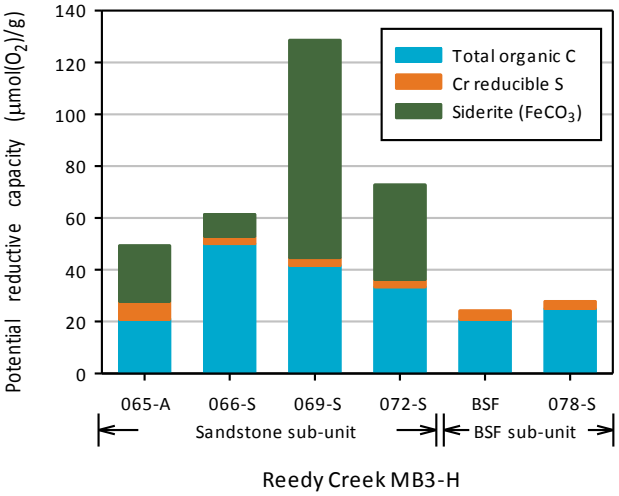

Figure 2.6: Components contributing to the potential reductive capacity (potential oxygen consumption) of the Precipice aquifer sediments at Reedy Creek

Sediment organic matter and siderite were found to be the two main contributors to the reductive capacity of the Precipice aquifer. Pyrite, on the other hand was not detected by XRD. However, a separate quantification of

chromium reducible sulphur (S_{Cr}) indicated that trace amounts of sulphide were present (≤0.012 % S_{Cr}). At such low concentrations sulphides are only minor contributor to the total PRC in comparison to the SOM and siderite (Figure 2.6). From these results it could be concluded that pyrite is unlikely to be a major and long-lasting source of metal/metalloid release should the aquifer sediments be oxidised by reinjection. The sandstone sub-unit of the Precipice aquifer has greater PRC than the BSF sub-unit, largely due to the presence of siderite in these sediments. The percent contribution to the PRC from SOM, siderite and pyrite for sample MB3-H 065-A were 42%, 44% and 14%, respectively, while they contributed 86%, 0% and 14%, respectively to the PRC of the MB3-H BSF sample.

2.4 Laboratory respirometer experiments with Reedy Creek sediments

The above discussed estimates of the potential reduction capacity of rocks and sediments may be determined from the analytically determined abundance of the reduced, i.e., potentially oxygen consuming phases (Hartog *et al.* 2002; Descourvieres *et al.* 2010a). However, their (slow) reactivity may limit their contribution as oxygen consuming process, at least over the time-scales relevant for the reinjection trials. Closed-system respirometry was used to assess the limitations imposed by such reactivity controls. Respirometer tests involve real time monitoring of any oxygen consumption and carbon dioxide production resulting from biotic and abiotic processes. In the case of aquifer sediments, these reactions are typically related to the microbial degradation of sediment organic matter and the chemical oxidation of sufficiently reactive mineral phases such as pyrite. Over the entire experimental period aqueous suspensions are equilibrated with atmospheric oxygen within the closed-system respirometer while the consumption of O_2 and evolution of CO_2 are monitored. The measured rates of oxygen consumption and carbon dioxide production can subsequently be related to changes in solution chemistry and the extent to which oxygen has reacted with the mineral phases and organic matter that is known or assumed to be present in the sediment sample.

The respirometer experiments for the Reedy Creek site were conducted using a sample from the sandstone sub-unit of the Precipice aquifer (MB3-H 065-A, 1302.6-1303.4 mBGL). Duplicate sub-samples were equilibrated for different incubation times with two different equilibrating solution compositions (low and high ionic strength) as outlined in Table 2.3. The two water compositions represent the low (Milli-Q) and high (simulated injectant) end members of possible injectant water composition, i.e., very low dissolved ions and ionic strength similar to that of the ambient groundwater, respectively. Initial major ion concentrations of the two equilibrating solutions are shown in Table 2.4 along with Reedy Creek ambient groundwater and injectant water of matching electrical conductivity (EC). The different incubation times indicated in Table 2.3 were chosen to describe potential changes in reaction kinetics during the course of the experiment.

Table 2.3: Water composition and incubation time associated with each respirometer duplicate sub-sample

INCUBATION TIME (DAYS)	WATER COMPOSITION		
	LOW IONIC STRENGTH (MILLI-Q)	HIGH IONIC STRENGTH (SIMULATED INJECTANT)	ANAEROBIC (MILLI-Q)
0	x	x	
1	x	x	
2	x		
5	x		
9	x		
14	x		
54	x	x	x

The methodology for the respirometer experiments was adapted from the procedure used by Descourvières *et al.* (2010). Moist sediment samples of 22.5 g (equivalent to approximately 20.94 g oven-dry weight) were mixed with 150 mL nitrogen saturated ultrapure laboratory grade (Milli-Q) water or simulated injectant water in 250 mL Duran bottles. The time zero samples were mixed briefly before supernatant collection (described below). The remaining samples plus two Milli-Q water blanks (no sediment) were connected to a close circuit respirometer (Micro-Oxymax, Columbus Instruments) and incubated at 24.2°C (±1.1°C). The head space was initially equilibrated with atmospheric O_2 and CO_2 concentrations with the respirometer automatically refreshing the head-space with air if O_2 or CO_2

concentrations fell outside the measurement range (19.3 to 21.5% for O_2 and 0 to 1.0% for CO_2). The sediment-water slurry was stirred using an orbital shaker (Thermocline Scientific) at 180 rpm to ensure a homogeneous chemical system and enhance oxygen diffusion between the head-space and the water phase.

Table 2.4: Composition of ambient groundwater and injectant from the Reedy Creek trial and respirometer equilibration solutions. All units in mg/L unless otherwise stated

	AMBIENT GW	INJECTANT 700EC	LOW IONIC STRENGTH WATER (MILLI-Q)	HIGH IONIC STRENGTH WATER (SIMULATED INJECTANT)
pH field (-)	7.85	9.30	6.60	8.90
pH lab (-)	8.14	9.31	8.00	9.30
EC (µS/cm)	796	687	2.7	732
Ca^{2+}	<1	<1	<0.1	<0.1
Mg^{2+}	<1	<1	<0.1	<0.1
K^{+}	3	<1	<0.1	<0.1
Na^{+}	178	153	<0.1	154
Cl^{-}	98	150	<1	170
SO_4^{2-}	<1	<1	<1	<1
HCO_3^{-}	319.64	112.24	9	153
CO_3^{2-}	0.6	25.2	<1	<1

Head space oxygen (O_2) and carbon dioxide (CO_2) concentrations in each sample were measured periodically (every 2.1 hrs) using electrochemical and infrared detection, respectively. Samples were removed from the respirometer according to the schedule in Table 2.3. Following the incubation, pH and EC were measured using a handheld pH and EC meter (WTW) with dissolved oxygen and oxidation reduction potential measured on the day 54 samples. The sediment samples were decanted in to 50 mL polypropylene centrifuge tubes and centrifuged at 4,000 rpm for 30 min. The filtered (0.45 µm) supernatant solutions were sent to a commercial laboratory (ChemCentre) for analysis of major ion (Ca, K, Mg, Na, Cl, SO_4, HCO_3), trace metal (Al, Ag, As, B, Ba, Be, Cd, Co, Cr, Cu, Fe, Mn, Mo, Ni, Pb, Sb, Se, Si, Sn, V, Zn), dissolved organic carbon (DOC), alkalinity, and acidity.

The oxygen consumption or measured reductive capacity (MRC) over the 54 day experiment ranged from 4.4 µmol/g for the low ionic strength water to 9.5 µmol/g for the simulated injectant water. These Precipice MRC values fall at the lower end of previously reported aquifer sediment MRC values (Hartog *et al.* 2002; Descourvieres *et al.* 2010a). The calculated MRC corresponds to between 9% and 19% of the total PRC, comparable to other reported aquifer sediments (Hartog *et al.* 2002; Descourvieres *et al.* 2010a). The rate at which oxygen was consumed decreased throughout the experiment as indicated by the curved response in Figure 2.7b, indicating that the reactivity of the minerals and organic matter present were decreasing throughout the experiment. Carbon dioxide was initially removed from the head space of the respirometer flasks as the N_2 saturated solution equilibrated with CO_2 and O_2 introduced into the head space. However, as observed by Descourvières *et al.* (2010), a greater consumption of CO_2 (removal from headspace) took place in the presence of carbonates due to increased CO_2 partial pressure resulting from the carbonate dissolution. Due to the presence of bicarbonate in the injectant solution, CO_2 equilibration was faster than observed in the Milli-Q samples (Figure 2.7c).

Oxidation of sediment organic matter (SOM) is likely to be the primary mechanism of oxygen consumption in the Precipice aquifer sediment from MB3-H 065-A. This can be concluded from the fact that the measured ratio of oxygen consumption to carbon dioxide production ratio was close to 1.0 (0.93 to 1.48) throughout the second half of the experimental period (day 25 to 54, Figure 2.7a). This ratio corresponds well with the stoichiometry of organic matter oxidation:

$$CCHH_2OO + OO_2 \rightarrow CCOO_2 + HH_2OO \quad (1)$$

While the calculation of the PRC suggest that siderite oxidation could contribute up to 44% of the PRC, it appears that its contributions to the MRC of the Reedy Creek samples is likely to be small, given that the measured CO_2:O_2

ratios were much lower than the 4:1 ratio predicted from the reaction stoichiometry of siderite. Duckworth and Martin (2004) showed that, under oxic and neutral to slightly alkaline pH (6<pH<10.3) conditions, the dissolution rate of siderite was low compared to more extreme acidic (pH<6) or alkaline (pH>10.3) conditions. They suggested that the precipitation of iron (hydr)oxides, which were observed on the surface of the siderite minerals, induced a decrease in apparent dissolution rates. Given that the pH of the respirometer experiments falls within the affected range (pH 6 to 10.3) (Figure 2.8c), this mechanism potentially limits the contribution of siderite towards the Precipice Sandstone sub-unit sediment MRC.

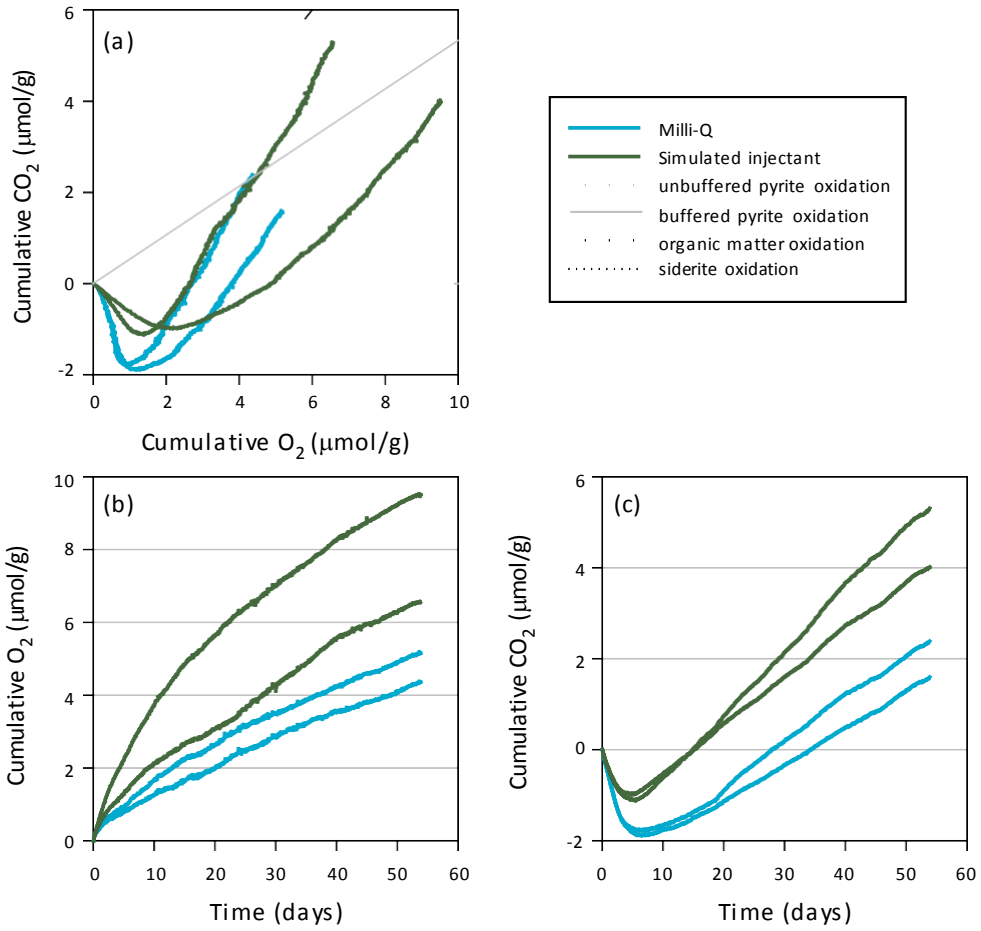

Figure 2.7: Cumulative consumption of O_2 and production of CO_2 during the 54 day incubation of Precipice aquifer sediment (MB3-H 065-A); (a) relative changes in CO_2 production with O_2 consumption; (b) and (c) temporal variation in O_2 consumption and CO_2 production, respectively. For comparison the lines representing the CO_2:O_2 stoichiometric ratio of the reactive minerals and organic matter are show in part (a)

While some arsenic mobilisation was observed in the initial phase of the incubation experiments with the Precipice aquifer sediment, its release appeared not to be related to the ongoing oxygen consumption. After the initial release during the first day of the experimental period, arsenic concentrations decreased successively over the duration of the experiment (Figure 2.8a). Regardless of the tested equilibrating solution, arsenic concentrations in the supernatant decreased after peaking at day 1 at a maximum of 26-28 µg/L. At the end of the experiment (day 54) concentrations ranged between <1 and 3 µg/L. Based on the data obtained from the experiment it is not possible to determine the mechanism that caused arsenic mobilisation at the beginning of the experiment, though desorption is the most probable mechanism. Also the most likely mechanism that caused concentration to decline is the adsorption to iron oxyhydroxides that have formed in conjunction with Fe(II) mineral oxidation, most likely the oxidation of siderite. While arsenic speciation determination was not undertaken for the supernatants that were produced in the respirometer experiments, it is reasonable to assume that oxidation of As(III) to As(V) has occurred and thus adsorption of both As(III) and As(V) is likely.

Increasing sulphate (SO_4) concentrations, which would have been a strong indicator of pyrite oxidation, were not observed in the experiments with the Precipice aquifer material (Figure 2.8b). This suggests that for the investigated

sediment sub-sample, pyrite oxidation was unlikely to be the source of the elevated dissolved As concentrations that was observed at the beginning of the experiment.

Dissolved organic carbon (DOC) was released during the incubation of the aquifer sediment with both the Milli-Q and simulated injectant equilibrating solutions (Figure 2.8d). This increase in DOC in the supernatant is potentially the result of SOM degradation/dissolution. Due to the age of the Precipice aquifer sediments and fluvial/lacustrine depositional environment, the SOM present in the aquifer is likely to have undergone significant degradation such that the remaining fraction is largely recalcitrant. While organic matter degradation was observed in the respirometer experiment, the increasing DOC in the supernatant solution suggests that SOM is being solubilised.

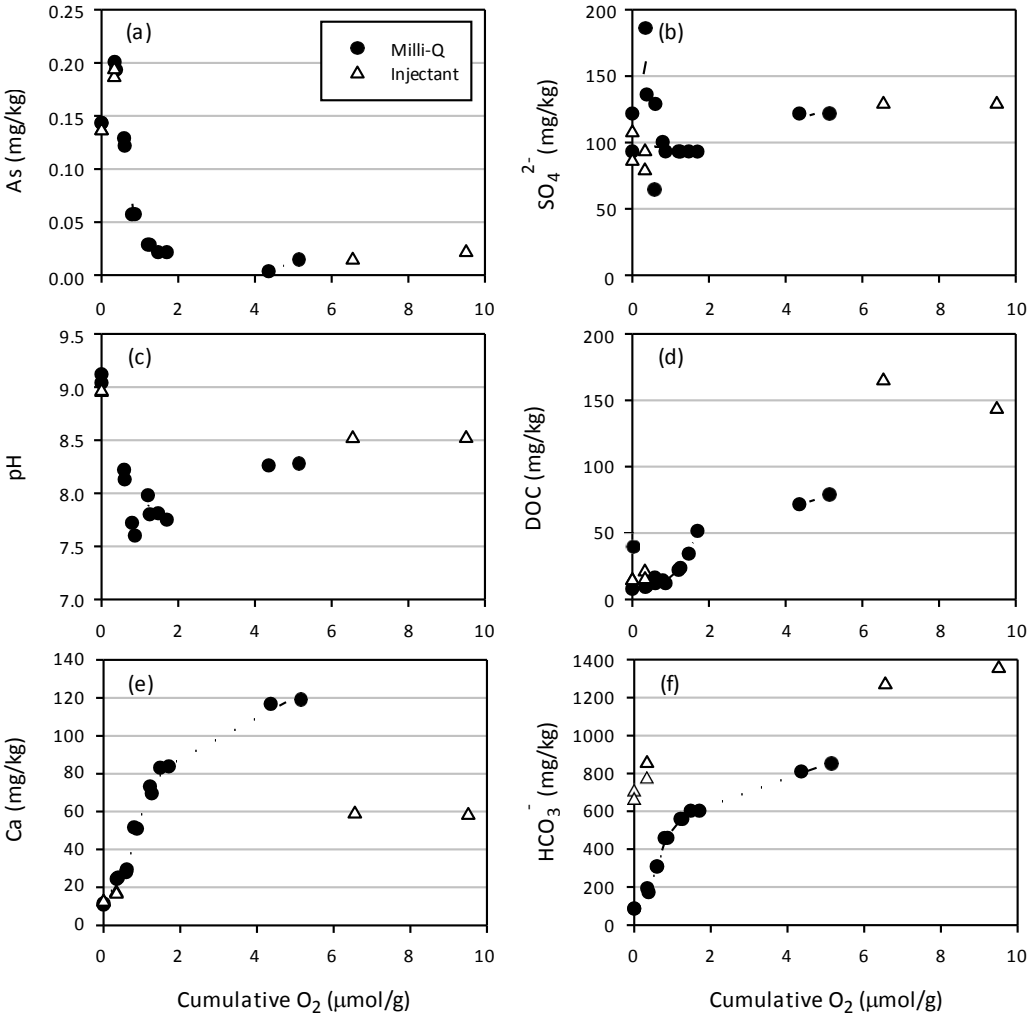

Figure 2.8: Change in supernatant chemistry (expressed as mg/kg of sediment) relative to consumption of oxygen during the incubation of Precipice aquifer sediment (MB3-H 065-A).

The other major mineral reaction that occurred in the experiments is the dissolution of carbonates, such as calcite. Carbonate dissolution results in the Ca and HCO_3 concentrations in the supernatant to increase over the incubation period (Figure 2.8e and 2.8f). While the Ca production rate was relatively stable up to day 14, there was a decrease in the production rate during the second part of the experiment. During the experiment the pH varied between an initially alkaline range (9.1) and a minimum of 7.6 before rising again towards the end of the incubation period (Figure 2.8c).

These findings need to be assessed with regard to the different sediment chemistry and hydraulic conductivities. The acid neutralisation capacity of the Precipice aquifer samples MB3-H 065-A and MB3-H BSF was determined to be 9.1 and 0.6 kg (H_2SO_4)/t, respectively. Therefore the sandstone sub-unit would have greater potential buffering capacity than the BSF sub-unit based on this limited information. The hydraulic conductivities of the aquifer will also determine the degree to which the injectant water interacts with the carbonates, especially as groundwater fluxes across the BSF sub-units are expected to be significantly higher than those across the sandstone sub-unit.

2.5 Laboratory-scale sorption experiments

A series of dedicated sorption experiments were performed with sediment material from the Precipice Sandstone aquifer at Reedy Creek to understand arsenic sorption under variable geochemical conditions. The material was prepared using a core (MB3-H-BSF) collected from the Reedy Creek injection trial site at a depth of 1,332.53-1,333.55 mBGL. The series of experiments included:

- Adsorption isotherms for As(III) at three constant pH; 6.1, 7.5 and 9.3;
- Variable pH experiments at a fixed As(III) concentration of 150 µg/L; and
- Assessment of competitive sorption effects with phosphate (PO_4).

The core material was ground and subsequently characterised with respect to the amount of arsenic that prevailed on the exposed mineral surfaces prior to the batch sorption experiments. Each of the batch experiments was conducted by mixing 40 mL of 6 mM sodium chloride (NaCl) solution with a sediment composite (4.00 g of MB3-H-BSF) in polypropylene centrifuge tubes. The resulting suspension was continuously mixed (end-over-end) on a rotating mixer at 25 revolutions per minute (rpm) for an equilibration time of 2 days.

Solutions were separated from sediment by centrifuging at 4,500 rpm for 10 min. The Na and Cl concentrations were selected to be comparable to those found in the ambient groundwater at the Reedy Creek site. Stock solutions of As(III) (arsenite) and phosphate were prepared using reagent grade 0.5M $NaAsO_2$ (Fluka) and KH_2PO_4 (Sigma-Aldrich). The As(III) extractions were conducted in the dark using light-impermeable brown centrifuge tubes to prevent photocatalysed oxidation of As(III). Also the extraction experiments were conducted in an anaerobic chamber (Coy Laboratory Products) containing a N_2 atmosphere. No attempt was made to suppress microbial activity.

Adsorption isotherms for As(III) were determined for concentrations ranging from 37.5 to 1500 µg/L As(III) at constant pH of either 6.1, 7.5 or 9.3. Arsenic speciation of filtered samples (0.45 µm) showed that >99% of the As has remained as As(III), i.e., oxidation to As(V) was successfully prevented. Adsorbed As(III) was determined from the difference between the initial and the final aqueous concentrations. Adsorption as a function of pH was measured for a constant initial As(III) concentration of 150 µg/L with pH values ranging from 4 to 10. Adjustment of pH was performed with 0.1 and 1.0 M HCl or NaOH.

The influence of phosphate on As(III) adsorption (pH 6.1 and 9.3) was determined using initial As(III) concentrations of 37.5, 75 and 150 µg/L at initial PO_4 concentrations ranging from 45, 90 and 180 µg/L. Given that the temperature of the injected water (18˚C) is significantly below the in-situ groundwater temperature of 62˚C it was also tested whether temperature changes could cause arsenic desorption. Therefore, selected arsenic sorption experiments were carried out at three different temperatures (25, 45 and 70˚C).

Dissolved As(III) concentrations in filtered samples (0.45 µm) were determined by the ChemCentre (Perth, WA) using ICP-MS (inductively coupled plasma-mass spectrometry) and hydride generation – AAS (atomic absorption spectroscopy).

2.6 Surface complexation model

All sorption experiments were jointly analysed through an inverse geochemical modelling approach. The objective of this step was to formulate a sorption model that could reproduce the observed arsenic sorption behaviour within the range of the tested geochemical conditions. This was achieved by defining a site-specific surface complexation model that specifically captures the sorption characteristics of the Precipice sandstone at the Reedy Creek site. This surface complexation model was defined within the geochemical model PHREEQC. The model was successively improved by adding/removing sorption reactions and by using the parameter estimation tool PEST (Doherty and Hunt 2009) to optimise:

- the reaction constants (log K_s) of the sorption reactions,
- the number of sorption sites (sorption site density) per volume of aquifer, and
- the concentrations of As(III) and PO_4 prevailing on the sorption sites prior to the start of the sorption experiments.

Where available the As(III) and PO_4 sorption reactions proposed by Stollenwerk *et al.* (2007) were adopted and their reported values for reaction constants were used as initial estimates for the optimisation. All reactions included in

the surface complexation model and the optimised parameter values are listed in Table 2.5. The optimised surface complexation model captures the arsenite and phosphate sorption behaviour over the entire pH range (4.5-10.0) tested (Figure 2.9).

Table 2.5: Optimised sorption constants (log K's) of the lab-derived SCM in comparison with selected literature data.

	LOG K (OPTIMISED FOR LAB EXPTS)	LOG K (OPTIMISED FOR FIELD TRIAL)	LOG K (STOLLENWERK *ET AL.* 2007)
Sorption reactions for arsenite with Reedy Creek Precipice (RCP) Sandstone			
$RCP\_wOH + AsO_3^{-3} + 4H^+ = RCP\_wH_3AsO_3^+ + H_2O$	48.06	52.56	-
$RCP\_wOH + AsO_3^{-3} + 3H^+ = RCP\_wH2AsO_3 + H_2O$	43.67	42.675	37.50
$RCP\_wOH + AsO_3^{-3} + 2H^+ = RCP\_wHAsO_3^- + H_2O$	18.14	28.14	32.10
$RCP\_wOH + AsO_3^{-3} + H^+ = RCP\_wAsO_3^{-2} + H_2O$	15.00	15.00	30.01
$RCP\_sOH + AsO_3^{-3} + 4H^+ = RCP\ sH3AsO_3^+ + H_2O$	53.71	-	-
$RCP\_sOH + AsO_3^{-3} + 3H^+ = RCP\_sH2AsO_3 + H_2O$	44.54	-	-
$RCP\_sOH + AsO_3^{-3} + 2H^+ = RCP\ sHAsO_3^- + H_2O$	18.14	-	-
$RCP\_sOH + AsO_3^{-3} + H^+ = RCP\_sAsO_3^{-2} + H_2O$	15.00	-	-
Sorption reactions for phosphate with Reedy Creek Precipice (RCP) Sandstone			
$RCP\_wOH + PO_4^{-3} + 4H^+ = RCP\_wH_3PO_4^+ + H_2O$	36.83	38.83	-
$RCP\_wOH + PO_4^{-3} + 3H^+ = RCP\ wH_2PO_4 + H_2O$	31.10	31.10	32.80
$RCP\_wOH + PO_4^{-3} + 2H^+ = RCP\_wHPO_4^- + H_2O$	24.40	25.37	24.89
$RCP\_wOH + PO_4^{-3} + H^+ = RCP\_wPO_4^{-2} + H_2O$	15.69	15.86	13.56
$RCP\_sOH + PO_4^{-3} + 4H^+ = RCP\_sH_3PO_4^+ + H_2O$	53.80	-	-
$RCP\_sOH + PO_4^{-3} + 3H^+ = RCP\_sH_2PO_4 + H_2O$	60.00	-	-
$RCP\_sOH + PO_4^{-3} + 2H^+ = RCP\_sHPO_4^- + H_2O$	40.89	-	-
$RCP\_sOH + PO_4^{-3} + H^+ = RCP\ sPO_4^{-2} + H_2O$	46.00	-	-

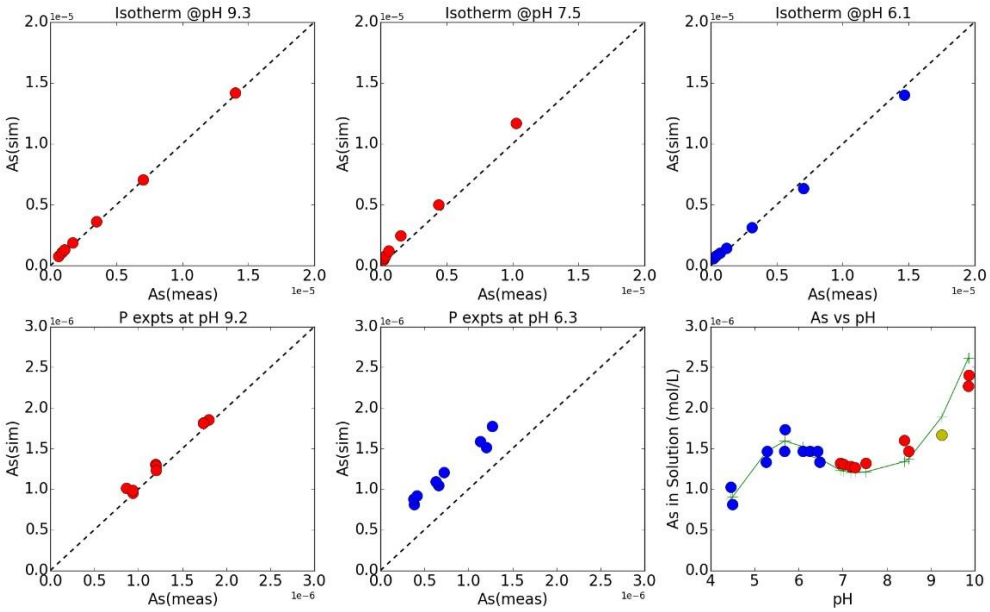

Figure 2.9: Comparison of simulated and laboratory-measured aqueous concentrations of As and P after estimation of lab-derived sorption constants. Red circles indicate values that were measured in the most relevant pH range (7-9.5), blue circles indicate experimental values from pHs < 7.

2.7 Injection experiment

The injection trial at Reedy Creek was undertaken as a push-pull experiment. Injection into the Precipice Sandstone commenced on 27th March, 2013 and continued intermittently through to 4th August, 2013. A total of 52.7 ML was injected, with injection occurring on 65 days during that period. Following the injection phase, a period of 64 days residence in the aquifer was designed to allow the injected water to react with the native groundwater and the aquifer matrix and thus to make weathering and other rates more identifiable. Following this period a pump was installed into the bore to recover the injected water. Recovery began on 8th October, 2013 and ran for a total of 309 days. Approximately 156 ML of water was extracted from the injection bore, representing approximately three times the total water injected. A summary of the injection rates and duration for each stage is shown in Table 2.6.

The injectant consisted of a combination of CSG water produced from a gas production pilot and water extracted from aquifers during hydraulic testing. CSG water from pilot wells was collected in the production gathering network and delivered as an aggregate from those wells to an existing pilot pond, where it was stored. Groundwater from hydraulic testing was pumped to the pilot pond through temporary pipework. The treatment system included several steps that were applied prior to injection:

- filtration of untreated water to remove suspended solids;
- reverse osmosis (RO) of filtered water (brine was stored in a separate compartment of the pilot pond);
- ultrafiltration (UF) of the raw water blend stream;
- blending of RO permeate and UF water streams to achieve similar or better quality than in-situ groundwater. The blending ratio was controlled through continual measurement of electrical conductivity (EC) and feedback to the feed pumps. Off-specification water was directed back to the pilot pond;
- disinfection by ultra-violet irradiation; and
- removal of dissolved gases by membrane de-oxygenation.

The water quality was closely monitored during the injection and recovery periods. Water quality parameters (DO, EC, pH, ORP and temperature) of the injectant were recorded at a 1 second interval by the process control system. Samples of the injectant were collected for laboratory analysis weekly for the first month (while injection was operational), then generally fortnightly until the end of the trial. During the extraction phase, water quality samples were collected twice per day for a period of two weeks. After two weeks the sampling frequency was decreased and weekly sampling was performed until the majority of the injected water was recovered, then on an intermittent basis. No monitoring bore was available within the predicted water quality impact zone.

A bromide tracer amendment was undertaken as part of the injection trial program to elucidate the physical transport behaviour and mechanisms. It was expected, for example, that the results could provide some indication on whether fracture flow and transport would play a role within the Precipice Sandstone aquifer. To minimise the required recovery period and to prevent excessive dilution to low bromide concentrations, tracer injection occurred in two pulses towards the end of injection phase. Sodium bromide (NaBr) was used as the tracer as bromide is generally considered to be conservative, and not expected to react with the formation or the in-situ groundwater. In total, 25 kg of laboratory grade NaBr powder was mixed into the 30,000 L blending tank and injected over approximately 4 hours. The Br concentrations that were recorded during the recovery provided important constraints for the subsequent calibration of the numerical model. The full details of the injection experiment and additional characterisation data are provided in APLNG (2013b).

Table 2.6: Injection/extraction rates and duration

Phase	Testing Stage		Average Flow Rate (m^3/hr)	Date(s)	EC Water Quality Target (µS/cm)
Injection	Commissioning		25	27/03/2013	755
			15		
			3		
Airlift re-development			70	17/04/2013 to 21/04/2013	NA
Injection	MRT 1	Step 1	25	13/05/2013	755
		Step 2	35	13/05/2013 to 14/05/2013	
		Step 3	47	15/05/2013 to 16/05/2013	
		Step 4	67	17/05/2013 to 18/05/2013	
	CRT 1		60	26/05/2013 to 25/06/2013	755
	MRT 2	Step 1	35	29/06/2013 to 30/06/2013	755
		Step 2	50	30/06/2013 to 01/07/2013	
		Step 3	67	01/07/2013 to 03/07/2013	
	CRT 2		60	05/07/2013 to 16/07/2013	755
	MRT 3	Step 1	35	19/07/2013 to 20/07/2013	790*
		Step 2	50	20/07/2013 to 21/07/2013	
		Step 3	67	21/07/2013 to 23/07/2013	
	CRT 3 - Permeate		50	23/07/2013 to 27/07/2013	790*/500/300/100
	MRT 4	Step 1	35	29/07/2013 to 30/07/2013	790*
		Step 2	50	30/07/2013 to 31/07/2013	
		Step 3	65	02/08/2013 to 03/08/2013	
		Step 4	87	03/08/2013 to 04/08/2013	
Residence in aquifer			0	04/08/2013 to 07/10/2013	NA
Recovery			31	08/10/2013 to 22/11/2014	NA

*the target EC was increased from 755 µS/cm to 790 µS/cm on 11th July, 2013 after it was observed that the TDS:EC ratio of the injectate (0.60) was less than originally assumed (0.65).

2.8 Model-based interpretation of field injection experiment

Numerical modelling was used as key tool to integrate and analyse the data collected during the field injection trial while also incorporating the conceptual understanding derived from the pre-trial hydrogeological and geochemical characterisation efforts and from the laboratory-scale investigations that were discussed in the previous sections.

2.8.1 MODELLING TOOLS AND APPROACHES

A local-scale reactive transport model was constructed to interpret the tracer, temperature and hydrochemical data that were collected during the Reedy Creek injection trial. MODFLOW (Harbaugh 2005), MT3DMS (Zheng and Wang 1999) and PHT3D (Prommer *et al.* 2003) were used as modelling tools to simulate groundwater flow, solute and reactive transport, respectively. The models were set up with the graphical user interface (GUI) ipht3d, developed at the University Bordeaux and Python was used for output data post-processing.

2.8.2 GROUNDWATER FLOW AND CONSERVATIVE SOLUTE TRANSPORT

As a first step of the field-scale modelling study a radial-symmetric multi-layer model was constructed on the basis of earlier models that were used to optimise the experimental conditions and to maximise the data worth of the injection trial. The final model that was used for simulating the injection trial and for the predictive simulations discretised the zone between 1278 mBGL and 1346.5 mBGL into 24 layers of varying thickness, porosity and hydraulic conductivity. The selected vertical discretisation honours the interpretation of the available hydrogeological logs and geophysical data, as provided by Origin. In the absence of more detailed data it was assumed that layers were homogenous and continuous in lateral direction. This assumption is probably reasonable over the spatial scale of the injection trial. However, it is expected to be a highly idealised translation of the larger-scale heterogeneity features of the Precipice aquifer.

Measured injection and recovery rates were discretised into daily steps. The initial estimates of porosity and hydraulic conductivity were refined during the initial model calibration, which used measured concentrations of bromide and chloride to constrain the processes and parameters controlling groundwater flow and nonreactive solute transport. The measured bromide recovery that resulted from two distinct bromide amendments during the injection phase provided the most valuable data for this part of the model calibration. The comparison between the simulated and measured bromide concentrations shows a good agreement with the breakthrough characteristics (Figure 2.10). This agreement was achieved without invoking a dual-domain approach, which suggests that fracture flow and transport may not be a dominant feature in the Precipice aquifer at Reedy Creek.

2.8.3 HEAT TRANSPORT

Geochemical reactions such as mineral dissolution and sorption reactions can be (strongly) temperature-dependent and both geochemical equilibria and reaction rates may be affected. The substantial temperature difference between the ambient groundwater in the Precipice Sandstone (~67 ºC) and the injected water (~20-30 ºC) made it necessary to account for potential temperature effects in the reactive transport simulations. In the modelling framework used for the injection trials heat transport was simulated by incorporating temperature as an additional, separate species, based on the similarity between solute and thermal energy transport (Anderson 2005; Ma *et al.* 2012; Seibert *et al.* 2014). Analogous with the instantaneous sorption formulation for a reactive species, thermal energy uptake by the sediments was simulated using a thermal distribution term defined as

$$K_{d,th} = \frac{c_S}{\rho_w c_w} \quad (2)$$

where, $K_{d,th}$ is the thermal distribution term, c_s is the specific heat capacity of the sediment and c_w and ρ_w represent the specific heat capacity and density of water as described in full detail by Ma *et al.* (2012) and Seibert *et al.* (2014). Thermal retardation was subsequently defined as

$$R_{th} = K_{d,th} \frac{\rho_b}{n_{eff}} \quad (3)$$

where, ρ_b represents the bulk density and n_{eff} the effective porosity of the sediment (Ma *et al.* 2012). Conductive heat transport was approximated using a (species-specific) thermal diffusion term ($D_{m,th}$), corresponding to the molecular diffusion for solutes, defined as

$$D_{m,th} = \frac{\kappa_0}{n_{tot}\ \rho_w c_w} \tag{4}$$

where, n_{tot} represents the total porosity (Thorne *et al.* 2006). The value for the bulk thermal conductivity κ_o was defined as

$$\kappa_0 = n_{tot}\kappa_w + (1 - n_{tot})\kappa_s \tag{5}$$

with κ_s and κ_w representing the thermal conductivity of the solid and water phase, respectively. Thermal dispersivity was assumed to have the same value as solute dispersivity (Bridger and Allen 2010; Ma *et al.* 2012; Engelhardt *et al.* 2013). The selected approach neglects rate-limited heat transfer and assumes temperature equilibrium between water and solid.

2.8.4 REACTIVE TRANSPORT MODEL SETUP

Based on the calibrated conservative transport model a multi-component reactive transport model was constructed. The investigated geochemical reactions included a range of mineral weathering reactions and, most importantly, the surface complexation model that captured the earlier discussed sorption phenomena under the spatially and temporally variable geochemical conditions that were induced during the injection trial. Geochemical reactions, where occurring, were dependent on (simulated) groundwater temperatures. Assuming that groundwater flow and (conservative) solute transport were captured with sufficient accuracy after the initial flow/conservative transport model calibration, the initial multi-species transport simulations were used to assess which (important) groundwater constituents were potentially affected by weathering or other types of reactions. This comparison showed that the observed concentration changes of many constituents were mostly well explained by purely conservative transport processes. The most pronounced differences were found for silica, phosphate and arsenic. The underestimation of simulated silica concentrations during the recovery phase in the absence of other substantial (reaction-induced) concentration changes suggested that quartz dissolution may have occurred. While quartz dissolution is generally considered to be a slow process, the combination of elevated temperatures and the elevated pH of the injectant may have promoted quartz dissolution. Reaction-induced concentration changes of phosphate and arsenic were attributed to surface complexation reactions, as supported by the previously discussed experimental work.

2.8.5 REACTIVE TRANSPORT MODEL DEVELOPMENT AND CALIBRATION

With the fate of most groundwater constituents being well matched by conservative transport, only quartz dissolution and surface complexation reactions were considered for the simulation of the injection trial. The laboratory-derived surface complexation model was initially used without modifications. However, the simulations were unable to closely replicate the phosphate and arsenic breakthrough behaviour that was observed in the recovery phase of the trial. Therefore, selected laboratory-derived sorption constants were further adjusted manually (see Table 2.5) until the field observed phosphate and arsenic concentrations were reasonably well matched by the simulations. A comparison of simulation results and corresponding field observations is shown in Figure 2.10. Note, that a direct comparison is only valid during the recovery phase, i.e. after day 200. Note, that during the injection phase the measured concentrations represent above ground concentrations prior to any contact with the aquifer. In contrast, the shown simulated concentrations represent in situ concentrations within the first model grid-cell. At the end of the current phase of the model calibration the validity of the sorption constants that were employed in these simulations was tested by employing them in the simulation of the laboratory sorption experiments. The comparison between simulated and measured data from the sorption experiments shows that the modified surface complexation model still captures the arsenite and phosphate sorption behaviour in the most relevant pH range (7.0-9.5) while failing to capture As sorption in the acidic pH range.

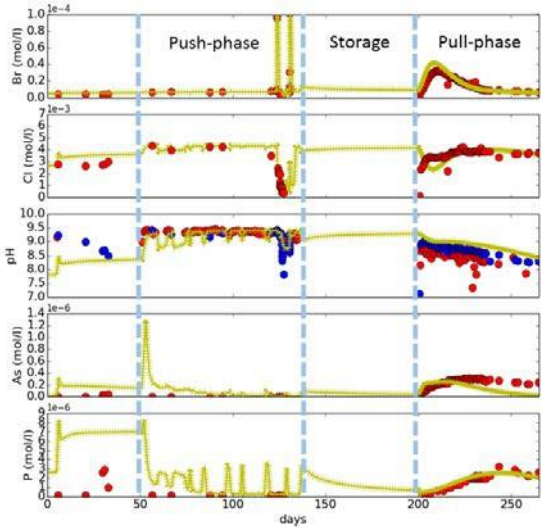

Figure 2.10: Selected simulated concentrations for the Reedy Creek injection trial (yellow lines) in comparison with the corresponding measured aqueous concentrations (red circles). In the case of pH red circles indicate field measured values and blue circles indicate laboratory results.

2.8.6 SIMULATED REACTIVE TRANSPORT BEHAVIOUR DURING THE INJECTION TRIAL

Figure 2.11 illustrates the simulated (reactive) transport behaviour within the target zone of the Precipice aquifer along a cross-section in radial direction for selected times after the start of the injection trial. The simulated concentration contours of the (artificial) tracer illustrate the variable lateral transport distances that are induced by the vertical variations of the hydraulic conductivities and porosities. The figure also highlights the degree of retardation that causes temperature changes to propagate at much slower rates than conservative solutes. Similarly the elevated pH of the injectant is also propagating at slower rates. During the injection phase arsenite is mobilised by desorption. The highest simulated arsenic concentrations at the end of the injection phase are found at the front of the high pH zone. During recovery dissolved arsenic is not (completely) re-adsorbed and at least partially extracted by pumping, which explains the elevated concentrations that were observed during the field trial.

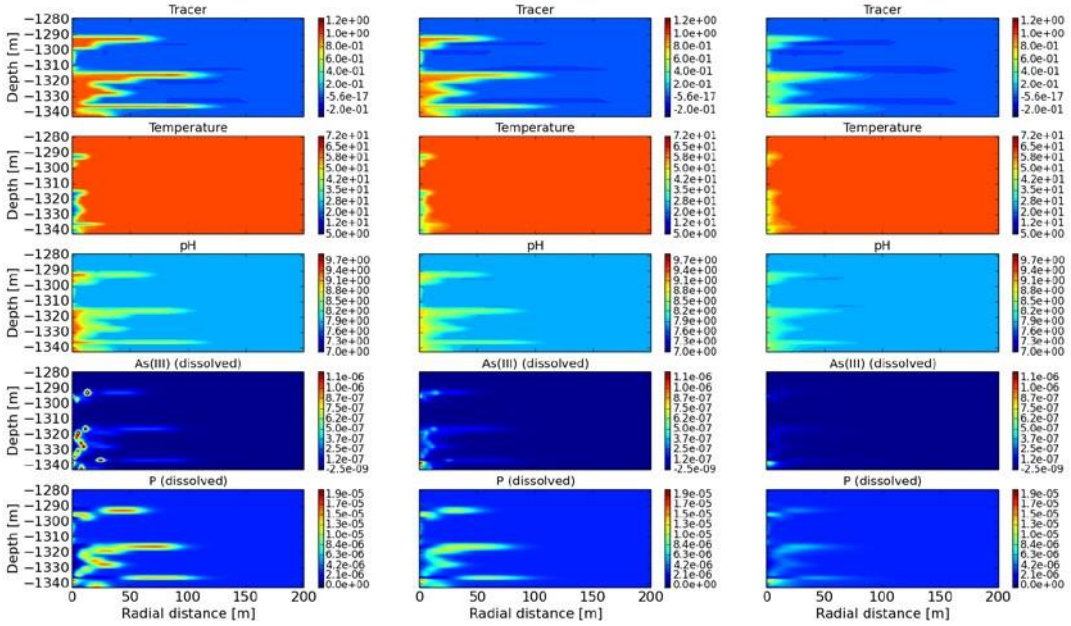

Figure 2.11: Contours of simulated concentrations 150 days (end of injection, left column), 240 (40 days after start of recovery, centre column) and 265 days (65 days after start of recovery, right column) after the start of the Reedy Creek injection trial.

3 Field Injection Experiments Condabri

3.1 Investigation program overview

Following on from the Reedy Creek injection trial and the finding that the alkaline nature of the injected water was the most likely cause of the observed arsenic mobilisation during the injection trial it was decided to perform a new series of injection trials in the Precipice Sandstone aquifer at a pristine site to evaluate this hypothesis and to investigate possible variations in the pre-treatment of the injectant. The new trials were performed at the Condabri site, which provided undisturbed aquifer conditions, i.e., no injection had previously occurred at that site. The major objectives of this series of new trials were to:

- confirm the mechanistic understanding of the processes affecting arsenic release within the Precipice Sandstone aquifer and in particular to verify the main hypothesis that the alkaline pH of the injectant represents the major risk for arsenic mobilisation;
- provide field-scale evidence that acid dosing could possibly eliminate As mobilisation; and to
- test the geochemical impact of eliminating the de-oxygenation step from the injectant treatment process.

The new trials were performed over a 251 day period between 28th October 2014 and 6th July 2015. In the absence of suitable monitoring wells in the vicinity of the injection borehole, the trials were also performed as a sequence of 3 push pulls tests (PPT1-PPT3).

- PPT1 (28th October 2014 to 7th January 2015) was performed to verify the impact of acid dosing on arsenic mobilisation. The injectant pH was controlled to remain in a neutral range throughout the entire injection phase.
- PPT2 (from 15th January 2015 to 22th April 2015) was performed as a "control" experiment to verify that some arsenic would be mobilised without acid dosing.
- PPT3 (from 24th April 2015 to 6th July 2015) was operated without deoxygenation.

3.2 Study Site

The Condabri trial injection site is located in the Surat Basin approximately 20 km north east of Condamine in southeast Queensland, Australia. The injection trial facility included a 200 ML feed pond, tied-in to the surrounding network gathering produced water from active CSG wells. The Precipice Sandstone trial injection bore (CON-INJ2-P) is located approximately 200 m south of the feed pond. The closest neighbouring bore is located approximately 6.7 km to the south of the trial injection site. The borehole from which mineralogical data was obtained (CON-MB9-H) is located approximately 6 km south-west of the trial injection bore. There are no identified springs or potentially baseflow-connected watercourses associated with the Precipice Sandstone in the vicinity of the trial site. The Precipice Sandstone is the earliest deposit in the Surat Basin sequence and is encountered at a depth of approximately 1,168 metres below ground level (mBGL) at the Condabri trial site. The lowermost portion of the Precipice Sandstone is known as the Braided Stream Facies (BSF). The BSF is considered to be the most permeable zone of the overall formation, comprising relatively coarse-grained material representative of a high energy fluvial depositional environment. As at Reedy Creek, the Evergreen Formation aquitard separates the Precipice Sandstone from the overlying Hutton Sandstone aquifer, approximately 150 m thick at the Condabri trial site and generally considered to be a significant regional aquitard. Within the Condabri Development Area, CSG and associated water are produced from the Jurassic age Walloon Coal Measures. These coal measures are separated from the Hutton Sandstone aquifer by the Eurombah Formation.

3.3 Injection experiment

The experiment was performed as a sequence of three separate push pull experiments (PPT1-PPT3). The PPTs commenced on 28th October, 2014 and continued intermittently through to 6th July, 2015, with injection occurring on 77 days during that period. Following each injection phase, a pump was installed into the bore to recover the

injected water and undertake water quality sampling. During PPT1 the maximum injection rate was limited to ~1ML/day while during PPT2 and PPT3 1.8-2.2 ML/day were reached during injection phase. The injection phases are characterised by several flow interruptions that resulted from operational problems. Compared to the injection phases, recovery rates were more constant, but remained limited to below 1 ML/day. The flow rates and their variability over time is illustrated in Figure 3.1.

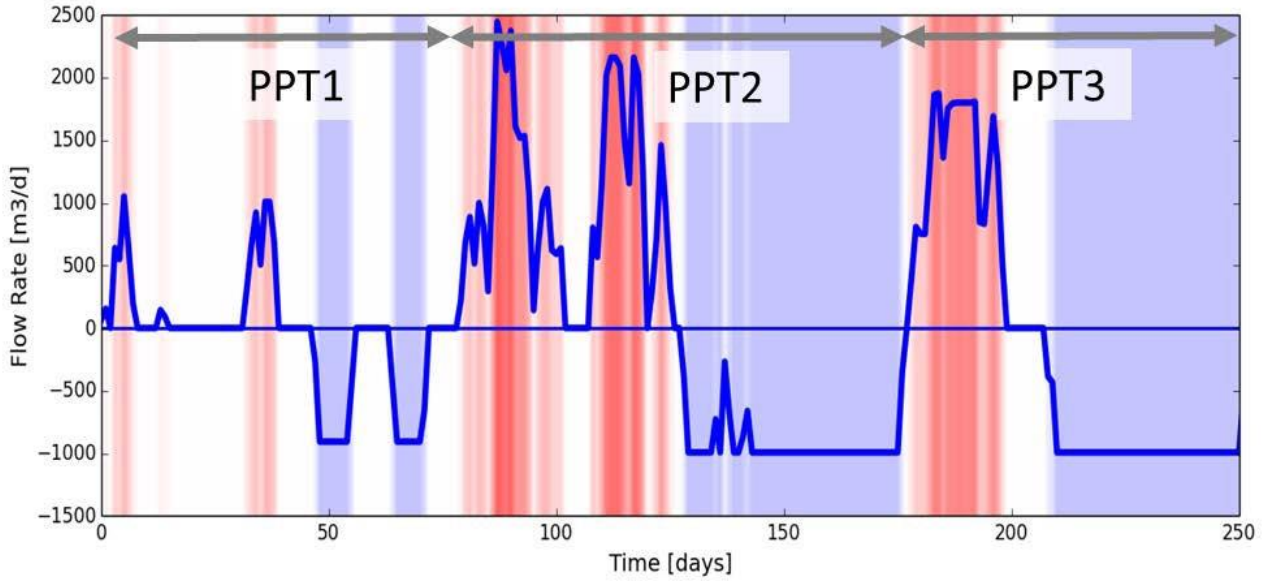

Figure 3.1: Measured and simulated injection/recovery rates during push pull tests PPT1 – PPT3 (red = injection phase, blue = extraction phase).

3.4 Mineralogy

Selected core samples from monitoring bore CON-MB9-H were analysed by X-ray diffraction (XRD). Quartz was found to be the predominant mineral in the Precipice Sandstone, with some clays, feldspar and carbonate minerals. In the BSF sub-unit the proportion of quartz increased further at the expense of other minerals. Laboratory X-ray fluorescence (XRF) analysis of the core samples was undertaken to provide a signature of trace elements in the aquifer matrix. The results show the majority of trace elements at concentrations below 100 ppm (mg/kg) and a minority of common rock-forming elements comprising the higher concentrations. Table A.11 and A.12 (A.2.2) in the appendix displays major and trace element geochemical analysis and mineralogical composition with depth for the Precipice Sandstone and BSF sub-unit at CON-MB9-H.

3.5 Ambient water quality

Baseline geochemical conditions were established by up to 12 sampling events prior to the injection experiment. The results indicate that the mean total dissolved solids (TDS) of the Precipice Sandstone was ~3,600 mg/L, clearly exceeding the Australian Drinking Water Guidelines (ADWG) (NHMRC–NRMMC 2011) aesthetic guideline value of 600 mg/L for all samples analysed. Samples also exceeded the aesthetic drinking water guideline values for sodium, chloride and iron and the health guideline limit for barium. All samples analysed met the guideline thresholds for livestock drinking water (ANZECC and ARMCANZ 2000), with the exception of TDS, which exceeded the lower guideline value for the majority of samples analysed. Field pH measurements showed a mean value of pH 7.6. Sodium was the dominant cation and chloride the dominant anion.

Table 3.1: Initial (ambient) and ranges of injectant concentrations during PPT1-PPT3 (in mol/L, except for pH and pe)

	AMBIENT	PPT1	PPT2	PPT3
pH	6.50	9.15	9.15	7.89
pe	-5.06	12	12	12
Al	1.85×10^{-7}	1.85×10^{-7}	1.85×10^{-7}	1.85×10^{-7}
As(+3)	6.67×10^{-9}	0.0	0.0	1.34×10^{-8}
As(+5)	0.0	4.00×10^{-8}	4.00×10^{-8}	0.0
B	1.11×10^{-5}	5.55×10^{-5}	5.55×10^{-5}	4.81×10^{-5}
Ba	1.57×10^{-5}	3.98×10^{-6}	3.98×10^{-6}	4.09×10^{-6}
Br	5.66×10^{-5}	6.41×10^{-5}	6.41×10^{-5}	3.53×10^{-5}
C(+4)	1.33×10^{-2}	1.22×10^{-2}	1.22×10^{-2}	4.59×10^{-3}
C(-4)	1.61×10^{-2}	0.0	0.0	0.0
Ca	2.62×10^{-3}	2.50×10^{-4}	2.50×10^{-4}	1.75×10^{-4}
Cd	0.0	0.0	0.0	0.0
Cl	4.70×10^{-2}	3.64×10^{-2}	3.64×10^{-2}	4.49×10^{-2}
F	1.58×10^{-5}	1.37×10^{-4}	1.37×10^{-4}	1.05×10^{-4}
Fe(+2)	5.93×10^{-6}	4.48×10^{-7}	4.48×10^{-7}	4.48×10^{-7}
Fe(+3)	1.00×10^{-7}	0.0	0.0	1.00×10^{-5}
K	1.25×10^{-3}	2.56×10^{-4}	2.56×10^{-4}	2.81×10^{-4}
Mg	5.76×10^{-4}	4.53×10^{-4}	4.53×10^{-4}	7.40×10^{-4}
Mn(+2)	2.91×10^{-7}	9.10×10^{-9}	9.10×10^{-9}	1.82×10^{-8}
Mn(+3)	0.0	0.0	0.0	0.0
N(+5)	0.0	3.57×10^{-7}	3.57×10^{-7}	3.57×10^{-7}
N(+3)	0.0	0.0	0.0	0.0
N(0)	0.0	0.0	0.0	0.0
Amm	1.32×10^{-4}	3.57×10^{-7}	3.57×10^{-7}	2.86×10^{-6}
Na	6.53×10^{-2}	5.96×10^{-2}	5.96×10^{-2}	5.66×10^{-2}
O(0)	0.0	2.00×10^{-5}	5.00×10^{-4}	2.00×10^{-5}
DOC	5.00×10^{-4}	1.33×10^{-3}	1.33×10^{-3}	5.00×10^{-4}
P	1.61×10^{-7}	1.62×10^{-7}	1.62×10^{-7}	1.62×10^{-7}
Pb		0.0	0.0	0.0
S(-2)	0.0	1.56×10^{-6}	1.56×10^{-6}	1.56×10^{-6}
S(+6)	0.0	0.0	0.0	0.0
Si	1.01×10^{-3}	8.58×10^{-4}	8.58×10^{-4}	9.58×10^{-4}
Sr	3.22×10^{-5}	1.27×10^{-5}	1.27×10^{-5}	1.47×10^{-5}

3.6 Injectant water quality

Raw CSG water was sourced directly from the Condabri gathering network and stored in an existing pond, formerly used for a CSG Pilot operation. From the pond, the raw water was fed directly into the portable treatment plant via a temporary inlet and suction line. Treatment prior to injection included (i) dosing with hydrochloric acid (PPT1 only); (ii) filtration to remove suspended solids; (iii) disinfection by ultra-violet irradiation; and (iv) removal of dissolved gases by membrane de-oxygenation (PPT1 and PPT2 only). The portable water treatment facility had a maximum design capacity of approximately 3 ML/day. Temporary amendment of a tracer was undertaken as part of the injection trial to (i) assess the physical transport characteristics of the Precipice Sandstone aquifer in terms of mixing and dispersion/dilution effects; and (ii) identify the potential contribution of fracturing to the flow and transport characteristics of the aquifer. Sodium bromide (NaBr) was used as the tracer as bromide is considered to be conservative, and was therefore not expected to react with the formation or the in-situ groundwater. Further, the use of this tracer was granted approval by the regulator. Towards the end of each injection phase 25 kg of laboratory grade NaBr powder was mixed into the 30 kL blending tank and injected over approximately 4 hrs.

3.7 Model-based data interpretations: Approaches and Tools

As for the data from the Reedy Creek injection trial, the data collected during the Condabri PPT1-PPT3 experiments were analysed through a numerical modelling study. The model development for the Condabri injection trial site included the main steps:

- Construction of a local-scale transient, radial-symmetric groundwater flow model for the Precipice Sandstone aquifer surrounding the injection well;
- Construction of a non-reactive solute transport model to estimate key physical transport model parameters, mostly from the interpretation of the three bromide tracer tests that were performed as part of PPT1-PPT3;
- Adaptation of the reaction network developed for the Reedy Creek injection trial to simulate reactive transport at Condabri;
- Reactive transport model calibration for PPT1-PPT3, constrained by the pre-trial geochemical characterisation and the hydrochemical data set collected during the trials; and
- Development and analysis of predictive scenarios for the anticipated long-term geochemical evolution and the associated fate of arsenic.

Like in the study for Reedy Creek simulation, the numerical models MODFLOW (Harbaugh 2005), MT3DMS (Zheng and Wang 1999) and PHT3D (Prommer et al. 2003) were employed to simulate groundwater flow, solute and reactive transport, respectively.

3.8 Conceptual hydrogeological and numerical groundwater flow model

In a first step a local-scale, radial-symmetric numerical flow model was constructed to simulate the groundwater flow processes during the injection trials. The vertical extent of the model was limited to the zone between 1213 m a.s.l and 1249 m a.s.l. Based on the hydrogeological logs and geophysical data it was concluded that unlike at Reedy Creek the zone targeted by the injection trial was relatively homogeneous and that it could possibly be represented by a single layer of 36m thickness. In radial direction the model domain used during the model calibration was limited to 400 m. During the trial phase the hydraulic gradients were dominated by the injection and extraction fluxes, which justifies the assumption of radial symmetry. In addition, it was assumed that the injection zone would be homogenous and continuous in lateral direction. The injection and recovery rates that were logged during the trial were discretised into daily time steps. The transient conditions persisting during PPT1-PPT3 are illustrated in Figure 3.1.

3.9 Conservative solute transport

Based on the transient flow model a non-reactive solute transport model was set up to simulate conservative (tracer) transport for chloride (Cl^-), bromide (Br^-) and boron (B). Using the measured breakthrough data as model calibration constraints, inverse modelling with PEST was used to provide an estimate for the longitudinal dispersivity,

α_L, which controls the degree of physical mixing that occurs during the injection, storage and recovery phases. In the model the injection of the (known) total mass of Br (distributed over a 1h long period) was simulated. The measured bromide concentrations during recovery provided the most valuable data for the conservative solute transport model calibration. Good matches between simulated and observed Br, Cl and B concentrations were achieved for α_L = 0.25-0.50 m (Figure 3.2), whereby Cl and B results were less sensitive to the selected dispersivity.

It should be noted that each of the Br amendments were made at a relatively late stage of the injection phases and that the travel distances of Br prior to recovery was less than the distances that other injected solutes had travelled. Given the well-known scale-dependency of longitudinal dispersion (Gelhar *et al.* 1992), it is possible that the calibrated value for Br underestimates the dispersion that other solutes have undergone during subsurface transport within the injection and recovery phase.

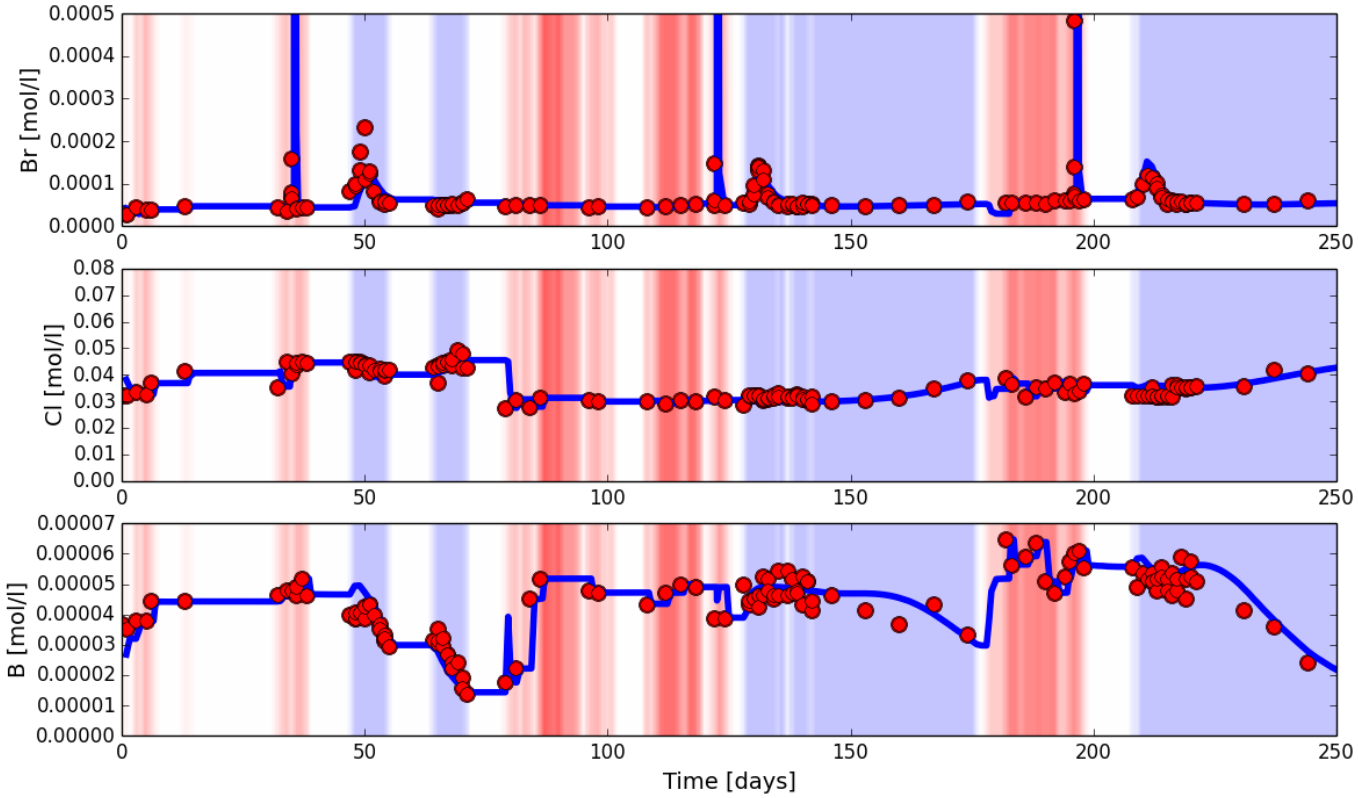

Figure 3.2: Results of conservative transport simulation. Comparison of simulated and measured Br^-, Cl^- and B concentrations for PPT1-PPT3. During the injection phase (red background) the red symbols represent the injected concentrations, during the recovery phases (blue background) the concentrations were measured in the extracted water.

3.10 Heat transport

Heat transport was included in the simulations following the same approach detailed in section 2.8.3. The results of the heat transport simulations (blue line) are shown in Figure 3.3 in comparison with the temperatures that were measured manually during groundwater sampling (red circles) and for PPT2 and PPT3 also a comparison with temperatures recorded in situ by temperature loggers (red lines). It can be seen that the manually measured temperatures, especially the higher temperatures, differ from the in situ logger data, suggesting that some cooling has already occurred at the time of manual sampling. Therefore model parameters were adjusted such that simulation results matched as close as possible with the temperatures measured by the data loggers. However, some discrepancies remained during each of the PPTs for the early parts of the recovery phases. The most likely explanation for the discrepancy is that (i) the simple radial-symmetric model does not account for vertical heat transfer from under- or overlying aquitards that could have occurred during the PPTs, especially during the storage (no-flow) phase or (ii) that the heat transfer between the water phase and the matrix was incomplete. In the subsequent reactive transport simulations the simulated temperatures were internally used to define the reaction temperature.

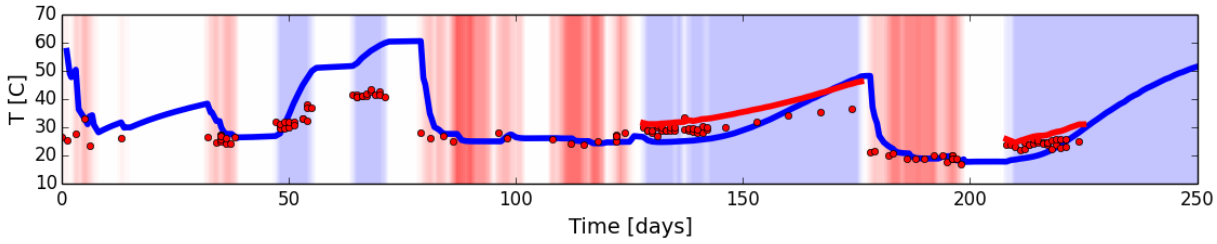

Figure 3.3: Comparison of simulated and measured temperatures during PPT1-PPT3. Red circles indicates the temperatures that were manually measured at the ground surface, the solid red line indicates the in situ temperature measurements that were continuously recorded by a data logger during PPT2 and PPT3 and the blue solid line indicates the simulated temperatures for the injection/extraction well.

3.11 Reactive transport

3.11.1 SELECTION OF SIMULATED REACTION NETWORK

Based on the calibrated conservative solute and heat transport model the reactive transport model was constructed. The model simulation employed the observed ambient concentrations of all relevant major and minor groundwater constituents as initial conditions for the simulations (see Table 3.1). Furthermore, the regularly measured injectant compositions (after treatment, prior to injection) were used to define the temporally changing water composition at the simulated injection well. The initial multi-species transport simulations were then performed in non-reactive mode and the comparison between model results and measured data was used to assess which groundwater constituents were potentially affected by reactive processes. This comparison showed that the observed concentration changes of most groundwater constituents were well explained by purely conservative transport processes. This confirmed the previous experience from the reactive transport simulations for the Reedy Creek injection trial, which was also performed within the Precipice Sandstone.

Over the time-scale of the injection trial the non-reactive model results showed that major ion concentrations were generally not strongly affected by reactive processes and their breakthrough curves during the recovery were largely controlled by physical transport processes.

However, at Condabri, sulphate concentrations during the recovery phase of PPT3 temporarily increased to ~0.15 mmol/L, despite being absent in the injected water. The sulphate concentration peak was accompanied by a peak in dissolved arsenic concentration of up to ~2.5 µmol/L (~185 µg/L). Given that deoxygenation was not operational during PPT3, the results clearly suggest that pyrite oxidation by dissolved oxygen has occurred in this phase of the trial, with

$$FeS_2 + 3.75\,O_2 + 3.5\,H_2O \leftrightarrow Fe(OH)_3 + 2SO_4^{2-} + 4H^+ \quad (6)$$

Therefore a kinetically controlled temperature-dependent pyrite oxidation reaction, as per earlier studies (Prommer and Stuyfzand 2005; Wallis *et al.* 2010; 2011), was incorporated into the reaction network:

$$r_{pyr} = \frac{f_{ar}(T_c)}{f_{ar}(T_{ref})}\left[(C_{O_2})^{0.5}(C_{H^+})^{-0.11}\left(10^{-10.19}\frac{A_{pyr}}{V}\right)\left(\frac{C}{C_0}\right)_{pyr}^{0.67}\right] \quad (7)$$

where, r_{pyr} is the specific oxidation rate for pyrite, C_{O_2} and C_{H^+} are the oxygen and proton groundwater concentrations, A_{pyr}/V is the ratio of mineral surface area to solution volume and (C/C_o) is a factor that accounts for changes in A_{pyr} resulting from the progressing reaction. The temperature dependency was quantified with:

$$f_{ar}(T_c) = -\exp\left(\frac{1}{T_c + 273.15}a_1 + a_2\right) \quad (8)$$

where, a_1 and a_2 are constants, T_c is the groundwater temperature in °C and T_{ref} is a reference temperature (for example the average temperature). The parameters controlling the temperature dependency were adopted from Prommer and Stuyfzand (2005).

The release of much higher arsenic concentrations during PPT3 compared to PPT1 and PPT2 and the observed increase of sulphate during recovery phase of PPT3 suggested a direct link between arsenic release and pyrite oxidation. This link has previously been identified in laboratory experiments (Descourvieres *et al.* 2010b) and during field experiments in artificially recharged deep aquifers (Wallis *et al.* 2010; 2011). In all these cases, oxidants such as molecular oxygen, nitrate or chlorine were oxidising pyrite while releasing arsenic that prevailed within the pyrite structure. In the numerical model arsenic release was directly linked to pyrite oxidation at a molar ratio of 0.04. Compared to previously reported ratios (e.g., 0.0053 in Wallis *et al.* (2010) for a Pleistocene aquifer in the Netherlands, 0.004 in Wallis *et al.* (2011) for the Suwannee Limestone, Florida) this represents a relatively high fraction of arsenic within the pyrite structure. Consistent with the model-based analysis of the Reedy Creek injection trial, the comparison of the conservative multi-species simulations with the measured data for PPT1-PPT3 suggested that silica (SiO_2) concentration may have been affected by quartz dissolution reactions. Therefore quartz dissolution was considered in the reaction network for the Condabri trials with a rate expression proposed by Rimstidt and Barnes (1980), as provided by the PHREEQC standard database:

$$r_q = k \frac{A}{V}\left(Q - 1\right)\left(\frac{K}{s}\right) \tag{9}$$

and

$$k = k_{25} \exp\left[\frac{E_a}{R}\left(\frac{1}{T_k} - \frac{1}{198.15}\right)\right] \tag{10}$$

where k_{25} is the reaction rate constant at 25°C (4.30×10^{-14} mol $m^{-2}s^{-1}$), E_a is the activation energy (75.0 kJ/mol), A/V is the area over which the reaction occurs per unit volume of fluid (m^2/m^3), T_K is the temperature in Kelvin, R is the gas constant (8.31456 J/mol/K), Q is the activity of aqueous SiO_2, and K_s is the equilibrium constant for dissolution of quartz reaction.

Precipitation of SiO_2 was modelled after Carroll *et al.* (1998), who investigated amorphous silica precipitation behaviour in simple laboratory experiments and more complex field experiments in the Wairaki geothermal field, New Zealand. They found that in simple laboratory solution supersaturated with the absence of chemical impurities, precipitation rates have a first-order form:

$$k_{ppt} = k_{ppt} \exp\left[\frac{E_a}{RT}\left(1 - \frac{Q}{K_{eq}}\right)\right] \tag{11}$$

where k_{ppt} is a rate constant of precipitation, $10^{-1.9}$ mol m^{-2} s^{-1} and E_a is the activation energy, 61±1 kJ/mol.

All other kinetically controlled mineral reactions that were considered concerned the iron cycle, i.e., siderite ($FeCO_3$), amorphous iron hydroxide ($Fe(OH)_3$(a)), and FeS(ppt). The reaction rates $r_{Fe\text{-}min}$ were simulated according to

$$r_{Fe-\min} = k_{Fe-\min}\left(1 - SR_{Fe-\min}\right) \tag{12}$$

where, $k_{Fe\text{-}min}$ is a reaction rate constant and $SR_{Fe\text{-}min}$ is the saturation ratio of the iron mineral.

The comparison between non-reactive simulations and measured data also suggested that dissolved organic carbon (DOC) and phosphate (PO_4) concentrations were influenced by reactive processes. The simulations suggested that at least for PPT2 and PPT3 the mass of DOC that was extracted during the recovery phase was greater than the mass of injected DOC. This suggests mobilisation of sediment organic matter must have occurred, most likely as response to the alkaline conditions that were locally and temporally induced in the vicinity of the injection well during PPT2 and PPT3 (Bastow, pers. communication). The observed phosphate release may be directly associated with the DOC release.

Finally, surface complexation reactions were incorporated into the reaction network to consider sorption/desorption reactions onto mineral surfaces. The surface complexation model that was recently compiled for simulating the impact of temperature variations on arsenic transport during aquifer thermal energy storage (Bonte *et al.* 2013) was used as a basis for the simulations and further modified to the site-specific conditions at Condabri.

3.11.2 INITIAL AND BOUNDARY CONDITIONS

The measured ambient (pre-trial) groundwater composition was used to define the initial concentrations and the measured ionic composition was used to define the temporally varying concentrations in the injection well. The ranges of the employed concentration values for PPT1, PPT2 and PPT3 are listed in Table 3.1.

3.11.3 MODEL DEVELOPMENT AND CALIBRATION

The model development and calibration phase was aimed at establishing and parameterising a geochemically plausible model that reproduces the measured field data as close as possible. This was achieved by a successive adjustment of included model parameters and, where needed, adjustments of the conceptual model. In this process it was attempted to keep the model as close as possible to previously reported conceptual (sub-)models, while not unnecessarily increasing model complexity.

3.11.4 SIMULATED REACTIVE TRANSPORT BEHAVIOUR DURING PPT1-PPT3

The most plausible and calibrated reactive transport model replicates, with few exceptions, the majority of the observed data that were collected during the injections trials PPT1-PPT3. Figure 3.4 shows a comparison between simulated results and observations for all relevant major and minor groundwater constituents. The comparison shows that some discrepancies between simulated breakthrough behaviour and measured data exist for DOC, phosphate and silica. However, additional model simulations (not shown) suggest that the simulated arsenic transport behaviour had a very low sensitivity with respect to small changes in the simulated concentrations of DOC, phosphate and silica.

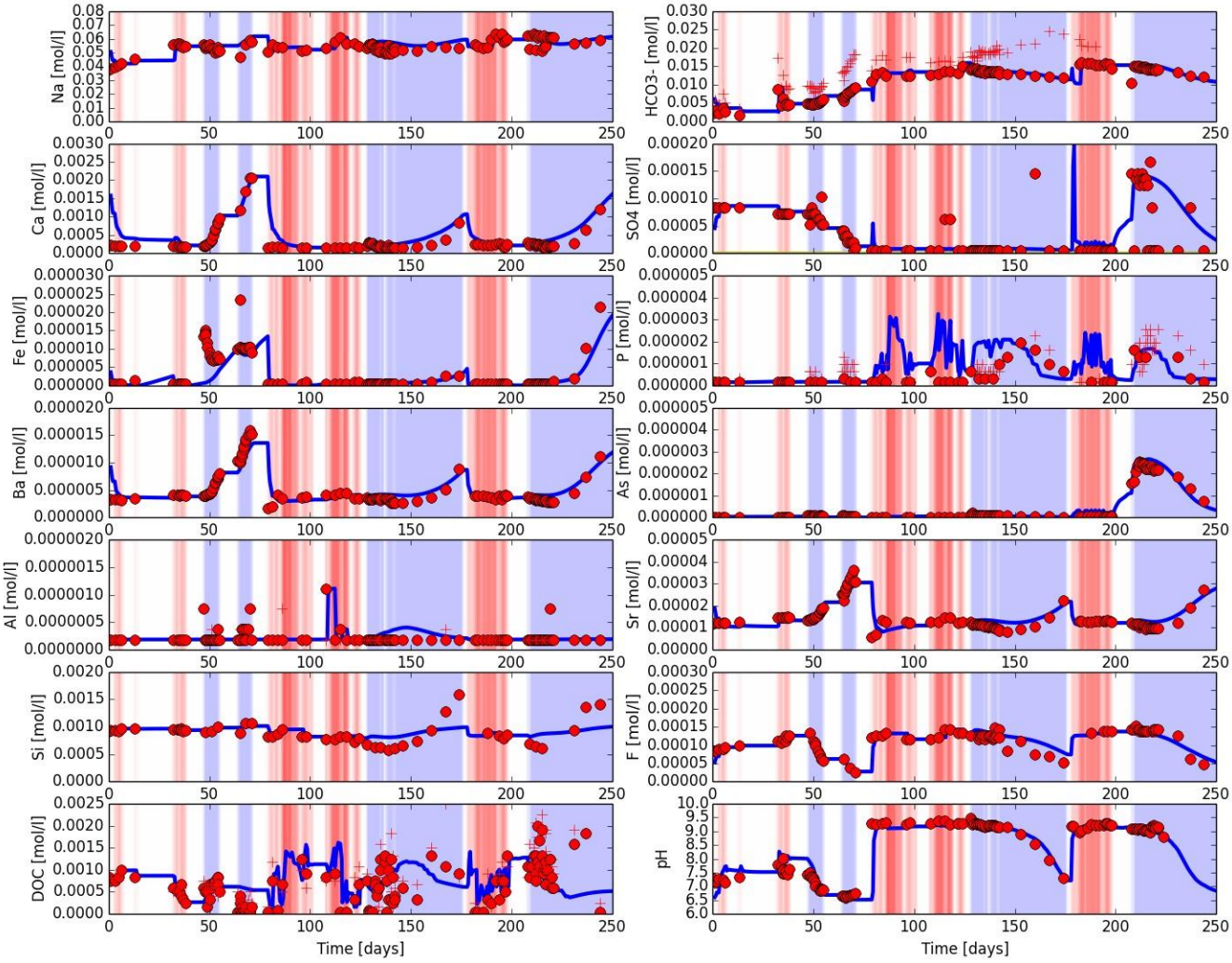

Figure 3.4: Comparison of selected simulated (solid blue lines) and observed concentrations (red circle symbols) for the simulation of the injection trials PPT1-PPT3 with the calibrated model. Note, that model results during the injection phase (red background) are taken from the first grid cell after the chemical reaction step and are therefore not directly comparable with the measured injectant composition (red '®' symbols) during the injection phases. Red '+' symbols represent measured DIC in addition to the measured alkalinity (red '®' symbols).

The most important insight of the model simulations for PPT1-PPT3 is that the high arsenic concentrations that were observed during PPT3 can be clearly attributed to the occurrence of pyrite oxidation and the associated release of

arsenic, which implies that the dissolved oxygen concentration in the injectant has a strong influence on the locations and rates at which geogenic arsenic might be released. While the models ability to reproduce the high arsenic concentrations that occurred during PPT3 has clearly shown to be important for accurately quantifying the release of arsenic as induced by an injectant containing dissolved oxygen, matching the lower observed arsenic concentrations during PPT1 and PPT2 under nominally oxygen free conditions was thought to hold the key for constraining the model parameters controlling arsenic sorption behaviour.

However, none of the simulations with models that attempted to ascribe arsenic mobilisation during PPT1 and PPT2 solely to desorption of arsenic from the aquifer matrix was able to even semi-quantitatively match the observations. Therefore other model variants that hypothesised that either (i) the injectant contained undetected low levels of oxidation capacity or (ii) that some (slow) dissolution of pyrite occurred in the absence of oxidants were also investigated. Under this assumption it was possible to approximately reproduce the observed arsenic concentrations for the recovery phases of PPT1 and PPT2, while at the same time also reproducing the observed concentrations of related species such as sulphate and iron.

4 Geochemical response to large-scale injection

The reactive models that were developed for the Reedy Creek and the Condabri injection trials, as described in the previous sections, were both used in predictive mode to assess the potential long-term geochemical changes and in particular to study the long-term fate of arsenic. The simulations were performed with a focus on (i) understanding the temporal and spatial evolution of dissolved arsenic concentrations and (ii) the impact of the injectant pre-treatment, including the impact of deoxygenation on the predicted arsenic concentrations.

Clearly, the predictions are subject to uncertainty due to a range of factors such as

- the physical heterogeneity within the Precipice Sandstone aquifer
- the limited understanding / data regarding the geochemical heterogeneity and to what extend the trial results can represent the larger-scale transport
- the limited identifiability (Doherty and Hunt 2009) of model parameters from single-well push-pull test

The model simulations were again performed for a radial-symmetric flow-field. This is a somewhat simplifying assumption as local heterogeneities will cause deviations from the idealised radial-symmetric conditions. However, given that the natural groundwater flow velocities are relatively slow in comparison with those generated by the injection and given that little information exists to consider aquifer heterogeneities the simplification to a radial-symmetric flow-field is also reasonable for the large-scale predictions.

4.1 Condabri

4.1.1 MODEL ASSUMPTIONS

For the predictive simulations all hydrogeological and geochemical parameters were generally left unchanged from those determined during the model calibration (see Section 3.11.3) and directly adopted form the model calibration phase. However, for the predictive simulations:

- the injection rate was increased to a constant rate of 3.0 ML/day over the entire simulation period of 10 years.
- the model dimension in radial direction was extended to 1000 m to accommodate for the larger transport distance over the 10 year duration
- the longitudinal dispersivity was increased from the calibrated value (1.5 m) to a slightly higher value of 4 m to account for the scale-dependency of longitudinal dispersion (Gelhar *et al.* 1992)

Predictive simulations were performed for 4 different types of injectant compositions:

- S1: An alkaline (pH = 9.15), anoxic injectant water composition, with concentrations set to those measured during PPT3, except for oxygen (here 0 mol/L), was assumed to be injected throughout the entire simulation period
- S2: As S1, but with 5×10^{-4} mol/L (8 mg/L) dissolved oxygen to represent conditions without deoxygenation
- S3: A more neutral, anoxic injectant water composition, with concentrations set to those measured during PPT1, except for sulphate (here 0 mol/L), was assumed to be injected throughout the entire simulation period
- S4: As S3 but with 5×10^{-4} mol/L (8 mg/L) dissolved oxygen

The water compositions that were employed as injectant composition in the four different scenarios are listed in Table 4.1.

Table 4.1: Initial and injectant concentrations assumed for the predictive simulations (in mol/L, except for pH and pe)

	AMBIENT	S1	S2	S3	S4
pH	6.50	9.15	9.15	7.89	7.89
pe	-5.06	12	12	12	12
Al	1.85×10^{-7}	1.85×10^{-7}	1.85×10^{-7}	1.85×10^{-7}	1.85×10^{-7}
As(+3)	6.67×10^{-9}	0.0	0.0	1.34×10^{-8}	1.34×10^{-8}
As(+5)	0.0	4.00×10^{-8}	4.00×10^{-8}	0.0	0.0
B	1.11×10^{-5}	5.55×10^{-5}	5.55×10^{-5}	4.81×10^{-5}	4.81×10^{-5}
Ba	1.57×10^{-5}	3.98×10^{-6}	3.98×10^{-6}	4.09×10^{-6}	4.09×10^{-6}
Br	5.66×10^{-5}	6.41×10^{-5}	6.41×10^{-5}	3.53×10^{-5}	3.53×10^{-5}
C(+4)	1.33×10^{-2}	1.22×10^{-2}	1.22×10^{-2}	4.59×10^{-3}	4.59×10^{-3}
C(-4)	1.61×10^{-2}	0.0	0.0	0.0	0.0
Ca	2.62×10^{-3}	2.50×10^{-4}	2.50×10^{-4}	1.75×10^{-4}	1.75×10^{-4}
Cd	0.0	0.0	0.0	0.0	0.0
Cl	4.70×10^{-2}	3.64×10^{-2}	3.64×10^{-2}	4.49×10^{-2}	4.49×10^{-2}
F	1.58×10^{-5}	1.37×10^{-4}	1.37×10^{-4}	1.05×10^{-4}	1.05×10^{-4}
Fe(+2)	5.93×10^{-6}	4.48×10^{-7}	4.48×10^{-7}	4.48×10^{-7}	4.48×10^{-7}
Fe(+3)	1.00×10^{-7}	0.0	0.0	1.00×10-5	1.00×10^{-5}
K	1.25×10^{-3}	2.56×10^{-4}	2.56×10^{-4}	2.81×10^{-4}	2.81×10^{-4}
Mg	5.76×10^{-4}	4.53×10^{-4}	4.53×10^{-4}	7.40×10^{-4}	7.40×10^{-4}
Mn(+2)	2.91×10^{-7}	9.10×10^{-9}	9.10×10^{-9}	1.82×10^{-8}	1.82×10^{-8}
Mn(+3)	0.0	0.0	0.0	0.0	0.0
N(+5)	0.0	3.57×10^{-7}	3.57×10^{-7}	3.57×10^{-7}	3.57×10^{-7}
N(+3)	0.0	0.0	0.0	0.0	0.0
N(0)	0.0	0.0	0.0	0.0	0.0
Amm	1.32×10^{-4}	3.57×10^{-7}	3.57×10^{-7}	2.86×10^{-6}	2.86×10^{-6}
Na	6.53×10^{-2}	5.96×10^{-2}	5.96×10^{-2}	5.66×10^{-2}	5.66×10^{-2}
O(0)	0.0	2.00×10^{-5}	5.00×10^{-4}	2.00×10^{-5}	5.00×10^{-4}
DOC	5.00×10^{-4}	1.33×10^{-3}	1.33×10^{-3}	5.00×10^{-4}	5.00×10^{-4}
P	1.61×10^{-7}	1.62×10^{-7}	1.62×10^{-7}	1.62×10^{-7}	1.62×10^{-7}
Pb		0.0	0.0	0.0	0.0
S(-2)	0.0	1.56×10^{-6}	1.56×10^{-6}	1.56×10^{-6}	1.56×10^{-6}
S(+6)	0.0	0.0	0.0	0.0	0.0
Si	1.01×10^{-3}	8.58×10^{-4}	8.58×10^{-4}	9.58×10^{-4}	9.58×10^{-4}
Sr	3.22×10^{-5}	1.27×10^{-5}	1.27×10^{-5}	1.47×10^{-5}	1.47×10^{-5}

4.1.2 PREDICTED LARGE-SCALE LONG-TERM TRANSPORT BEHAVIOUR

The predicted flow, heat and conservative solute transport of all considered cases was identical. The key results of these simulations are illustrated in Figure 4.1. The figure shows the profiles of simulated chloride concentration at selected times as a function of the radial distance, whereby chloride can be seen as a proxy for non-reactive solute transport behaviour. In addition the figure shows the simulated temperature profiles. Under the assumed radial-symmetric conditions the simulated concentration profiles indicate that the injectant plume reaches diameters of ~440m, ~800m and ~1500m after 1, 3 and 10 years simulation time, respectively. The simulated temperature fronts lag behind the conservative solute front and therefore the predicted diameters with cooler groundwater temperatures are ~80m, ~160m and ~300m respectively. Note, that these simulations neglect that in reality some heat is transferred from the underlying and overlying aquitards, thus the distance travelled by the heat front would be expected to be somewhat overestimated.

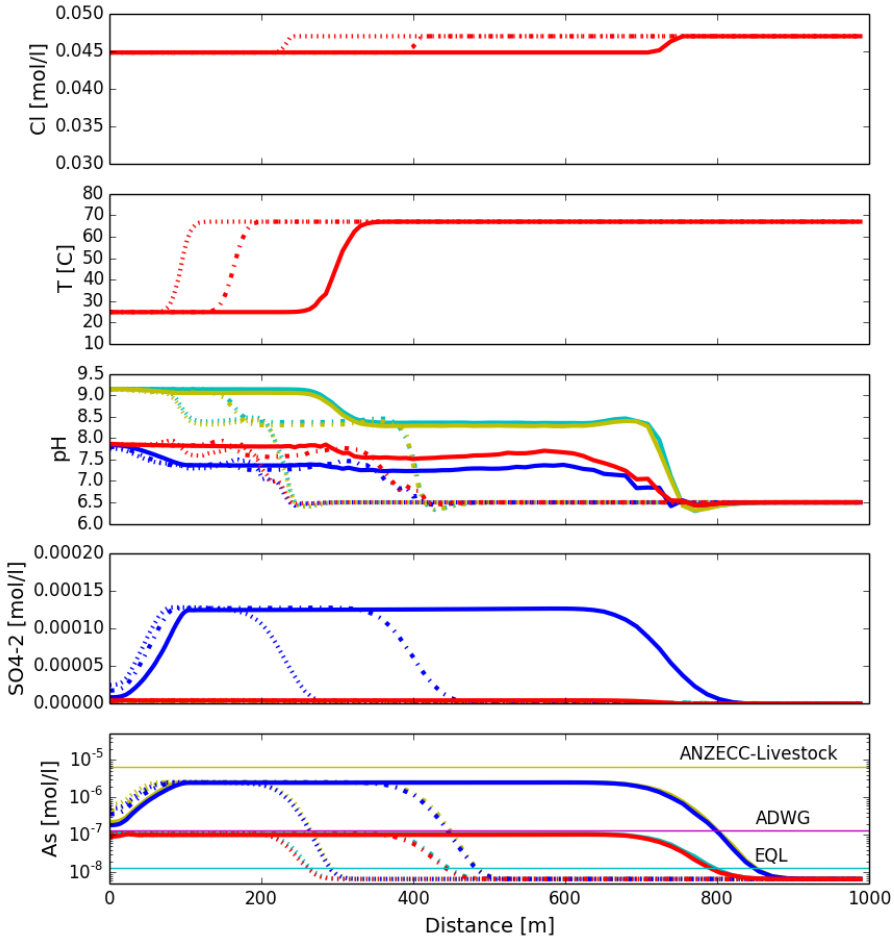

Figure 4.1: Evolution of selected groundwater quality parameters after 1 year (dotted lines), 3 years (dashed lines) and 10 years (solid lines) for continuous injection of 3ML/day. Simulation results for Cl- and temperature are similar for all 4 cases (S1-S4). Results for pH, sulphate and arsenic are shown for the considered cases S1 (cyan), S2 (yellow), S3 (red) and S4 (blue).

The simulation results for pH indicate that the pH front migrates at a similar rate as the injectant front. This is a result of the almost negligible pH buffering capacity that was identifiable during the model calibration. Figure 4.1 illustrates the migration of the pH front over time and some of the differences among the 4 simulation cases S1-S4. Figure 4.1 also illustrates the sulphate release that is induced by pyrite oxidation in cases S2 and S4, i.e., the two cases without active deoxygenation of the injectant. In the absence of sulphate reduction, which was assumed not to occur in the model, sulphate concentrations quickly stabilise at a constant concentration once the oxygen within the injectant is depleted. The bottom panel of Figure 4.1 shows the simulated arsenic concentrations. Corresponding to the postulated direct link with pyrite oxidation, predicted concentrations reach up to 2.5×10^{-6} mol/L (185 µg/L) in

cases S2 and S4, while persistently remaining below the ADWG limit of 10 µg/L in cases S1 and S3. In all cases the predicted concentrations are not effectively attenuated during transport away from the injection well. This is due to the essentially negligible impact of the considered arsenic sorption reactions (surface complexation reactions) relative to the magnitude of the As released.

4.2 Reedy Creek

4.2.1 INVESTIGATED SCENARIOS

Based on the additional insights gained from the Condabri injection trials a set of revised model scenarios was defined to predict the large-scale impact of reinjection at Reedy Creek. In terms of the assumed groundwater flow rates the scenarios were based on the historical and currently estimated injection rates for individual Reedy Creek injection wells, as provided by Origin. It was assumed that the total injection rate was equally distributed amongst ten of the eleven operational injection bores. The current estimates suggest a rapid initial increase in the injection rates with rates reaching their maximum between 2018 and 2025, before subsequently declining until the end of the simulation time in 2053 (see Figure 4.2). These estimated rates were incorporated into the previously constructed radial-symmetric flow model. For simplicity interactions between multiple wells were neglected. Hydraulic interactions between wells would impact the detailed injectant plume shape but are expected to have a minor impact on the size of the geochemically impacted zone. The transient flow model simulation served as a basis for the reactive transport simulations, which investigated a range of key scenarios. Different scenarios were simulated in order to illustrate the impact of injectant pre-treatment and to illustrate the impact of model uncertainties in the conceptual geochemical model on predicted results.

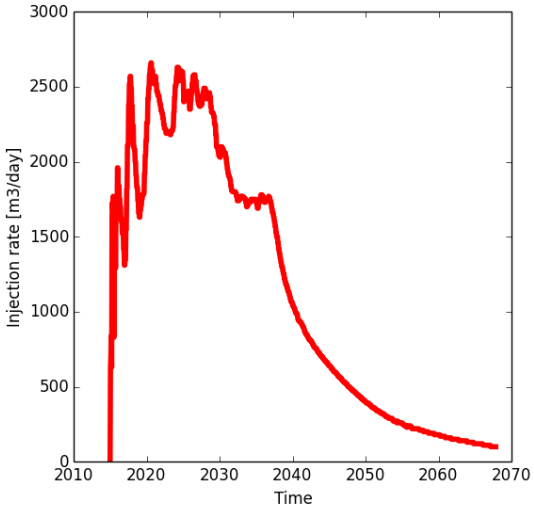

Figure 4.2: Anticipated Reedy Creek well injection rates 2016-2053, as applied in the radial-symmetric flow model.

Compared to the previously discussed observations and simulations for the Reedy Creek injection trial, the simulated injectant composition was adjusted to the actually measured injectant quality that is produced in the full-scale injection scheme. This injectant composition is far less alkaline (S1 in Table 4.3) than the injectant that was used during the injection trials (up to ~9.3). This is expected to have a beneficial effect for reducing the likelihood that arsenic is mobilised through desorption. Table 4.2 provides an overview of the key model scenarios for which results will be discussed in this document. Table 4.3 shows the ambient and injectant water compositions that were used in the predictive model simulations.

Table 4.2: Key model scenarios

SCENARIO	DESCRIPTION
S1	Base case. Simulation assuming that the injectant is effectively deoxygenated and pyrite oxidation in the target aquifer is omitted
S2	Similar to S1 but assuming that the injectant is not de-oxygenated (DO = 8mg/L)
S3	As S2, but assuming zero sorption capacity on freshly precipitated ferrihydrite
S4	As S2, without any sorption reactions
S5	As S2, with phosphate included in the injectant

Table 4.3: Initial (ambient) and injectant concentrations assumed for the predictive simulations (in mol/L, except for pH, pe and Temperature)

	AMBIENT	S1	S2, S3, S4	S5
pH	7.8	7.6	7.6	7.6
pe	-5.0	10.0	13	13
Temperature	62	18	18	18
O(0)	0	1.876×10^{-6}	5×10^{-4}	5×10^{-4}
N(5)	0	0	0	0
N(3)	0	0	0	0
N(0)	0	0	0	0
Amm	2.788×10^{-5}	0	0	0
Al	2.596×10^{-6}	0	0	0
As(3)	1.600×10^{-8}	0	0	0
As(5)	0	0	0	0
Ba	2.040×10^{-7}	0	0	0
Br	4.609×10^{-6}	5.884×10^{-6}	5.884×10^{-6}	5.884×10^{-6}
C(4)	2.584×10^{-3}	1.321×10^{-3}	1.321×10^{-3}	1.321×10^{-3}
Ca	1.248×10^{-5}	1.522×10^{-5}	1.522×10^{-5}	1.522×10^{-5}
Cl	2.709×10^{-3}	3.813×10^{-3}	3.813×10^{-3}	3.813×10^{-3}
Fe(2)	4.483×10^{-7}	0	0	0
Fe(3)	0	0	0	0
K	1.279×10^{-5}	0	0	0
Mg	1.235×10^{-4}	0	0	0
Na	4.927×10^{-3}	5.047×10^{-3}	5.047×10^{-3}	5.047×10^{-3}
Orgc	4.169×10^{-4}	0	0	0
P	2.584×10^{-6}	0	0	2.584×10^{-6}
S(6)	0	0	0	0
S(-2)	0	0	0	0
Si	5.330×10^{-4}	2.248×10^{-5}	2.248×10^{-5}	2.248×10^{-5}

4.2.2 PREDICTED FLOW AND PHYSICAL TRANSPORT BEHAVIOUR

The predicted flow, heat and conservative solute transport of all considered cases (S1-S5) is identical. All employed physical model parameters were adopted from the results of the earlier described model calibration, except for the value employed for longitudinal dispersivity (4 m), which was increased to account in a simplistic way for the scale-dependency of the dispersion process. The results of the heat transport simulations and other results are illustrated in Figure 4.3. It shows the simulated temperature profiles for model layer 15 for 3 different simulation times, i.e., after 1, 10 and 38 years. Results are displayed for this layer as the transport occurs faster than within other layers. For comparison the simulated temperatures are shown for the model that used the calibrated heat transport parameters (with sediment water injections, SWI) and for the case where heat transfer to the aquifer matrix and within the matrix was neglected (no SWI). Thus the no SWI case essentially represents conservative transport behaviour. The comparison among the two cases illustrates the strong retardation of the heat transport due to heat transfer (in this case a transfer of lower temperatures) from the aqueous phase towards the aquifer matrix. The "no SWI" case indicates that the injectant plume in layer 15 extends to ~400, ~1250 and ~1500m after 1, 10 and 38 years (2053, end of simulation time), respectively. The reason for the slow growth in temperature in the "no SWI" case over the last 28 years of the simulation period is two-fold. First, transport distance decreases due to the radial-symmetric flow field and secondly due to the successively decreasing flow rates (as indicated in Figure 4.2).

4.2.3 PREDICTED REACTIVE TRANSPORT BEHAVIOUR

Scenario S1 (Base case)

The simulation results for the base case (S1) pH (Figure 4.3) indicate that the injection causes only minor changes within the aquifer. However, the small pH increase that occurs in response to the injection migrates at a similar rate as the 'conservative' injectant front. This is a consequence of the almost negligible pH buffering capacity that was identifiable during the model calibration. It is, however, possible that the absence of identifiable buffering reactions stems from the relative short trial duration and that over the much longer prediction period some slower buffering reactions could still play a more pronounced role.

For this base case scenario (S1) the predicted arsenic concentrations remain clearly below the ADWG limit of 10 µg/L because both previously identified arsenic mobilisation mechanisms (alkaline conditions and pyrite oxidation) remain inactive. It should be noted that this model scenario represents the current reinjection configuration at the full-scale injection scheme at Reedy Creek. The results suggests therefore that arsenic concentrations may not be expected to increase as a result of the implemented reinjection scheme.

Scenario S2

The simulation for scenario S2 shows key differences in the simulated concentration profiles for pH, sulphate and arsenic (Figure 4.4). Sulphate concentrations are increased as a result of pyrite oxidation and a sulphate plume is growing successively. While iron is also released during pyrite oxidation it is largely re-precipitating as ferrihydrite. In the model it is assumed that the freshly precipitating ferrihydrite can serve as sorption surface.

The maximum sulphate concentration is limited by the stoichiometric relationship between the pyrite oxidation reaction and the oxygen concentration that is contained in the injectant. Compared to the simulated pH in scenario S1 (base case) the simulated pH in S2 is lowered due to the acidity produced by pyrite oxidation. In the model simulations little pH buffering occurs, as already discussed for S1, and therefore the zone in which the pH decreases to below 7 is successively growing.

The simulation results show a successively growing arsenic plume, with a maximum size of ~500 m reached at the end of the simulation and concentrations clearly exceeding the ADWG level of 10 µg/L but being well below the ANZECC-Livestock guidelines. However, the arsenic plume grows at a much slower rate than the injectant plume as a results of arsenic sorption to the two types of mineral surfaces that were considered in this model scenario. Note that the magnitude of the predicted concentrations depends strongly on the assumed stoichiometric ratio between As release and pyrite oxidation. For the present simulation the ratio (0.04) that was determined from the interpretation of the Condabri injection trial PPT3 was used.

Scenario S3

The simulation scenario S3 was performed to assess the importance of ferrihydrite on the attenuation of dissolved arsenic concentrations. To test the impact, this model variant excluded all surface complexation reactions with the ferrihydrite mineral surface while the sorption reactions to other surfaces remained active. However, as can be seen from the comparison of Figure 4.5 (S3 results) and Figure 4.4 (S2 results) there is no significant difference in the simulated arsenic concentration profiles. This implies that sorption to freshly precipitated ferrihydrite is expected to have a minor impact on the arsenic transport behaviour.

Scenario S4

Following from Scenario 3, all other surface complexation reactions were also excluded in the S4 model variant. The corresponding results are displayed in Figure 4.6. The results of S4 confirm that arsenic transport in S2 and S3 was strongly controlled by surface complexation (sorption) to the pre-existing sorption sites in the aquifer rather than surface complexation to the sorption sites provided by the newly precipitated ferrihydrite.

Scenario S5

In scenario S5 the impact of the dissolved phosphate concentration within the injectant was tested to make sure that the arsenic attenuation that occurred in S2 was not related to the fact that the simulated injectant composition did not include dissolved phosphate, which is a strong competitor for sorption sites. However the results (not shown) did not show any significant changes in the simulated concentration profiles.

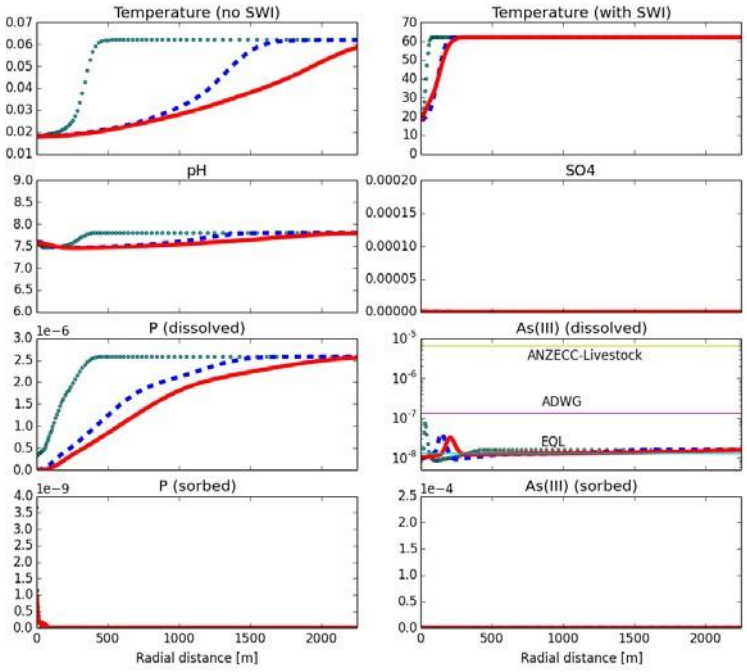

Figure 4.3: Evolution of selected groundwater quality parameters after 1 year (green lines), 10 years (dashed blue lines) and 38 years (solid red lines) for scenario S1 (Base case with deoxygenation). "No SWI" means "no sediment water interaction" and represents the hypothetical case that no heat adsorption by sediments occurs. Simulated temperatures are shown as ˚C Celcius.

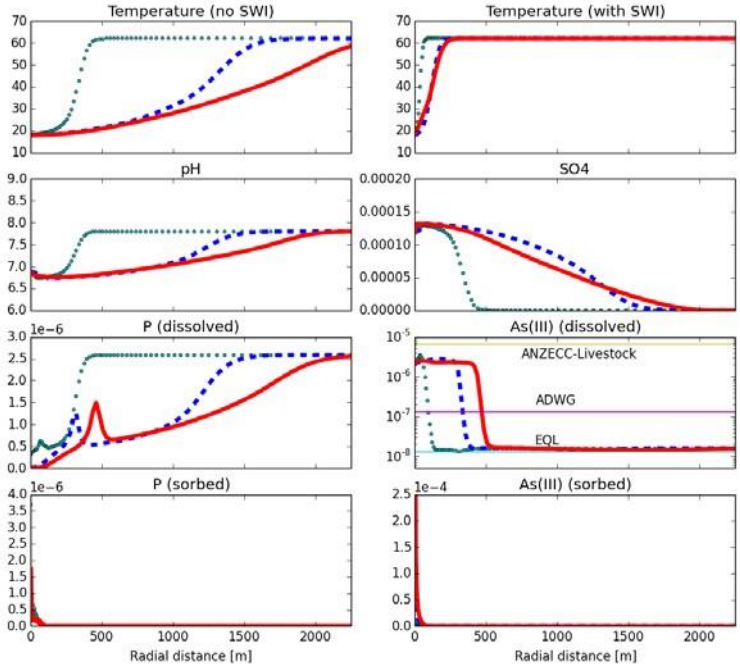

Figure 4.4: Evolution of selected groundwater quality parameters after 1 year (green lines), 10 years (dashed blue lines) and 38 years (solid red lines) for scenario S2. "No SWI" means "no sediment water interaction" and represents the hypothetical case that no heat adsorption by sediments occurs. Simulated temperatures are shown as ˚C Celcius.

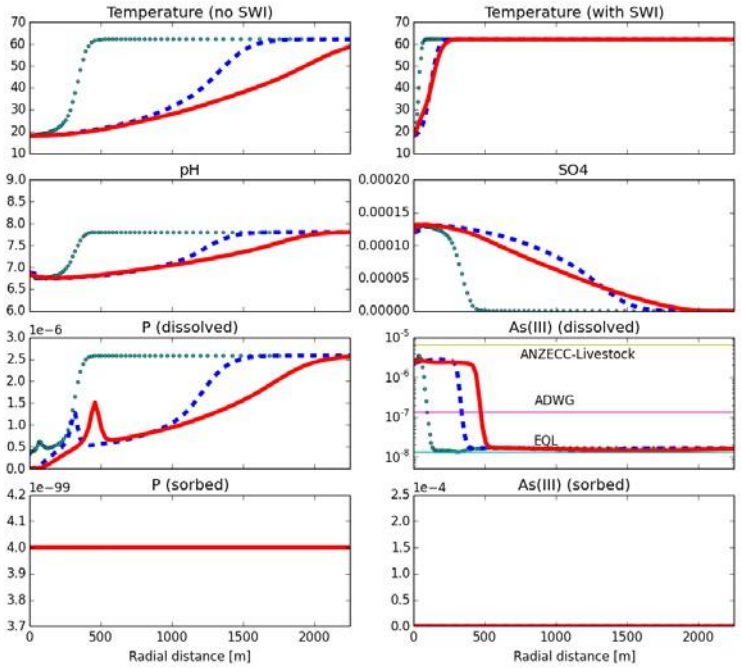

Figure 4.5: Evolution of selected groundwater quality parameters after 1 year (green lines), 10 years (dashed blue lines) and 38 years (solid red lines) for scenario S3. "No SWI" means "no sediment water interaction" and represents the hypothetical case that no heat adsorption by sediments occurs. Simulated temperatures are shown as ˚C Celcius.

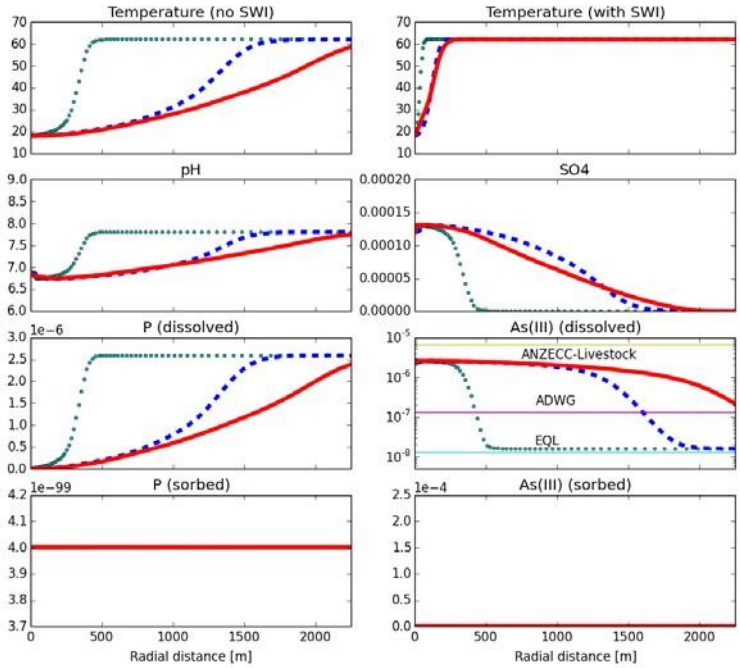

Figure 4.6: Evolution of selected groundwater quality parameters after 1 year (green lines), 10 years (dashed blue lines) and 38 years (solid red lines) for scenario S4. "No SWI" means "no sediment water interaction" and represents the hypothetical case that no heat adsorption by sediments occurs. Simulated temperatures are shown as ˚C Celcius.

5 Discussion

This study provides the first detailed data set and interpretation of the geochemical response to the injection of CSG product waters. Therefore the study provides important information for the planning of future injection schemes, particularly for schemes in the Precipice Sandstone aquifer. The study illustrates the importance of field-scale injection trials and the role of a model-based data interpretation in understanding and predicting potential water quality impacts.

5.1 Conclusions and recommendations

The results of this study suggest that the injection of large volumes of highly treated CSG product water will cause no foreseeable uncontrollable adverse impacts on groundwater quality. For the investigated sites the most critical problem for the proposed large-scale injection has shown to be the potential for arsenic mobilisation. However, from the combined experimental and numerical modelling work it can be concluded that the mobilisation of arsenic can largely be eliminated through a suitable pre-treatment of the injectant, most importantly through deoxygenation. Due to the relatively short times-scale of the injection trials and in the absence of monitoring wells it was not possible to uniquely identify the degree to which attenuation mechanisms would naturally reduce arsenic levels in case of their mobilisation near the injection wells. Future investigations might be able to clarify whether, for example, arsenic sorption would be sufficient to eliminate arsenic migration over longer travel distances even in cases where the injectant is not deoxygenated. Based on the current investigations deoxygenation of the injectant is recommended until the occurrence of arsenic attenuation mechanisms can be further verified.

To advance the knowledge gained in this study the following recommendations can be made:

- If technically feasible, the model predictions made for the Reedy Creek injection scheme, in particular the predicted absence of arsenic mobilisation, might be verified through groundwater sampling
- As an extension of the predictive scenarios regional-scale groundwater quality simulations could clarify the degree of arsenic attenuation that would occur through mixing and dilution alone. In case the predictions would show sufficient mixing/dilution deoxygenation of the injectant might not be required
- There is still some residual uncertainty on wether pyrite oxidation may have contributed to the occurrence of arsenic during the Reedy Creek injection trial that was performed with deoxygenated water. Future injection trials may include additional analytes (e.g., S-isotopes) to clarify this issue
- The results of the injection trial PPT3 at Condabri suggested that the observed DOC concentrations might be attributed to an in situ mobilisation by the injectant. In future trials the DOC, if occurring might be further characterised in order to better understand its origin and whether its presence could affect ionic mobility and/or the mobility of metal(loids)

Key recommendation from the study is that:

- The planning and implementation of large-scale reinjection schemes in aquifers that have not previously been investigated for their suitability as target aquifer require: (i) a detailed characterisation of the geochemical and mineralogical characteristics; and (ii) field trials such as push-pull test that provide sufficiently comprehensive data sets to underpin the development of conceptual and numerical models of the potential groundwater impacts.

References

Anderson, MP (2005) Heat as a Ground Water Tracer. *Ground Water* **43**, 951-968.

ANZECC, ARMCANZ, 2000. Australia and New Zealand Guidelines for Fresh and Marine Water Quality. Australian and New Zealand Environment and Conservation Council, Agriculture and Resource Management Council of Australia and New Zealand.

APLNG (2013b) Aquifer Injection Trial at Reedy Creek – Precipice Sandstone Technical Feasibility.

Appelo, CAJ, Vet, WWJM (2003) Modeling in situ iron removal from groundwater with trace elements such as As. In 'Arsenic in Ground Water: Geochemistry and Occurrence.' (Eds AH Welch, KG Stollenwerk.) pp. 381-401. (Springer US: Boston, MA)

Bonte, M, Röling, WFM, Zaura, E, van der Wielen, PWJJ, Stuyfzand, PJ, van Breukelen, BM (2013) Impacts of Shallow Geothermal Energy Production on Redox Processes and Microbial Communities. *Environmental Science & Technology* **47**, 14476-14484.

Bridger, DW, Allen, DM (2010) Heat transport simulations in a heterogeneous aquifer used for aquifer thermal energy storage (ATES). *Canadian Geotechnical Journal* **47**, 96-115.

Carroll, S, Mroczek, E, Alai, M, Ebert, M (1998) Amorphous silica precipitation (60 to 120°C): comparison of laboratory and field rates. *Geochimica Et Cosmochimica Acta* **62**, 1379-1396.

Descourvieres, C, Hartog, N, Patterson, BM, Oldham, C, Prommer, H (2010a) Geochemical controls on sediment reactivity and buffering processes in a heterogeneous aquifer. *Applied Geochemistry* **25**, 261-275.

Descourvières, C, Hartog, N, Patterson, BM, Oldham, C, Prommer, H (2010) Geochemical controls on sediment reactivity and buffering processes in a heterogeneous aquifer. *Applied Geochemistry* **25**, 261-275.

Descourvieres, C, Prommer, H, Oldham, C, Greskowiak, J, Hartog, N (2010b) Kinetic Reaction Modeling Framework for Identifying and Quantifying Reductant Reactivity in Heterogeneous Aquifer Sediments. *Environmental Science & Technology* **44**, 6698-6705.

Doherty, J, Hunt, RJ (2009) Two statistics for evaluating parameter identifiability and error reduction. *Journal of Hydrology* **366**, 119-127.

Duckworth, OW, Martin, ST (2004) Role of molecular oxygen in the dissolution of siderite and rhodochrosite. *Geochimica Et Cosmochimica Acta* **68**, 607-621.

Engelhardt, I, Prommer, H, Moore, C, Schulz, M, Schüth, C, Ternes, TA (2013) Suitability of temperature, hydraulic heads, and acesulfame to quantify wastewater-related fluxes in the hyporheic and riparian zone. *Water Resources Research* **49**, 426-440.

Feitz, AJ, Ransley, TR, Dunsmore, R, Kuske, TJ, Hodgkinson, J, Preda, M, Spulak, R, Dixon, O, Draper, J, 2014. Geoscience Australia and Geological Survey of Queensland Surat and Bowen Basins Groundwater Surveys Hydrochemistry Dataset (2009-2011). Canberra Australia.

Gelhar, LW, Welty, C, Rehfeldt, KR (1992) A critical review of data on field-scale dispersion in aquifers. *Water Resources Research* **28**, 1955-1974.

Harbaugh, AW (2005) MODFLOW-2005: the U.S. Geological Survey modular ground-water model - the ground-water flow process. *Book 6: Modeling techniques, Section A. Ground-water*

Hartog, N, Griffioen, J, Van der Weijden, CH (2002) Distribution and reactivity of O_2-reducing components in sediments from a layered aquifer. *Environmental Science & Technology* **36**, 2338-2344.

Jones, GW, Pichler, T (2007) Relationship between pyrite stability and arsenic mobility during aquifer storage and recovery in southwest central Florida. *Environmental Science & Technology* **41**, 723-730.

Ma, R, Zheng, C, Zachara, JM, Tonkin, M (2012) Utility of bromide and heat tracers for aquifer characterization affected by highly transient flow conditions. *Water Resources Research* **48**, n/a-n/a.

McNab, WW, Singleton, MJ, Moran, JE, Esser, BK (2009) Ion exchange and trace element surface complexation reactions associated with applied recharge of low-TDS water in the San Joaquin Valley, California. *Applied Geochemistry* **24**, 129-137.

Neil, CW, Yang, YJ, Jun, YS (2012) Arsenic mobilization and attenuation by mineral-water interactions: implications for managed aquifer recharge. *Journal of Environmental Monitoring* **14**, 1772-1788.

NHMRC–NRMMC, 2011. Australian Drinking Water Guidelines, NHMRC and NRMMC, Canberra. http://www.nhmrc.gov.au/_files_nhmrc/publications/attachments/eh52_aust_drinking_water_guidelines_update_120710_0.pdf.

OGIA (2016) Underground Water Impact Report for the Surat Cumulative Management Area. Department of Natural Resources and Mines.

Prommer, H, Barry, DA, Zheng, C (2003) MODFLOW/MT3DMS-Based Reactive Multicomponent Transport Modeling. *Ground Water* **41**, 247-257.

Prommer, H, Stuyfzand, PJ (2005) Identification of Temperature-Dependent Water Quality Changes during a Deep Well Injection Experiment in a Pyritic Aquifer. *Environmental Science & Technology* **39**, 2200-2209.

Rimstidt, JD, Barnes, HL (1980) The kinetics of silica-water reactions. *Geochimica Et Cosmochimica Acta* **44**, 1683-1699.

Seibert, S, Prommer, H, Siade, A, Harris, B, Trefry, M, Martin, M (2014) Heat and mass transport during a groundwater replenishment trial in a highly heterogeneous aquifer. *Water Resources Research* **50**, 9463-9483.

Stollenwerk, KG, Breit, GN, Welch, AH, Yount, JC, Whitney, JW, Foster, AL, Uddin, MN, Majumder, RK, Ahmed, N (2007) Arsenic attenuation by oxidized aquifer sediments in Bangladesh. *Science of the Total Environment* **379**, 133-150.

Thorne, D, Langevin, CD, Sukop, MC (2006) Addition of simultaneous heat and solute transport and variable fluid viscosity to SEAWAT. *Computers & Geosciences* **32**, 1758-1768.

Vanderzalm, JL, Dillon, PJ, Barry, KE, Miotlinski, K, Kirby, JK, La Salle, CL (2011) Arsenic mobility and impact on recovered water quality during aquifer storage and recovery using reclaimed water in a carbonate aquifer. *Applied Geochemistry* **26**, 1946-1955.

Wallis, I, Moore, C, Post, V, Wolf, L, Martens, E, Prommer, H (2014) Using predictive uncertainty analysis to optimise tracer test design and data acquisition. *Journal of Hydrology* **515**, 191-204.

Wallis, I, Prommer, H, Pichler, T, Post, V, B. Norton, S, Annable, MD, Simmons, CT (2011) Process-Based Reactive Transport Model To Quantify Arsenic Mobility during Aquifer Storage and Recovery of Potable Water. *Environmental Science & Technology* **45**, 6924-6931.

Wallis, I, Prommer, H, Simmons, CT, Post, V, Stuyfzand, PJ (2010) Evaluation of Conceptual and Numerical Models for Arsenic Mobilization and Attenuation during Managed Aquifer Recharge. *Environmental Science & Technology* **44**, 5035-5041.

Wendling, L, Prommer, H, Patterson, B (2013) Understanding and quantifying the geochemical responses to reinjection of CSG water permeates, brines and blends. Task 2: Assessment of mineralogical and other geochemical characterization and analytical data collected by APLNG from core samples. No. GISERA Report Number W1 1114.

Zheng, C, Wang, PP (1999) 'MT3DMS v5.3 - A modular three - dimensional multispecies transport model for simulation of advection, dispersion and chemical reactions of contaminants in groundwater systems. Documentation and User's Guide. Prepared for the U.S. Army Corps of Engineers.' Department of Geological Sciences, Tuscaloosa, AL)

Appendix A Assessment of mineralogical and other geochemical characterization and analytical data collected by APLNG from core samples

Gas Industry Social & Environmental Research Alliance

Understanding and quantifying the geochemical response to reinjection of CSG water permeates, brines and blends

GISERA Project Number W1 1114

Laura Wendling, Henning Prommer, Bradley Patterson

February 2013

Task 2: Assessment of mineralogical and other geochemical characterization and analytical data collected by APLNG from core samples

A.1 Background

Analysis of the mineralogy and geochemistry of core samples from aquifers with potential to receive treated coal seam gas (CSG) waters was undertaken to facilitate assessment of potential (bio)geochemical interactions between aquifer materials and injected waters, and inform future monitoring and sampling schemes associated with aquifer recharge activities. The objective of this assessment was to investigate the potential for mineral precipitation (clogging) and the likelihood of trace/toxic element mobilisation following injection of CSG waters based on mineralogical and geochemical examination of aquifer materials.

A.2 Mineralogical and Geochemical Analysis of Core Samples

Mineralogical and geochemical analyses of Condabri MB1-G, Talinga MB3-H, Reedy Creek MB3-H, Reedy Creek MB1-G, Talinga MB9-G and Condabri MB9-H core samples were performed by Weatherford Laboratories (Australia) Pty Ltd (Weatherford Laboratories, 2011a, 2011b, 2011c, 2011d, 2012, 2013). Details of core samples analysed are given in Apx Table A.1. In brief, rock samples provided to Weatherford Laboratories by Origin Energy were finely ground using a tungsten carbide ring mill. Representative sub-samples of ground rock samples were analysed by powder X-ray diffraction (XRD) using a Philips PW-1830 diffractometer with Cu-Kα radiation and mineral phases were identified using the ICDD Powder Diffraction Database. Quantitative analyses of crystalline mineral phases in each sub-sample were performed using Siroquant™ interpretation software (Taylor, 1991). Additional sub-samples of each ground rock sample were fused with lithium metaborate and cast into a disc (Norrish and Hutton, 1969). Fused discs were analysed for major elements by X-ray fluorescence (XRF) spectrometry using a Philips PW 2400 spectrometer and SuperQ software (PANanytical B.V., Almelo, The Netherlands). The results were expressed as percentages of major element oxides. Trace element (mg/kg) analyses of powdered rock sub-samples were performed using a Philips PW2400 spectrometer XRF system and Pro-Trace interpretation software (PANanytical B.V., Almelo, The

Netherlands). International coal and mineral standards were used to calibrate XRD and XRF systems prior to analyses.

Apx Table A.1: Description of Talinga MB9-G, Reedy Creek MB1-G, Condabri MB1-G, Talinga MB3-H, Reedy Creek MB3-H, and Condabri MB9-H cores sub-sampled and subjected to mineralogical and geochemical analyses (from Weatherford Laboratories, 2011a, 2011b, 2011c, 2011d, 2012, 2013).

Core	Sample	Depth (m)	Length (m)	Formation	Description
Reedy Creek MB1-G	001	200.85-201.18	0.33	Gubberamunda	-
Reedy Creek MB1-G	002	216.19-216.31	0.12	Gubberamunda	-
Condabri MB1-G	#1	376.49-376.59	0.10	Gubberamunda	-
Condabri MB1-G	#2	381.43-381.60	0.17	Gubberamunda	-
Condabri MB1-G	#3	381.69-381.80	0.11	Gubberamunda	-
Condabri MB1-G	#4	394.10-394.59	0.49	Gubberamunda	-
Condabri MB1-G	#5	402.67-402.86	0.19	Gubberamunda	-
Talinga MB3-H	003	673.00-673.58	0.58	Hutton	Coarse-grained sandstone
Talinga MB3-H	013	703.37-703.88	0.51	Hutton	Medium- to coarse-grained sandstone
Talinga MB3-H	019	732.04-732.64	0.60	Hutton	Interbedded fine sandstone / siltstone
Talinga MB3-H	022	743.61-744.16	0.55	Hutton	Coarse sandstone / conglomerate
Talinga MB3-H	028	766.27-766.74	0.47	Hutton	Fine-grained sandstone, carbonaceous laminae
Talinga MB3-H	034	794.40-794.92	0.52	Hutton	Fine-grained sandstone, carbonaceous siltstone clasts
Talinga MB3-H	043	837.48-838.00	0.52	Hutton	Siltstone, fissile
Talinga MB3-H	052	873.66-874.12	0.46	Hutton	Fine- to medium-grained sandstone
Talinga MB3-H	055	884.02-884.52	0.50	Hutton	Fine-grained sandstone
Talinga MB3-H	060	910.74-911.32	0.58	Hutton	Interbedded fine-grained sandstone / siltstone (20%)
Talinga MB3-H	066	928.91-929.39	0.48	Hutton	Fine- to medium-grained sandstone with coal
Talinga MB3-H	069	937.11-937.66	0.55	Hutton	Medium-grained sandstone
Reedy Creek MB3-H	007-S	842.35-842.85	0.50	Hutton	Medium gravel
Reedy Creek MB3-H	003-S	853.45-853.95	0.50	Hutton	Wood and coal fragments
Reedy Creek MB3-H	006-S	857.64-858.14	0.50	Hutton	Coal fragments
Reedy Creek MB3-H	013-S	891.00-891.49	0.49	Hutton	Medium-grained sandstone
Reedy Creek MB3-H	019-S	920.97-921.52	0.55	Hutton	Sandstone, massive
Reedy Creek MB3-H	022-S	930.84-931.35	0.51	Hutton	Sandstone, massive
Reedy Creek MB3-H	028-S	977.90-978.40	0.50	Hutton	Fine-grained sandstone
Reedy Creek MB3-H	031-S	994.90-995.39	0.49	Hutton	Medium-grained sandstone
Reedy Creek MB3-H	034-S	1011.11-1011.62	0.51	Hutton	Fine- to medium-grained sandstone
Reedy Creek MB3-H	037-S	1024.93-1025.42	0.49	Hutton	Fine- to medium-grained sandstone

Reedy Creek MB3-H	042-S	1061.16-1061.72	0.56	Hutton	Fine- to medium-grained sandstone
Reedy Creek MB3-H	048-S	1094.85-1095.35	0.50	Hutton	Siltstone, siltstone laminae
Reedy Creek MB3-H	051-S	1102.77-1103.27	0.50	Hutton	Fine- to medium-grained sandstone
Reedy Creek MB3-H	057-S	1147.50-1148.00	0.50	Hutton	Fine- to medium-grained sandstone
Reedy Creek MB3-H	060-S	1232.40-1232.70	0.30	Hutton	Very fine- to fine-grained sandstone
Reedy Creek MB3-H	063-S	1250.87-1251.25	0.38	Hutton	Fine- to medium-grained sandstone, carbonaceous
Reedy Creek MB3-H	1	1300.87-1301.00	0.13	Precipice Sst	Medium- to coarse-grained sandstone, high porosity
Reedy Creek MB3-H	2	1303.19-1303.40	0.21	Precipice Sst	Medium- to coarse-grained sandstone, high porosity
Reedy Creek MB3-H	066-S	1303.58-1304.06	0.48	Precipice Sst	Coarse-grained sandstone, coal seam at 1304.04
Reedy Creek MB3-H	3	1307.29-1307.46	0.17	Precipice Sst	Fine-grained sandstone, low porosity
Reedy Creek MB3-H	069-S	1311.10-1311.63	0.53	Precipice Sst	Coarse-grained sandstone, high porosity
Reedy Creek MB3-H	4	1315.08-1315.20	0.12	Precipice Sst	Medium- to coarse-grained sandstone, high porosity
Reedy Creek MB3-H	072-S	1317.72-1318.22	0.50	Precipice Sst	Coarse-grained sandstone, high porosity
Reedy Creek MB3-H	5	1322.23-1322.43	0.20	Precipice Sst	Fine- to medium-grained sandstone, deformed wispy black laminate
Reedy Creek MB3-H	6	1325.87-1326.00	0.13	Precipice Sst	Fine- to medium-grained sandstone, 1-3 mm grey/black horizontal to subhorizontal laminations every 2-10 mm
Reedy Creek MB3-H	7	1329.55-1329.73	0.18	Precipice BSF	Fine- to medium-grained sandstone, 1-3 mm grey/black horizontal to subhorizontal laminations every 2-10 mm
Reedy Creek MB3-H	8	1333.00-1333.20	0.20	Precipice BSF	Medium- to coarse grained sandstone, medium/high strength, moderate to well-cemented, 5-10% fine gravel
Reedy Creek MB3-H	9	1335.00-1335.16	0.16	Precipice BSF	Medium- to coarse grained sandstone, medium/high strength, moderate to well-cemented, 5-10% fine gravel
Reedy Creek MB3-H	10	1336.90-1337.04	0.14	Precipice BSF	Medium- to coarse grained sandstone, medium/high strength, moderately to well-cemented, 5-10% fine gravel, high porosity
Reedy Creek MB3-H	11	1337.76-1338.00	0.24	Precipice BSF	Shale

Reedy Creek MB3-H	12	1343.00-1343.35	0.35	Precipice BSF	Medium-to coarse-grained sandstone, 10% fine gravel, high strength, high porosity, moderately to well-cemented
Reedy Creek MB3-H	13	1344.48-1344.65	0.17	Precipice BSF	Medium-to coarse-grained sandstone, 10% fine gravel, high strength, high porosity, moderately to well-cemented
Reedy Creek MB3-H	14	1346.68-1346.80	0.12	Precipice BSF	Medium-to coarse-grained sandstone, 10% fine gravel, high strength, high porosity, moderately to well-cemented
Reedy Creek MB3-H	15	1348.03-1348.20	0.17	Precipice BSF	Medium-to coarse-grained sandstone, 10% fine gravel, high strength, high porosity, moderately to well-cemented
Reedy Creek MB3-H	078-S	1349.37-1349.87	0.50	Precipice BSF	Coarse-grained sandstone
Talinga MB9-G	US#10	62.28-62.70	0.42	Gubberamunda	Medium-grained sandstone, low-medium strength
Talinga MB9-G	US#11	64.70-64.93	0.23	Gubberamunda	Medium- to coarse-grained sandstone, medium strength
Talinga MB9-G	US#12	77.30-77.65	0.35	Gubberamunda	Coarse-grained sandstone, low-medium strength
Talinga MB9-G	US#13	75.95-76.28	0.33	Gubberamunda	Coarse-grained sandstone, high strength
Talinga MB9-G	US#14	77.93-78.43	0.50	Gubberamunda	Coarse-grained sandstone / fine gravel, medium-high strength
Condabri MB9-H	3	1051.95-1052.45	0.50	Hutton	Coarse sandstone, well cemented
Condabri MB9-H	9	1093.70-1094.06	0.36	Hutton	Coarse sandstone
Condabri MB9-H	12	1106.80-1107.30	0.50	Hutton	Medium-grained sandstone
Condabri MB9-H	24	1161.53-1161.83	0.30	Hutton	Coarse sandstone / conglomerate
Condabri MB9-H	27	1170.87-1171.17	0.30	Hutton	Coarse sandstone / conglomerate
Condabri MB9-H	36	1198.86-1199.36	0.50	Hutton	Fine-grained sandstone
Condabri MB9-H	39	1210.76-1211.26	0.50	Hutton	Interbedded fine sandstone / siltstone
Condabri MB9-H	58	1247.42-1247.95	0.53	Hutton	
Condabri MB9-H	51	1284.85-1285.35	0.50	Hutton	Fine- to medium-grained sandstone
Condabri MB9-H	54	1289.28-1289.78	0.50	Hutton	Fine- to medium-grained sandstone
Condabri MB9-H	59	1291.35-1291.85	0.50	Hutton	Coarse sandstone
Condabri MB9-H	42	1294.71-1295.04	0.33	Hutton	Interbedded fine sandstone / siltstone
Condabri MB9-H	57	1294.92-1295.42	0.50	Hutton	Coarse sandstone, well cemented
Condabri MB9-H	65	1460.40-1460.90	0.50	Precipice Sst	Fine-grained sandstone
Condabri MB9-H	82	1475.74-1476.25	0.55	Precipice Sst	Fine-grained sandstone
Condabri MB9-H	68	1489.62-1490.18	0.56	Precipice BSF	Medium-grained sandstone
Condabri MB9-H	73	1499.75-1500.32	0.57	Precipice BSF	Medium-grained sandstone

Condabri MB9-H	83	1512.87-1513.41	0.54	Precipice BSF	Medium-grained sandstone
Condabri MB9-H	78	1537.92-1538.43	0.51	Precipice BSF	Fine-grained sandstone
Condabri MB9-H	81	1545.42-1545.97	0.55	Precipice BSF	-

A.2.1 CORE SAMPLE MINERALOGY

Table 2 through Table 4 list the percentages of the minerals identified in Reedy Creek MB1-G, Condabri MB1-G, Talinga MB3-H, Reedy Creek MB3-H, Talinga MB9-G and Condabri MB9-H samples from the respective Siroquant interpretations. Additional data, including the relative error in the estimated weight percentages of individual mineral phases (estimated standard deviation) for each sample are given in the respective analytical reports from Weatherford Laboratories (Weatherford Laboratories, 2011a, 2011b, 2011c, 2011d, 2012).

In general, quartz (SiO_2) was the dominant mineral in all core samples examined with substantial proportions of kaolinite ($Al_4Si_4O_{10}(OH)_8$), illite ($K_{1.0\text{-}1.5}Al_4(Si,Al)_8O_{20}(OH)_4$) and/or mixed layers of illite and smectite ($M^+_{0.7}(Y^{3+},Y^{2+})_{4\text{-}6}(Si,Al)_8O_{20}(OH)_4nH_2O$) (Table 2 – Table 4) Kaolinite in the sandstone samples is likely due to dissolution of feldspar and mica minerals during sandstone diagenesis and subsequent re-precipitation of Si and Al as kaolinite. Most samples also contained minor quantities of feldspar minerals. For Reedy Creek MB1-G, Talinga MB3-H, Reedy Creek MB3-H, Talinga MB9-G and Condarbi MB9-H core samples albite ($NaAlSi_3O_8$) was used to represent plagioclase feldspar and orthoclase ($KAlSi_3O_8$) selected to represent K-feldspar. Mixtures of plagioclase and orthoclase feldspar minerals including a wider range of minerals were likely present in each sample. Plagioclase feldspar in some Condabri MB1-G samples was reported as albite, whilst in some samples plagioclase feldspar was identified as anorthite ($CaAlSi_2O_8$) and in others as both albite and anorthite. A range of feldspar minerals is likely present, some of which have structures closer to that of albite and some with structures closer to anorthite (Ward et al., 1999).

Reedy Creek MB1-G, Condabri MB1-G, Talinga MB9-G core samples are from different locations within the Gubberamunda Sandstone formation. The Gubberamunda sandstone formation, an Upper Jurassic lithographic sequence, was deposited by braided and meandering freshwater stream systems and is largely comprised of sandstone with some siltstone and conglomerate. Petrographic investigation has shown that Gubberamunda sandstone contains approximately 50% quartz and feldspar is predominant; Gubberamunda sandstone is primarily comprised of quartz, feldspar and fragments of siltstone, shale, and quartzite, with trace muscovite, biotite, iron oxide, and garnet (Exon, 1972). In this study, quartz, feldspar, and clay minerals were identified in Reedy Creek MB1-G, Condabri MB1-G, Talinga MB9-G core samples from different locations within the Gubberamunda Sandstone formation, along with varying quantities of carbonate minerals (e.g. calcite, dolomite, siderite, ankerite) (Table 2, Table 4).

Quantitative XRD examination showed that in the uppermost Talinga MB9-G core samples (e.g. 62-65 m), quartz, smectite and feldspar minerals were co-dominant along with major kaolinite. Both the total clay (kaolinite, illite and smectite) and feldspar mineral content decreased with depth in the Talinga MB9-G core samples (ca. 62-78 m), whilst the relative proportion of quartz concomitantly increased. The Reedy Creek MB1-G core samples were dominated by quartz, with the core sample at approximately 216 m (no. 002) exhibiting substantial calcite ($CaCO_3$) content. The Condabri MB1-G core (*ca.* 201-403 m) exhibited increasing total clay mineral content with depth. Talinga MB9-G and Condabri MB1-G core samples contained transient minor siderite ($FeCO_3$) whereas the Reedy Creek MB1-G core samples contained calcite and dolomite ($CaMg(CO_3)_2$).

The Talinga MB3-H core samples and upper core samples from Reedy Creek MB3-H and Condabri MB9-H (Table 2 - Table 4) were taken from different locations within the Hutton sandstone formation. Hutton sandstone, in the Lower Jurassic lithographic sequence, is mainly comprised of quartz with some fragments of metamorphic and volcanic rocks and feldspar and chlorite ($(Mg,Fe)_3(Si,Al)_4O_{10}(OH)_2\cdot(Mg,Fe)_3(OH)_6$) is common in some areas (Exon, 1976). Whilst calcite cements are relatively common in sub-surface Hutton sandstone, and although kaolinite partially fills some pores, the sandstone itself is generally porous (Exon, 1976). The mineralogical composition of Hutton sandstone varies considerably within the formation (Houston, 1972).

Apx Table A.2: Mineralogical composition (wt. %) of Reedy Creek MB1-G (RC), Condabri MB1-G (C) and Talinga MB3-H (T) core sub-samples in order of increasing depth.

	Mean depth (mBGL)	Quartz SiO_2	Kaolinite $Al_4Si_4O_{10}(OH)_8$	Illite $K_{1.0\text{-}1.5}Al_4(Si,Al)_8O_{20}(OH)_4$	Smectite $M^+_{0.7}(Y^{3+},Y^{2+})_{4\text{-}6}(Si,Al)_8O_{20}(OH)_4nH_2O$	Illite/smectite	Illite + illite/smectite	Plagioclase feldspar (albite)$NaAlSi_3O_8$	Plagioclase feldspar (anorthite)$CaAlSi_2O_8$	Orthoclase feldspar (microcline) $KAlSi_3O_8$	Calcite $CaCO_3$	Dolomite $Ca,Mg(CO_3)_2$	Siderite $FeCO_3$	Anatase TiO_2	Rutile TiO_2	Apatite $Ca_5(PO_4)_3(OH,F,Cl)$	Chlorite $(Mg,Fe)_3(Si,Al)_4O_{10}(OH)_2\cdot(Mg,Fe)_3(OH)_6$	Ankerite $Ca(Fe,Mg,Mn)(CO_3)_2$	Total
RC001	201.02	44.2	7.4				2.7	8.0		11.6	26.1								100.0
RC002	216.25	73.8	6.3	0.5				4.1		12.2		3.1							100.0
C#1	376.54	63.7	14.4			7.2			9.3	5.4									100.0
C#2	381.52	85.4	7.0			1.8		1.7		4.0									99.9
C#3	381.75	60.5	11.7						7.3	4.6			15.9						100.0
C#4	394.35	51.5	19.5	1.6		4.7		5.6	11.6	2.4			3.2						100.1
C#5	402.77	24.8	19.0	12.5		23.8		5.3	5.8	4.8			4.1						100.1
T003	673.29	93.9	3.3					2.8											100.0
T013	703.63	76.5	10.5	2.1				4.0		6.9									100.0
T019	732.34	22.2	23.0				27.4	5.6		0.5			20.2	1.1					100.0
T022	743.89	83.1	10.3	4.1				2.5											100.0
T028	766.51	60.2	12.2				11.8	7.8		7.6				0.4					100.0
T034	794.66	68.9	7.2	4.0				12.3		7.6									100.0
T043	837.74	21.0	30.4				40.8	6.0		0.1			1.1	0.5					99.9
T052	873.89	68.5	10.5				9.0	5.8		5.8				0.5					100.1
T055	884.27	64.4	12.4				11.3	7.0		4.9									100.0
T060	911.03	35.5	26.8	7.9		16.9		8.7		4.2									100.0
T066	929.15	45.2	10.6	3.2		13.9		12.9		1.6	12.7								100.1
T069	937.39	63.8	16.3	4.6				12.6									2.7		100.0

Apx Table A.3: Mineralogical composition (wt. %) of Reedy Creek MB3-H core sub-samples in order of increasing depth.

	Mean depth (mBGL)	Quartz SiO_2	Kaolinite $Al_4Si_4O_{10}(OH)_8$	Illite $K_{1.0\text{-}1.5}Al_4(Si,Al)_8O_{20}(OH)_4$	Smectite $M^+_{0.7}(Y^{3+}, Y^{2+})_{4\text{-}6}(Si,Al)_8O_{20}(OH)_4nH_2O$	Illite/smectite	Illite + illite/smectite	Plagioclase feldspar (albite)$NaAlSi_3O_8$	Plagioclase feldspar (anorthite)$CaAlSi_2O_8$	Orthoclase feldspar (microcline)$KAlSi_3O_8$	Calcite $CaCO_3$	Dolomite $Ca,Mg(CO_3)_2$	Siderite $FeCO_3$	Anatase TiO_2	Rutile TiO_2	Apatite $Ca_5(PO_4)_3(OH,F,Cl)$	Chlorite $(Mg,Fe)_3(Si,Al)_4O_{10}(OH)_2\cdot$	Ankerite $Ca(Fe,Mg,Mn)(CO_3)_2$	Total
007-S	842.6	59.8	21.4	2.9		1.7		9.4		4.8									100.0
003-S	853.7	36.8	12.7	4.4		9.8		15.0		3.7	0.2		17.3						99.9
006-S	857.9	25.6	5.3	9.8		29.0		28.5		1.6	0.2								100.0
013-S	891.2	52.3	16.2	8.0		6.2		13.4		3.9									100.0
019-S	921.2	72.7	10.9	5.5		2.7		8.2											100.0
022-S	931.1	62.4	14.0	6.4		4.3		7.4		3.5	2.0								100.0
028-S	978.2	54.5	18.6	11.5		0.6		9.6		5.0									99.8
031-S	995.1	66.6	14.3	6.2				8.6		4.2									99.9
034-S	1011.4	72.3	9.8	6.6		0.9		10.4											100.0
037-S	1025.2	74.2	7.3	5.4		0.2		12.6		0.2									99.9
042-S	1061.4	56.9	12.0	8.2		1.6		16.4		4.9									100.0
048-S	1095.1	60.0	10.0	7.5		1.2		16.1		5.2									100.0
051-S	1103.0	60.7	9.3	8.1		1.1		16.8		3.4	0.5								99.9
057-S	1147.8	71.1	11.5	7.1				10.3											100.0
060-S	1232.6	25.8	7.3	6.9		36.3		19.0		4.6	0.2								100.1
063-S	1251.1	41.3	7.4	5.4		34.7		10.9		0.2	0.1								100.0
1	1300.9	68.5	18.4	1.4						9.5			1.2	1.0					100.0
2	1303.3	77.1	12.1	0.8						8.3			1.3	0.4					100.0
066-S	1303.8	71.3	10.3			1.0		1.1		4.7	11.3		0.4						100.1
3	1307.4	63.4	4.4	0.7						5.4	25.6			0.5					100.0
069-S	1311.4	61.1	17.1	4.7		4.2		1.5		7.3	0.3		3.9						100.1

4	1315.1	68.9	15.1	2.5		2.2				8.3			1.9	1.1				100.0
072-S	1318.0	74.3	15.1	2.7		1.4		0.5		4.2			1.7					99.9
5	1322.3	61.8	21.0	3.9						9.8			2.7	0.8				100.0
6	1325.9	87.4	8.8	3.5										0.3				100.0
7	1329.6	95.3	3.6	1.1														100.0
8	1333.1	96.0	3.0	0.8										0.2				100.0
9	1335.1	95.5	3.7	0.8														100.0
10	1337.0	94.5	4.0	1.3										0.2				100.0
11	1337.9	27.5	57.9	12.4										2.2				100.0
12	1343.2	96.6	2.7	0.5										0.2				100.0
13	1344.6	96.5	3.2	0.3														100.0
14	1346.7	97.9	1.9	0.2														100.0
15	1348.1	97.4	2.5	0.1														100.0
078-S	1349.6	92.7	3.9	2.3						1.1								100.0

Apx Table A.4: Mineralogical composition (wt.%) of Talinga MB9-G (T) and Condabri MB9-H (C) core sub-samples in order of increasing depth.

	Mean depth (mBGL)	Quartz SiO_2	Kaolinite $Al_4Si_4O_{10}(OH)_8$	Illite $K_{1.0\text{-}1.5}Al_4(Si,Al)_8O_{20}(OH)_4$	Smectite $M^+_{0.7}(Y^{3+},Y^{2+})_{4\text{-}6}(Si,Al)_8O_{20}(OH)_4.nH_2O$	Illite/smectite	Illite + illite/smectite	Plagioclase feldspar (albite)$NaAlSi_3O_8$	Plagioclase feldspar (anorthite)$CaAlSi_2O_8$	Orthoclase feldspar (microcline)$KAlSi_3O_8$	Calcite $CaCO_3$	Dolomite $Ca,Mg(CO_3)_2$	Siderite $FeCO_3$	Anatase TiO_2	Rutile TiO_2	Apatite $Ca_5(PO_4)_3(OH,F,Cl)$	Chlorite $(Mg,Fe)_3(Si,Al)_4O_{10}(OH)_2$·	Ankerite $Ca(Fe,Mg,Mn)(CO_3)_2$	Total
TUS#10	62.5	30.1	14.4	6.9	23.4			18.1		7.2									100.1
TUS#11	64.8	31.8	13.2	0.7	24.2			17.7		8.0			4.3						99.9
TUS#12	72.5	57.8	22.0	4.8				11.5		3.9									100.0
TUS#13	76.1	80.2	12.4					3.1		2.8			1.5						100.0
TUS#14	78.2	72.1	16.8					6.1		3.5			1.2					0.3	100.0
C3	1052.2	39.3	24.1				8.7	8.0		3.3	16.5								99.9
C9	1093.9	73.9	12.8				0.9	4.3		7.3	0.8								100.0
C12	1107.1	39.2	18.8				3.2	6.5		7.9	23.5			0.9					100.0
C24	1161.7	80.3	9.2				1.7	2.4		6.0			0.4						100.0
C27	1171.0	90.0	4.1				3.0	1.9						0.2	0.8				100.0
C36	1199.1	49.8	16.3				8.7	15.3		9.0	1.0								100.1
C39	1211.0	41.6	28.5				17.8	7.2		4.9									100.0
C58	1247.7	73.2	16.3				0.6	6.2			0.4			0.5		2.8			100.0
C51	1285.1	56.3	19.4				7.8	7.4		9.1									100.0
C54	1289.5	72.4	10.3				1.7	6.5		9.0									99.9
C59	1291.6	67.3	13.1				2.5	6.0		9.6				1.4					99.9
C42	1294.8	35.0	33.7				15.6	6.2		8.6				1.0					100.1
C57	1295.2	34.1	12.8				10.2	9.8		6.4	26.8								100.1
C65	1460.7	47.8	11.7				10.5	5.2		10.1	11.8		2.2	0.7					100.0
C82	1476.0	38.8	38.1				9.0	0.5		2.1			11.0	0.4					99.9

C68	1489.9	92.6	7.4															100.0
C73	1500.0	96.3	3.7															100.0
C83	1513.1	91.4	7.6				1.0											100.0
C78	1538.2	45.9	22.8				14.8	0.5		9.2			6.2	0.6				100.0
C81	1545.7	43.2	16.3				7.4	0.5		6.0	25.0		1.6					100.0

The core samples from the Hutton sandstone formation examined herein showed substantial variability in quartz and clay content; however, quartz was generally predominant with lesser quantities of kaolinite and/or illite and illite/smectite and minor feldspar minerals (Table 2 - Table 4). Calcite was commonly identified in Talinga MB3-H, Reedy Creek MB3-H, and Condabri MB9-H core samples from the Hutton sandstone formation. Siderite was less commonly observed but comprised a substantial portion of one sample from each the Talinga MB3-H core (no. 019) and the Condabri MB9-G (no. 003) core. Chlorite was identified in only one core sample from Hutton sandstone, no. 0.69 in the Talinga MB3-H core (Table 2) and one sample from the Condabri MB9-H core (Table 4) contained minor apatite ($Ca_5(PO_4)_3(OH,F,Cl)$). Trace quantities of anatase (TiO_2) were present in several samples from the Talinga MB3-H and Condabri MB9-H cores whilst both anatase and rutile (TiO_2), a second titanium dioxide polymorph, were detected in one sample from the Condabri MB9-H core.

Lower core samples from Reedy Creek MB3-H (*ca.* 1300-1350 m, no.066-078 in Table 3) and Condabri MB9-H (*ca.* 1460-1546 m, no. 65-81 in Table 4) were taken from different locations within the Precipice sandstone formation. The Precipice sandstone formation, in the Lower Jurassic lithographic sequence, is characterised by quartzose sandstone which is fine-textured in upper portions of the formation and becomes more coarse-textured with depth (Exon, 1976). In upper portions of the formation, Precipice sandstone also contains some siltstone and minor lithic grains, feldspar, muscovite, mica, and coaly fragments are found throughout. Precipice sandstone is generally laminated and micaceous, with thin seams of coal and carbonaceous shale common (Exon, 1976).

Quartz predominated in Reedy Creek MB3-H and Condabri MB9-H core samples from the Precipice sandstone formation (Table 3, Table 4) with lesser quantites of kaolinite. Minor quantities of illite, illite/mica ($K_{1-1.5}Al_4(Si_{7-6.5}Al_{1-1.5}O_{20})(OH)_4$, present in Reedy Creek MB3-H samples 1-15 and denoted as illite in Table 3) and/or illite/smectite and feldspar minerals were commonly observed. In Reedy Creek MB3-H and Condabri MB9-H core samples from the Precipice formation, quartz exhibited a general increase with depth whilst clay, feldspar, and siderite content decreased. Minor to trace quantities of siderite were also common in Precipice sandstone samples from Reedy Creek MB3-H and Condabri MB9-H cores. Some Reedy Creek MB3-H and Condabri MB9-H core samples exhibited minor to significant (e.g. Reedy Creek MB3-H sample 3) calcite content, whilst the deepest core sample analysed, Condabri MB9-H sample no. 81, was comprised of 25% calcite. The single shale sample analysed, Reedy Creek MB 3-H sample 11, was comprised primarily of kaolinite and quartz along with illite/mica and trace anatase. Reedy Creek MB3 -H core samples contained 1.4-8.1% (generally <5%) poorly ordered phases not identifiable via XRD analysis which were likely organic materials, disordered clay minerals and/or poorly crystalline mineral phases.

A.2.2 CORE SAMPLE GEOCHEMISTRY

Sandstones are sediments composed of fragments, or clasts, of pre-existing minerals and rock which originate from the weathering of parent rocks and are the transported or washed residues from this weathering process (Pettijohn, 1963). As a result, sandstones are comprised of the relatively more chemically inert and mechanically more durable minerals as compared to parent rocks. The bulk composition of sandstone is a function of the parent rock composition, nature and duration of weathering and diagenic processes, and the degree of biochemical (e.g. shell debris) and other contamination (Morton and Hallsworth, 1999; Pettijohn, 1963). Whole-rock elemental concentrations provide important information for characterisation of sandstone aquifers.

Major and trace element content for each sample analysed, including the loss on ignition (LOI) at 1050°C, chromium-reducible S (S_{Cr}), total organic carbon (TOC), and oxalate-extractable Al, Fe and Mn, are presented in Tables 5-14. Figures 1-10 illustrate core lithology and stratigraphy, sample mineralogy and major ion composition, chromium-reducible S, TOC, and oxalate-extractable Al, Fe and Mn with depth in cores Condabri MB1-G, Talinga MB3-H, Reedy Creek MB3-H, Talinga MB9-G and Condabri MB9-H. Where reported values were less than analytical limits of detection they were assumed to equal half the detection limit for graphing purposes. Where no lithological data were provided, sandstone was the assumed sample lithology.

The results of major and trace element geochemical analyses were consistent with mineralogical results obtained for the sandstone core samples. Overall, the core samples analysed showed relatively similar composition of major elements. Major element analysis showed that all core samples were primarily comprised of Si (as SiO_2) with lesser quantities of Al_2O_3 (Table 5, Table 8, Table 11). Simple correlation analyses showed that the SiO_2 content of core samples was strongly correlated (r=0.92) with quartz content whereas Al_2O_3 content was strongly correlated (r=0.95) with total clay (e.g. kaolinite, illite, smectite and illite/smectite) content. A few core samples contained major Fe_2O_3 or CaO; contents of all other major elements in the core samples examined were minor. Iron as quantified by XRF (Fe_2O_3) was largely (r=0.72) accounted for by siderite, and calcite and CaO content were highly correlated (r=0.96).

The Na and K content of core samples can be primarily attributed to the presence of illite, smectite and alkali feldspar minerals within the sandstone matrices.

Sequential LOI is a widely-used technique for estimating the organic and carbonate content of soils and sediments. In the sequential process, organic matter (OM) is oxidised to CO_2 and ash at 500-550°C, then CO_2 is evolved from carbonate at 900-1000°C leaving oxides. Temperature control is essential for accurate OM determination, as loss of volatile salts, structural water and inorganic C may also occur depending on the ignition temperature (Dean, 1974; Sutherland, 1998). Across all samples, the LOI at 1050°C was strongly correlated (r=0.75) with total carbonate mineral content as determined by quantitative XRD (Table 5, Table 8, Table 11). The LOI at 1050°C was also moderately correlated (r=0.56) with total clay content of the samples.

Trace element content of the core samples examined was generally low (Table 6, Table 9, Table 12), with the mean total trace element content of all cores samples equivalent to *ca.* 0.1% by mass (0.11 ± 0.05 % w/w). Some trace elements readily substitute for major elements. For example, Sr readily substitutes for Ca in feldspar and clay minerals and Ti in rutile is readily replaced by Nb (Preston et al., 1998). In addition, Rb or Cs may substitute for K and thus can be expected to be relatively more abundant in samples containing substantial feldspar and/or micaceous clay minerals such as illite. The Sr content of core samples was more strongly correlated to the total clay mineral content (r=0.64) than to feldspar (r=0.43) or calcite (r=0.19) content. Whilst there was no apparent correlation between Nb and rutile content, the core samples showed a moderate correlation (r=0.63) between Nb and anatase. The Rb and K contents of core samples were strongly correlated (r=0.94) to one another and both Rb and K were strongly correlated (r=0.81 and r=0.71, respectively) with the total clay content of core samples.

Apx Table A.5: Major elemental composition (wt. %, as oxides) of Reedy Creek MB1-G (RC), Condabri MB1-G (C) and Talinga MB3-H (T) core sub-samples in order of increasing depth. <DL = less than detection limit.

	Mean depth (mBGL)	SiO_2	Al_2O_3	TiO_2	Fe_2O_3	MnO	CaO	MgO	Na_2O	K_2O	P_2O_5	SO_3	LOI	Sum %
RC001	201.02	58.33	6.10	0.28	1.73	0.15	15.78	0.37	1.18	1.78	0.07	0.10	13.93	99.90
RC002	216.25	87.68	5.27	0.33	1.78	0.02	0.21	0.53	0.99	1.45	0.07	0.06	1.00	99.39
C#1	376.54	85.29	6.81	1.88	0.03	0.54	0.24	0.33	0.52	1.84	0.03	<DL	1.58	99.09
C#2	381.52	89.42	5.16	1.09	0.02	0.32	0.17	0.19	0.27	1.60	0.01	<DL	1.08	99.32
C#3	381.75	77.13	4.75	9.10	0.30	0.31	0.29	0.59	0.32	1.32	0.05	<DL	5.40	99.56
C#4	394.35	81.96	7.63	3.41	0.11	0.82	0.30	0.27	0.83	1.85	0.04	0.02	2.63	99.86
C#5	402.77	57.80	20.16	5.43	0.08	1.03	0.52	0.87	1.06	2.60	0.09	0.08	10.73	100.44
T003	673.29	95.71	2.22	0.11	0.79	0.01	-	0.34	0.65	0.26	0.06	0.06	0.40	100.60
T013	703.63	86.71	6.38	0.35	1.37	0.01	0.03	0.44	1.04	0.77	0.07	0.09	1.80	99.05
T019	732.34	48.33	18.61	1.113	13.70	0.29	0.49	1.23	1.17	2.24	0.15	0.07	11.91	99.32
T022	743.89	93.49	3.40	0.24	0.90	0.01	0.01	0.37	0.72	0.31	0.06	0.07	0.93	100.51
T028	766.51	79.73	10.66	0.56	1.85	0.01	0.14	0.62	1.46	1.66	0.09	0.08	2.69	99.55
T034	794.66	84.69	7.96	0.49	1.43	0.01	0.10	0.51	1.86	1.10	0.09	0.07	1.54	99.85
T043	837.74	56.14	23.07	1.39	3.97	0.07	0.35	0.73	1.47	3.01	0.12	0.36	9.50	100.17
T052	873.89	86.33	7.51	0.26	1.69	0.02	0.10	0.46	1.11	0.97	0.07	0.07	1.80	100.38
T055	884.27	82.87	8.68	0.41	1.86	0.02	0.10	0.56	1.53	1.37	0.10	0.06	2.06	99.61
T060	911.03	66.67	16.83	0.73	3.99	0.02	0.58	0.93	1.71	2.36	0.10	0.08	5.75	99.75
T066	929.15	60.19	12.82	0.48	4.08	0.32	8.20	0.54	1.70	1.35	0.12	0.10	10.06	99.96
T069	937.39	80.66	9.61	0.35	3.39	0.02	0.10	0.46	1.82	0.40	0.10	0.05	2.68	99.63

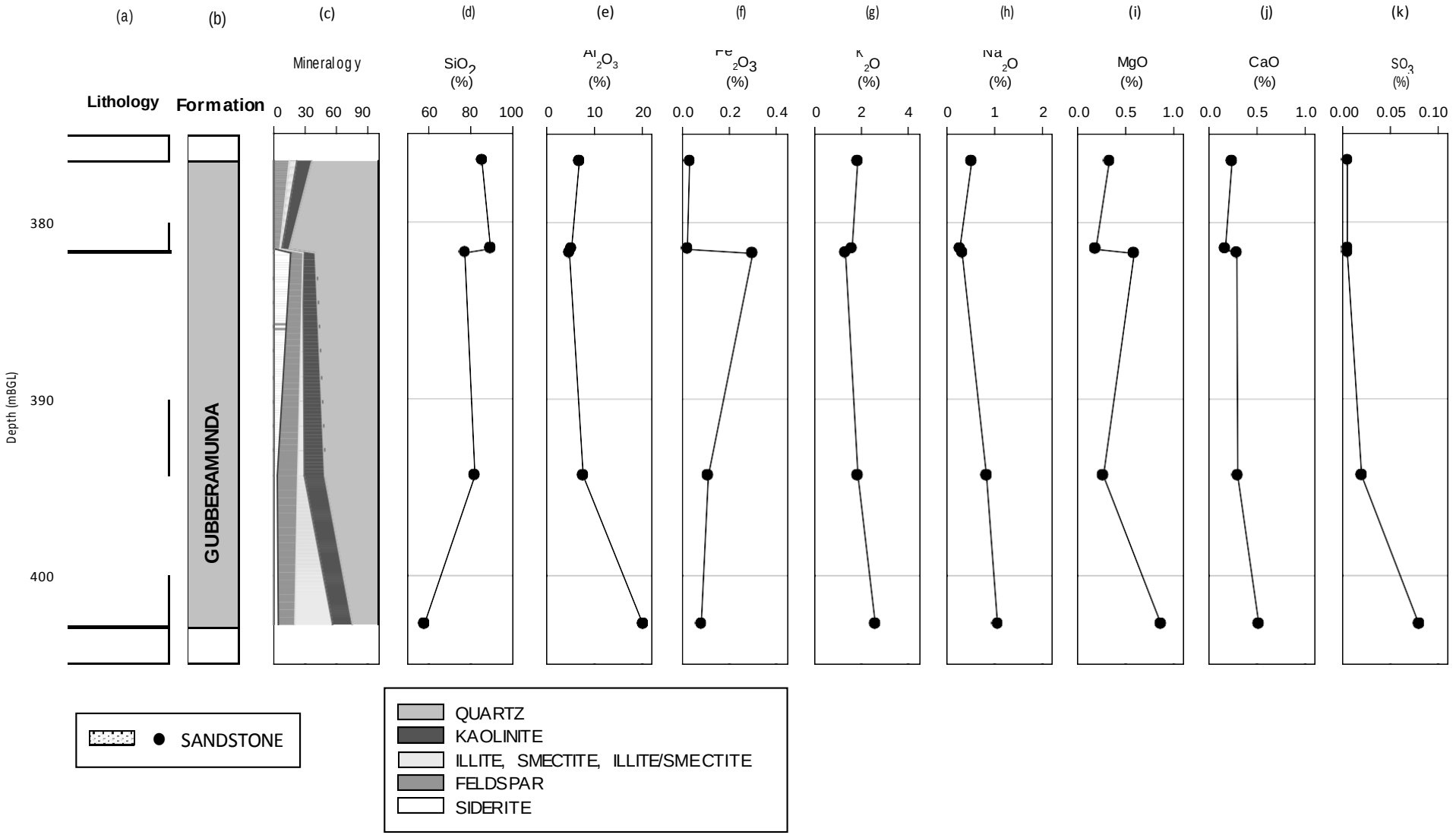

Figure A.1: Depth profile of Condabri MB1-G core showing (a) lithology, (b) stratigraphy, (c) mineralogy, and (d-k) major ions. Depth is reported as metres below ground level (mBGL).

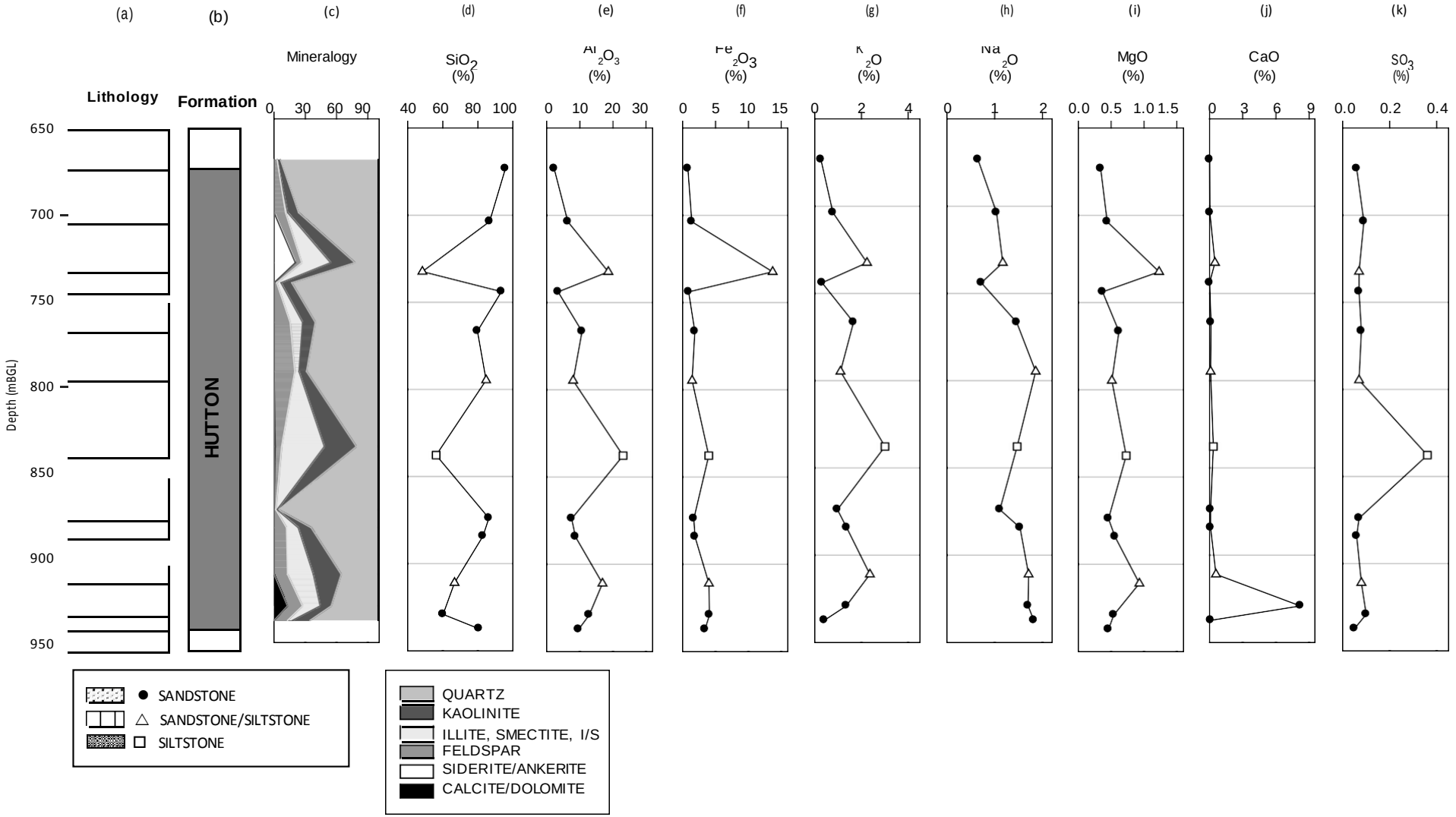

Figure A.2: Depth profile of Talinga MB3-H core showing (a) lithology, (b) stratigraphy, (c) mineralogy, and (d-k) major ions. Depth is reported as metres below ground level (mBGL).

Apx Table A.6 Trace elemental composition (ppm) of Reedy Creek MB1-G (RC), Condabri MB1-G(C) and Talinga MB3-H (T) core sub-samples in order of increasing depth. nm = not measured; <DL = less than detection limit.

	Ag	As	Ba	Bi	Br	Cd	Ce	Co	Cr	Cs	Cu	Ga	Ge	Hf	Hg	I	La	Mn	Mo	Nb
RC001	nm	3.9	244.7	nm	nm	<DL	35.3	1.3	60.2	nm	7.0	6.8	nm	nm	nm	nm	nm	nm	0.5	<DL
RC002	nm	3.9	347.2	nm	nm	1.1	26.3	2.6	**121.9**†	nm	6.3	5.9	nm	nm	nm	nm	nm	nm	0.9	<DL
C#1	<DL	**25.2**†	215.9	6.1	2.9	<DL	21.0	21.6	22.5	5.4	12.5	8.1	<DL	2.7	<DL	<DL	8.7	107.4	1.1	6.7
C#2	<DL	19.4	180.9	4.4	2.5	<DL	25.1	12.6	44.5	3.9	4.0	6.7	<DL	2.3	**3.1**‡	<DL	7.7	83.6	0.5	3.8
C#3	<DL	**32.2**†	106.9	10.1	4.0	<DL	8.1	9.7	19.1	5.1	6.0	6.4	<DL	0.8	<DL	<DL	4.8	1674.6	0.7	4.1
C#4	<DL	**26.9**†	106.8	6.9	3.3	<DL	26.1	11.5	40.3	10.8	1.9	8.9	<DL	3.8	<DL	<DL	9.8	988.2	1.8	10.9
C#5	<DL	**28.6**†	121.4	8.5	3.5	<DL	52.1	18.2	38.4	11.9	19.7	22.5	<DL	8.8	<DL	<DL	17.5	426.3	1.8	15.5
T003	nm	4.8	60.1	nm	nm	0.6	13.6	6.1	**243.8**†	nm	6.0	3.3	nm	nm	nm	nm	nm	nm	1.2	<DL
T013	nm	5.2	174.8	nm	nm	1.4	29.4	13.1	**147.4**†	nm	8.0	7.3	nm	nm	nm	nm	nm	nm	0.8	<DL
T019	nm	8.1	740.5	nm	nm	**3.3**†	53.5	41.2	**96.6**†	nm	33.3	19.7	nm	nm	nm	nm	nm	nm	3.4	14.2
T022	nm	4.8	71.2	nm	nm	0.3	22.5	6.3	**118.3**†	nm	5.4	3.8	nm	nm	nm	nm	nm	nm	0.5	<DL
T028	nm	6.9	485.3	nm	nm	1.0	47.3	5.9	68.1	nm	8.3	10.6	nm	nm	nm	nm	nm	nm	<DL	1.4
T034	nm	5.7	286.2	nm	nm	**2.7**†	49.2	4.2	**116.7**†	nm	6.0	7.0	nm	nm	nm	nm	nm	nm	2.3	<DL
T043	nm	**21.2**†	937.0	nm	nm	**2.9**†	56.3	62.1	55.7	nm	38.0	23.5	nm	nm	nm	nm	nm	nm	2.1	8.5
T052	nm	5.4	233.0	nm	nm	1.5	27.2	5.3	74.9	nm	6.6	7.1	nm	nm	nm	nm	nm	nm	0.1	<DL
T055	nm	6.9	304.3	nm	nm	1.8	39.5	5.3	61.5	nm	7.0	9.0	nm	nm	nm	nm	nm	nm	1.3	<DL
T060	nm	9.1	541.0	nm	nm	**2.1**†	61.6	15.0	49.6	nm	15.5	17.6	nm	nm	nm	nm	nm	nm	2.4	4.5
T066	nm	8.2	220.7	nm	nm	0.9	39.4	7.3	58.3	nm	9.5	12.0	nm	nm	nm	nm	nm	nm	0.1	1.6
T069	nm	4.9	90.9	nm	nm	0.4	24.6	12.0	**120.4**†	nm	6.8	8.1	nm	nm	nm	nm	nm	nm	0.8	<DL

†Concentration exceeds ANZECC/ARMCANZ (2000) ISQG-low (trigger value) recommended sediment quality guidelines.

‡Concentration exceeds ANZECC/ARMCANZ (2000) ISQG-high recommended sediment quality guidelines.

Table A.6 (continued): Trace elemental composition (ppm) of Reedy Creek MB1-G (RC), Condabri MB1-G (C) and Talinga MB3-H (T) core sub-samples in order of increasing depth. nm = not measured; <DL = less than detection limit.

	Nd	Ni	Pb	Rb	Sb	Sc	Se	Sm	Sn	Sr	Ta	Te	Th	Tl	U	V	W	Y	Yb	Zn	Zr
RC001	nm	8.6	11.4	43.6	<DL	nm	nm	nm	<DL	112.3	nm	nm	<DL	nm	2.2	32.6	nm	10.6	nm	19.4	72.8
RC002	nm	6.7	9.8	35.8	**2.7**†	nm	nm	nm	<DL	59.8	nm	nm	1.7	nm	3.4	43.7	nm	11.9	nm	20.0	91.6
C#1	9.5	4.9	10.1	50.7	<DL	4.4	1.1	3.9	5.7	66.1	2.7	11.5	4.8	9.7	4.4	13.9	197.1	12.8	0.3	**353.2**†	120.3
C#2	13.3	4.2	10.6	42.5	<DL	4.5	1.1	2.9	3.3	52.4	<DL	8.5	2.6	7.7	3.8	15.3	89.9	9.0	<DL	**222.2**†	86.8
C#3	5.9	3.4	8.7	35.6	<DL	1.6	1.9	3.3	4.0	48.4	0.1	15.1	1.6	11.7	5.7	9.1	112.2	8.6	2.4	111.6	94.6
C#4	11.9	4.6	10.1	49.9	<DL	4.9	1.5	3.0	3.0	72.9	1.1	9.9	9.0	10.0	5.1	<DL	85.0	14.8	<DL	**226.0**†	295.4
C#5	22.8	**24.4**†	19.2	102.5	<DL	8.9	1.5	7.6	5.9	126.7	5.2	12.0	12.2	9.8	7.3.	27.0	15.8	29.5	3.8	**966.4**‡	228.1
T003	nm	7.9	2.7	12.7	**5.5**†	nm	nm	nm	<DL	20.2	nm	nm	<DL	nm	<DL	20.3	nm	7.8	nm	9.5	44.3
T013	nm	13.7	8.3	26.2	**4.9**†	nm	nm	nm	<DL	51.4	nm	nm	2.3	nm	2.1	53.0	nm	13.6	nm	28.3	135.6
T019	nm	**30.1**†	17.9	86.9	<DL	nm	nm	nm	2.4	175.5	nm	nm	6.2	nm	4.9	173.3	nm	34.3	nm	73.8	247.7
T022	nm	11.2	3.1	13.8	**8.0**†	nm	nm	nm	<DL	25.5	nm	nm	1.4	nm	0.9	26.0	nm	6.3	nm	14.1	95.6
T028	nm	10.9	15.4	54.1	**3.7**†	nm	nm	nm	<DL	96.4	nm	nm	4.2	nm	3.5	54.9	nm	19.0	nm	37.4	220.0
T034	nm	8.4	13.3	13.3	**5.8**†	nm	nm	nm	<DL	66.4	nm	nm	3.9	nm	0.6	37.7	nm	15.3	nm	19.9	336.1
T043	nm	**44.7**†	23.1	23.1	<DL	nm	nm	nm	<DL	251.2	nm	nm	5.0	nm	3.8	206.0	nm	41.9	nm	110.8	254.9
T052	nm	8.0	9.3	9.3	2.0	nm	nm	nm	<DL	53.2	nm	nm	2.4	nm	3.7	33.7	nm	10.8	nm	19.4	85.2
T055	nm	8.4	13.1	13.1	1.9	nm	nm	nm	<DL	70.6	nm	nm	2.7	nm	2.9	47.0	nm	16.6	nm	29.4	192.9
T060	nm	14.6	25.0	25.0	2.0	nm	nm	nm	<DL	198.8	nm	nm	8.5	nm	7.3	94.2	nm	31.7	nm	73.9	252.8
T066	nm	12.1	16.0	16.0	<DL	nm	nm	nm	<DL	182.8	nm	nm	3.5	nm	5.0	71.9	nm	18.4	nm	60.2	125.5
T069	nm	9.9	11.5	11.5	<DL	nm	nm	nm	<DL	49.0	nm	nm	1.3	nm	3.3	58.3	nm	10.7	nm	34.6	80.0

†Concentration exceeds ANZECC/ARMCANZ (2000) ISQG-low (trigger value) recommended sediment quality guidelines.

‡Concentration exceeds ANZECC/ARMCANZ (2000) ISQG-high recommended sediment quality guidelines.

Apx Table A.7: Chromium-reducible S (SCr, %), total organic carbon (TOC, %) and oxalate-extractable Al, Fe and Mn content of Condabri MB1-G (C) and Talinga MB3-H (T) core sub-samples in order of increasing depth.

	S_{Cr} (%)	TOC (%)	Al_{OX} (mg/L)	Fe_{OX} (mg/L)	Mn_{OX} (mg/L)
C#1	<0.01	0.04	1299	2578	21
C#2	<0.01	0.04	833	1508	21
C#3	0.01	0.03	970	35227	1440
C#4	<0.01	0.06	1268	12853	623
C#5	0.02	1.34	2465	47158	1494
T003	0.06	0.04	188	322	16
T013	0.01	0.1	880	1539	38
T019	0.01	0.63	1620	119287	4525
T022	0.03	0.04	533	3389	99
T028	0.02	0.08	760	2148	69
T034	0.03	0.04	671	1489	43
T043	0.03	0.09	852	1826	95
T052	0.09	1.19	1186	9013	512
T055	0.01	0.06	981	1980	90
T060	0.02	0.6	1741	4287	108
T066	0.02	0.15	2059	5643	3091
T069	0.01	0.07	2116	5846	156

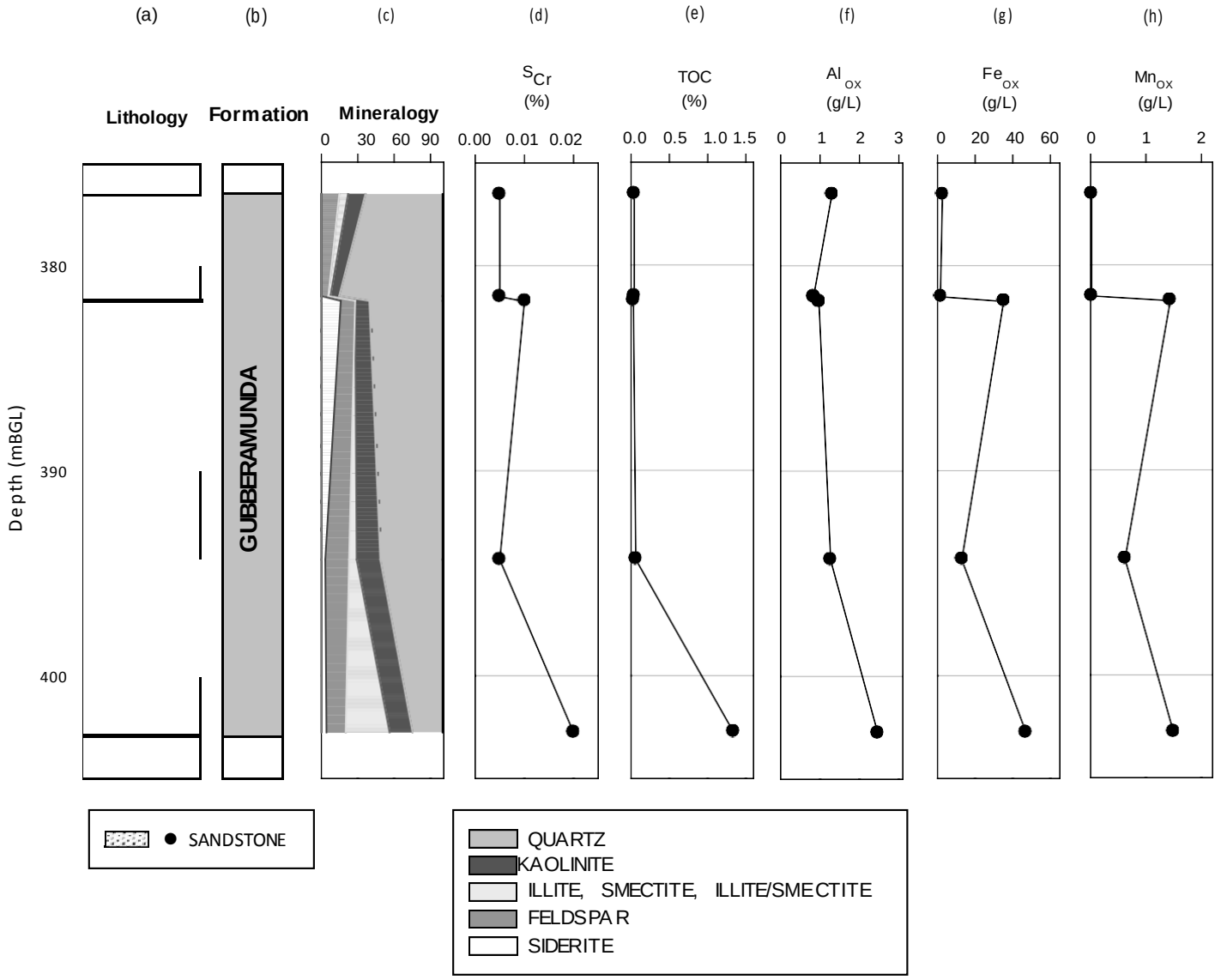

Figure A.3: Depth profile of core Condabri MB1-G showing (a) lithology, (b) stratigraphy, (d) chromium-reducible S (SCr), (e) total organic C (TOC), and oxalate-extractable Al (f), Fe (g) and Mn (h). Depth is reported as metres below ground level (mBGL).

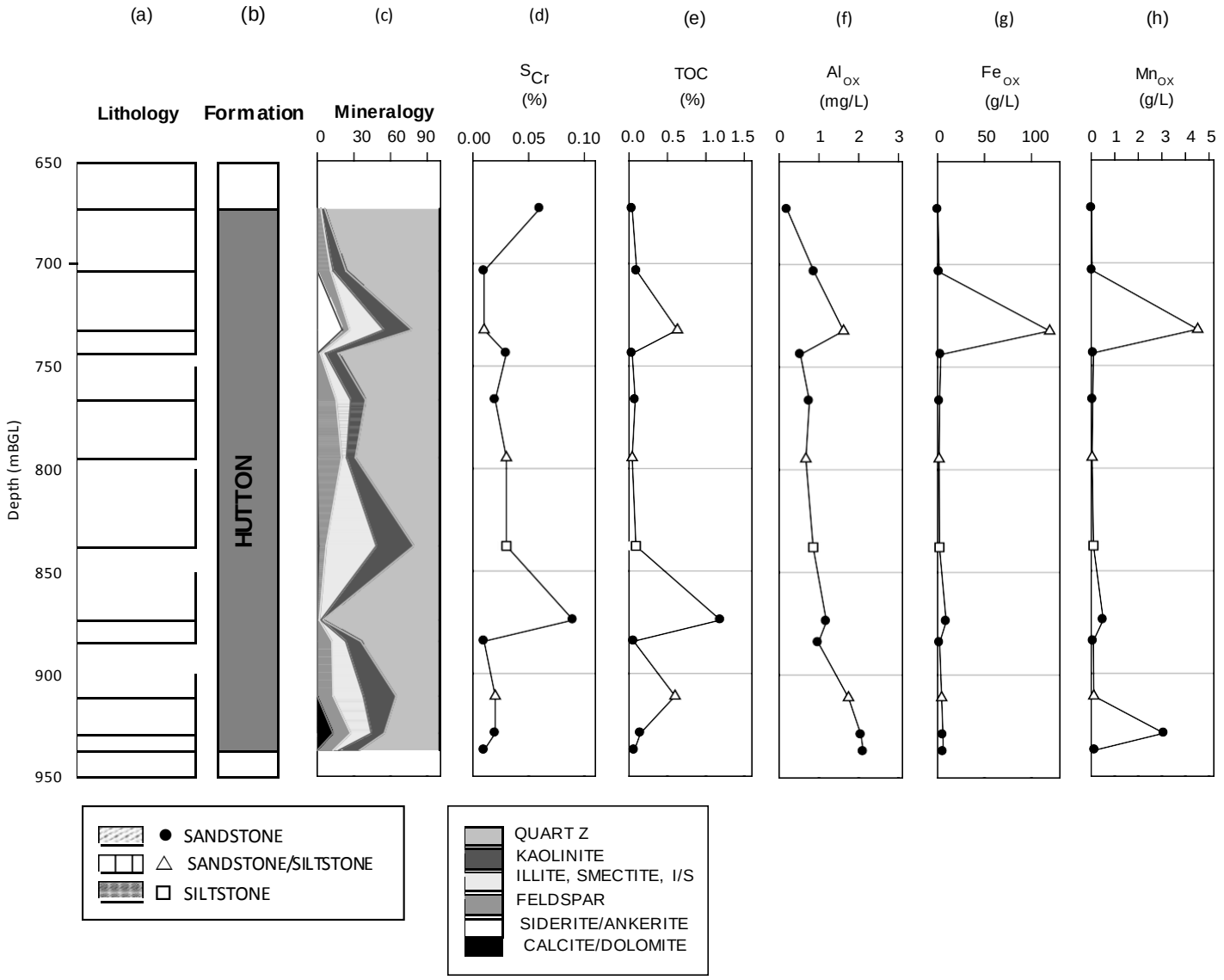

Figure A.4: Depth profile of core Talinga MB3-H showing (a) lithology, (b) stratigraphy, (d) chromium-reducible S (SCr), (e) total organic C (TOC), and oxalate-extractable Al (f), Fe (g) and Mn (h). Depth is reported as metres below ground level (mBGL).

Apx Table A.8 Major elemental composition (wt. %, as oxides) of Reedy Creek MB3-H core sub-samples in order of increasing depth. <DL = less than detection limit.

	Mean depth (mBGL)	SiO_2	Al_2O_3	TiO_2	Fe_2O_3	MnO	CaO	MgO	Na_2O	K_2O	P_2O_5	SO_3	LOI	Sum %
007-S	842.6	86.04	7.68	0.33	1.95	0.01	0.18	0.35	1.23	1.06	0.05	0.03	1.75	100.66
003-S	853.7	63.99	11.49	0.61	11.36	0.31	0.95	0.90	1.53	1.64	0.15	0.06	7.20	100.17
006-S	857.9	70.02	16.72	0.71	3.28	0.02	1.26	0.84	2.40	2.09	0.11	0.07	4.00	101.52
013-S	891.2	76.11	12.30	0.53	4.06	0.02	0.20	0.57	1.54	1.66	0.04	0.08	3.24	100.34
019-S	921.2	86.06	6.97	0.34	2.43	0.02	0.07	0.30	0.55	1.08	0.03	0.01	2.20	100.05
022-S	931.1	79.35	9.65	0.64	2.45	0.07	1.25	0.35	0.84	1.68	0.04	0.01	3.59	99.90
028-S	978.2	78.17	11.94	0.65	2.56	0.01	0.13	0.39	0.80	2.06	0.04	<DL	3.46	100.22
031-S	995.1	87.26	7.09	0.39	1.47	0.02	0.09	0.17	0.85	1.54	0.04	0.01	1.50	100.42
034-S	1011.4	88.46	6.04	0.50	1.65	0.02	0.18	0.19	0.72	1.27	0.04	0.01	1.30	100.38
037-S	1025.2	88.77	5.52	0.46	1.51	0.02	0.18	0.18	1.03	1.21	0.04	<DL	1.17	100.10
042-S	1061.4	80.71	10.47	0.47	1.89	0.02	0.18	0.32	1.84	1.92	0.06	<DL	2.26	100.14
048-S	1095.1	81.13	10.07	0.33	2.22	0.02	0.36	0.35	1.58	2.02	0.04	<DL	2.23	100.36
051-S	1103.0	83.27	8.58	0.38	1.75	0.03	0.50	0.33	1.46	1.62	0.04	<DL	3.00	100.97
057-S	1147.8	87.95	7.40	0.39	1.29	0.01	0.30	0.20	1.00	1.16	0.03	0.05	1.04	100.80
060-S	1232.6	65.04	18.38	0.78	3.24	0.02	1.44	0.82	2.09	2.11	0.10	0.04	6.48	100.55
063-S	1251.1	69.66	15.07	0.63	2.76	0.02	0.99	0.81	1.27	1.98	0.06	0.01	7.26	100.51
066-S	1303.8	78.97	4.58	0.17	1.01	0.08	6.83	0.12	0.06	1.38	0.02	<DL	6.88	100.09
069-S	1311.4	76.87	11.73	0.49	2.48	0.04	0.41	0.39	0.16	2.63	0.08	0.04	4.64	99.93
072-S	1318.0	84.88	7.90	0.39	2.30	0.05	0.19	0.22	-	1.57	0.07	0.05	3.07	100.72
078-S	1349.6	96.89	1.53	0.39	0.39	0.01	0.01	0.03	0.01	0.10	0.01	<DL	0.72	100.10

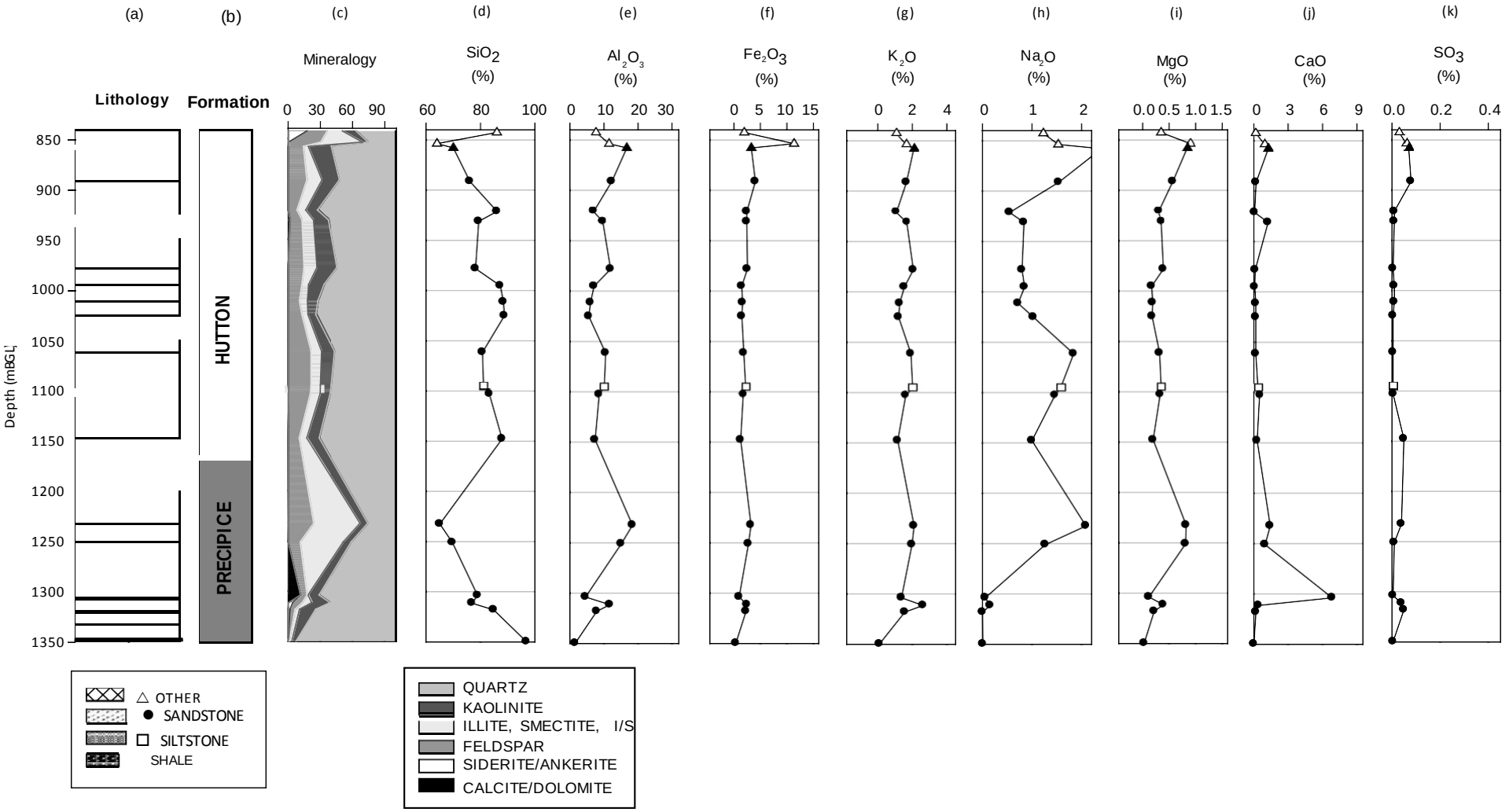

Figure A.5: Depth profile of core Reedy Creek MB3-H showing (a) lithology, (b) stratigraphy, (c) mineralogy, and (d-k) major ions. Depth is reported as metres below ground level (mBGL).

Apx Table A.9: Trace elemental composition (ppm) of Reedy Creek MB3-H core sub-samples in order of increasing depth. nm = not measured; <DL = below detection limit.

	Ag	As	Ba	Bi	Br	Cd	Ce	Co	Cr	Cs	Cu	Ga	Ge	Hf	Hg	I	La	Mn	Mo	Nb
007-S	<DL	24.9†	226.0	6.1	2.6	<DL	29.9	7.7	56.4	7.7	4.9	9.5	<DL	4.6	5.4‡	<DL	11.5	60.2	0.6	5.7
003-S	<DL	38.3†	196.6	10.7	3.7	<DL	25.6	12.7	50.7	5.5	12.7	12.9	<DL	2.5	<DL	<DL	6.6	1455.3	1.7	6.0
006-S	<DL	26.1†	372.7	6.2	2.5	<DL	27.0	7.7	71.2	5.1	12.8	16.7	<DL	5.2	2.2‡	<DL	10.6	118.8	1.3	7.0
013-S	<DL	30.5†	287.4	8.0	3.6	<DL	29.1	8.2	62.9	4.7	8.4	15.7	<DL	5.6	<DL	<DL	12.7	99.1	1.0	10.4
019-S	<DL	27.0†	196.7	6.8	3.5	<DL	32.3	12.3	76.9	10.1	8.6	9.4	<DL	3.1	4.3‡	<DL	5.7	79.3	0.8	11.0
022-S	<DL	28.2†	248.6	5.8	2.3	<DL	44.3	10.3	91.9†	5.1	9.0	12.5	<DL	4.7	2.5‡	<DL	23.2	579.9	2.2	13.6
028-S	<DL	21.5†	291.8	5.1	2.6	<DL	42.8	6.2	63.1	8.8	6.7	12.8	<DL	4.8	2.4‡	<DL	21.9	91.4	1.9	11.7
031-S	<DL	21.1†	293.7	5.4	2.9	<DL	29.1	4.4	56.6	8.0	3.0	7.4	<DL	1.9	2.9‡	<DL	15.4	60.4	1.0	7.3
034-S	<DL	19.6	189.7	4.6	2.7	<DL	31.7	4.1	70.8	8.2	3.2	6.8	<DL	4.2	4.9‡	<DL	15.1	84.3	1.5	8.6
037-S	<DL	20.0	235.1	5.4	2.6	<DL	34.3	2.8	73.8	7.5	3.1	6.1	<DL	5.5	5.4‡	<DL	18.0	89.2	1.9	7.8
042-S	<DL	21.0†	390.6	4.4	2.0	<DL	43.5	6.1	51.2	5.3	3.6	10.7	<DL	4.6	2.6‡	<DL	20.2	80.8	1.3	8.4
048-S	<DL	25.8†	418.8	6.3	2.6	<DL	29.1	6.3	43.4	5.4	4.4	10.2	<DL	2.8	2.3‡	<DL	14.2	126.1	0.5	6.5
051-S	<DL	23.4†	325.0	5.7	2.3	<DL	22.6	5.1	49.9	7.3	3.5	9.5	<DL	3.4	5.5‡	<DL	16.7	151.2	1.3	7.2
057-S	<DL	20.5†	258.8	4.8	2.1	<DL	27.6	4.3	102.8†	2.4	3.9	2.8	<DL	2.8	5.8‡	<DL	10.5	87.3	1.5	7.0
060-S	<DL	33.1†	397.5	6.9	2.5	<DL	69.2	11.3	30.6	7.7	18.0	23.3	<DL	8.3	2.4‡	<DL	29.0	109.3	2.8	14.6
063-S	<DL	26.0†	489.5	6.0	2.6	<DL	45.9	7.5	26.4	10.3	15.1	19.8	0.2	7.0	2.7‡	<DL	18.4	93.6	2.3	13.6
066-S	<DL	29.0†	245.5	7.2	2.9	<DL	13.4	2.7	120.8†	5.8	4.0	5.6	<DL	2.9	5.1‡	<DL	12.9	664.0	0.6	2.6
069-S	<DL	27.5†	416.4	7.0	2.5	<DL	27.2	7.1	124.0†	8.8	8.1	12.7	<DL	2.0	3.6‡	<DL	10.8	256.5	1.2	7.2
072-S	<DL	24.7†	179.9	5.9	2.4	<DL	19.3	8.3	108.5†	<DL	4.8	8.2	<DL	2.7	1.9‡	<DL	9.4	292.1	1.2	5.1
078-S	<DL	18.0	<DL	4.9	2.5	<DL	19.5	0.3	109.2†	3.7	2.9	2.2	<DL	2.8	7.0‡	<DL	7.6	16.9	1.5	6.8

†Concentration exceeds ANZECC/ARMCANZ (2000) ISQG-low (trigger value) recommended sediment quality guidelines.

‡Concentration exceeds ANZECC/ARMCANZ (2000) ISQG-high recommended sediment quality guidelines.

Table A.9 (continued): Trace elemental composition (ppm) of Reedy Creek MB3-H core sub-samples in order of increasing depth. nm = not measured; <DL = below detection limit.

	Nd	Ni	Pb	Rb	Sb	Sc	Se	Sm	Sn	Sr	Ta	Te	Th	Tl	U	V	W	Y	Yb	Zn	Zr
007-S	15.8	5.3	8.0	41.6	<DL	9.1	0.9	0.7	3.9	74.1	1.7	11.4	4.7	8.8	5.3	12.5	4.1	13.4	<DL	323.5†	104.5
003-S	13.7	9.4	9.0	51.2	<DL	7.4	1.5	<DL	3.7	218.5	1.8	14.3	6.3	10.8	6.8	49.5	4.0	26.9	4.9	504.2‡	136.1
006-S	15.9	7.9	10.1	69.4	<DL	3.9	1.2	5.0	4.9	419.2	3.8	11.2	6.4	8.9	6.5	29.2	7.6	16.2	<DL	741.7‡	169.0
013-S	15.3	11.3	9.8	65.4	<DL	5.3	1.5	3.8	6.1	122.9	4.1	11.6	7.0	10.3	6.1	23.2	7.3	20.0	1.6	723.3‡	168.0
019-S	11.8	12.4	10.3	42.0	<DL	3.3	1.1	3.9	4.0	50.0	2.6	9.9	5.4	9.0	5.3	20.1	4.3	13.7	1.7	500.0‡	121.6
022-S	21.5	14.5	9.0	66.4	<DL	4.8	1.1	7.8	5.2	125.0	2.6	12.6	10.3	8.3	6.1	12.8	6.8	25.8	0.6	577.0‡	446.6
028-S	21.3	12.6	11.6	72.2	<DL	3.7	0.7	7.4	4.7	79.1	2.8	10.2	9.2	8.4	4.9	<DL	5.7	22.3	1.4	534.9‡	372.8
031-S	13.5	5.7	8.8	47.7	<DL	3.1	0.8	5.4	3.0	55.1	1.7	9.6	6.0	7.0	4.0	<DL	2.4	11.5	0.3	156.7	201.7
034-S	15.1	5.9	8.4	40.5	<DL	1.2	0.8	3.6	4.2	51.1	1.4	8.4	7.2	7.1	4.9	<DL	2.9	12.8	0.3	159.0	358.0
037-S	19.1	3.9	9.6	38.6	<DL	0.5	1.1	5.6	3.8	49.4	<DL	8.5	7.6	7.6	4.9	<DL	3.0	13.7	<DL	111.7	336.0
042-S	18.8	7.0	12.1	63.2	<DL	3.4	0.8	4.0	3.6	85.1	2.4	9.4	7.5	6.5	5.0	<DL	6.0	16.3	<DL	316.1	258.6
048-S	15.6	7.9	11.6	69.0	<DL	2.6	1.0	6.0	3.1	94.6	2.5	9.7	5.6	9.2	5.2	4.6	2.8	14.2	2.7	299.0†	99.8
051-S	8.8	6.2	10.6	56.9	<DL	2.4	0.9	4.9	3.9	87.5	0.3	9.5	6.2	8.3	5.2	<DL	2.9	14.8	<DL	238.0†	202.4
057-S	14.1	4.6	8.2	41.1	<DL	1.7	0.9	4.2	3.2	54.4	2.1	9.4	5.2	7.3	4.5	<DL	3.8	12.0	<DL	210.0†	228.4
060-S	30.6	11.5	19.9	95.1	<DL	9.3	0.9	9.2	6.9	486.0	5.1	11.0	14.8	8.4	8.9	21.9	11.3	32.2	1.8	1066.7‡	311.3
063-S	21.9	8.7	17.4	93.7	<DL	7.6	0.9	3.6	6.9	407.4	5.8	11.2	12.5	8.6	8.0	17.2	8.8	27.3	1.9	780.5‡	238.0
066-S	6.5	3.5	5.2	46.5	<DL	2.2	0.8	6.2	4.6	244.6	0.3	12.2	2.8	10.3	6.1	9.0	3.7	10.6	<DL	86.2	63.9
069-S	12.6	7.0	14.3	79.9	<DL	3.1	1.2	2.8	5.7	63.3	3.2	13.0	7.3	9.4	6.0	25.2	5.3	16.0	1.0	477.2‡	135.2
072-S	10.6	7.2	8.1	39.9	<DL	3.9	1.1	2.9	2.2	35.5	2.6	7.9	5.0	7.8	4.2	11.5	5.9	13.3	<DL	380.8†	98.0
078-S	9.5	2.6	5.4	3.4	<DL	<DL	0.9	2.2	4.9	24.3	<DL	9.8	4.8	7.4	4.0	<DL	2.3	8.6	<DL	100.9	271.8

†Concentration exceeds ANZECC/ARMCANZ (2000) ISQG-low (trigger value) recommended sediment quality guidelines.

‡Concentration exceeds ANZECC/ARMCANZ (2000) ISQG-high recommended sediment quality guidelines.

Apx Table A.10: Chromium-reducible S (S_{Cr}, %), total organic carbon (TOC, %) and oxalate-extractable Al, Fe and Mn content of Reedy Creek MB3-H core sub-samples in order of increasing depth.

	S_{Cr} (%)	TOC (%)	Al_{ox} (mg/L)	Fe_{ox} (mg/L)	Mn_{ox} (mg/L)
007-S	0.02	0.23	2603	50975	2310
003-S	<0.01	0.1	1687	4453	152
006-S	<0.01	0.03	1868	3425	59
013-S	<0.01	0.06	2893	6107	99
019-S	<0.01	0.25	1402	3130	75
022-S	<0.01	0.11	1649	2999	843
028-S	<0.01	0.24	1954	3765	100
031-S	<0.01	0.06	1119	2071	52
034-S	<0.01	0.04	1287	2483	65
037-S	<0.01	0.04	1155	2247	97
042-S	<0.01	0.16	1658	2617	68
048-S	<0.01	0.06	2144	3760	144
051-S	<0.01	0.08	1396	2271	110
057-S	<0.01	0.11	1518	1835	70
060-S	<0.01	0.31	2134	3422	97
063-S	<0.01	0.9	2021	2372	65
066-S	<0.01	0.06	479	2740	549
069-S	<0.01	0.05	1030	8513	229
072-S	<0.01	0.04	806	8307	308
078-S	<0.01	0.03	386	212	6

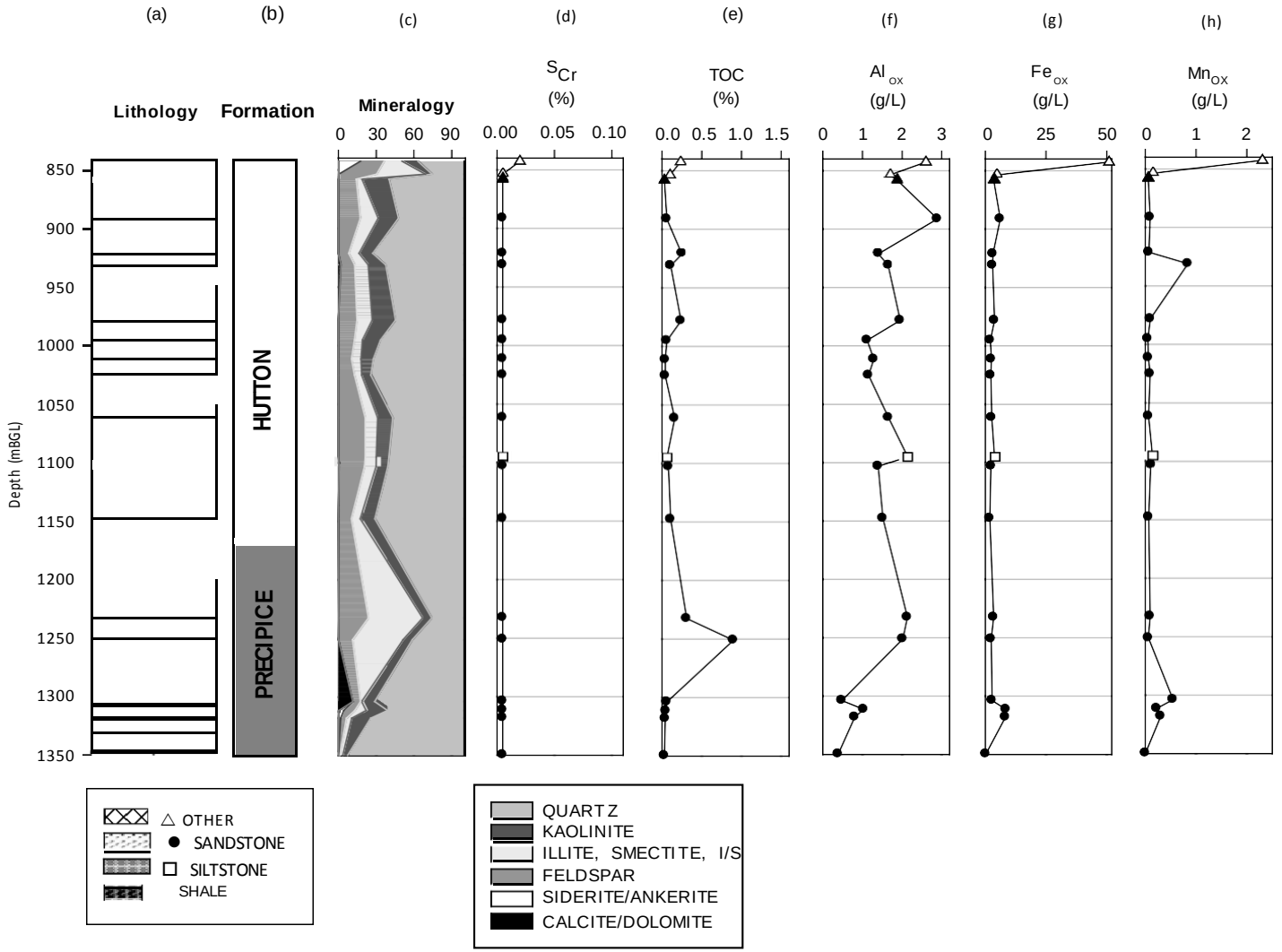

Figure A.6: Depth profile of core Reedy Creek MB3-H showing (a) lithology, (b) stratigraphy, (d) chromium-reducible S (S_{Cr}), (e) total organic C (TOC), and oxalate-extractable Al (f), Fe (g) and Mn (h). Depth is reported as metres below ground level (mBGL).

Apx Table A.11: Major elemental composition (wt. %, as oxides) of Talinga MB9-G (T) and Condabri MB9-H (C) core sub-samples in order of increasing depth. <DL = below detection limit.

	Mean depth (mBGL)	SiO_2	Al_2O_3	TiO_2	Fe_2O_3	MnO	CaO	MgO	Na_2O	K_2O	P_2O_5	SO_3	LOI	Sum %
TUS#10	62.5	72.31	14.00	0.50	3.29	0.02	0.79	0.70	2.02	2.14	0.09	<DL	5.42	101.28
TUS#11	64.8	67.12	10.10	0.48	3.84	0.08	0.58	0.52	1.39	1.54	0.07	<DL	14.71	100.53
TUS#12	72.5	84.95	7.98	0.40	1.63	0.02	0.59	0.26	0.92	1.44	0.04	<DL	2.29	100.53
TUS#13	76.1	92.80	3.08	0.13	1.91	0.06	0.09	0.12	0.20	0.84	0.01	<DL	1.09	100.32
TUS#14	78.2	91.50	3.96	0.49	2.68	0.07	0.18	0.33	0.19	0.72	0.01	<DL	0.99	101.12
C3	1052.2	67.39	10.83	0.61	2.23	0.27	6.58	0.61	1.87	1.21	0.08	0.13	7.95	99.76
C9	1093.9	88.42	5.73	0.25	1.04	0.02	0.83	0.35	0.90	0.78	0.06	0.10	2.00	100.48
C12	1107.1	64.55	7.33	0.46	2.23	0.35	11.34	0.45	1.02	1.14	0.07	0.15	11.05	100.14
C24	1161.7	91.56	4.05	0.21	1.46	0.04	0.04	0.36	0.69	0.77	0.07	0.06	1.29	100.59
C27	1171.0	94.51	2.07	0.13	0.99	0.01	0.01	0.33	0.64	0.51	0.06	0.09	0.65	99.99
C36	1199.1	78.58	9.54	0.43	1.52	0.03	0.72	0.52	2.30	1.56	0.08	0.07	2.28	97.63
C39	1211.0	71.72	14.48	0.79	2.50	0.01	0.20	.08	1.50	2.25	0.09	0.06	4.39	98.07
C58	1247.7	79.22	4.41	0.37	5.50	0.03	2.33	0.54	0.88	0.29	1.30	0.11	4.13	99.11
C51	1285.1	81.25	9.02	0.38	2.88	0.02	0.20	0.66	1.45	1.57	0.09	0.05	2.17	99.73
C54	1289.5	89.51	5.20	0.38	1.00	0.01	0.12	0.39	1.16	0.82	0.07	0.08	1.19	99.93
C59	1291.6	86.82	4.05	2.79	1.47	0.03	0.29	0.43	0.93	0.68	0.08	0.09	1.15	98.81
C42	1294.8	70.20	15.13	0.95	3.94	0.01	0.34	0.70	1.54	1.94	0.10	0.06	4.73	99.65
C57	1295.2	61.35	10.00	0.42	1.58	0.31	11.10	0.47	1.71	1.78	0.09	0.15	10.91	99.87
C65	1460.7	64.26	11.74	0.53	5.19	0.11	4.64	0.95	0.94	2.78	0.12	0.14	7.77	99.16
C82	1476.0	58.95	17.44	0.74	7.36	0.09	0.31	0.72	0.48	1.03	0.13	0.11	11.44	98.80
C68	1489.9	95.01	2.21	0.14	0.42	0.01	0.02	0.28	0.51	0.16	0.06	0.08	0.96	99.85
C73	1500.0	95.81	1.30	0.17	0.56	0.01	0.02	0.27	0.45	0.15	0.07	0.06	0.65	99.52
C83	1513.1	95.64	1.55	0.11	0.41	0.01	<DL	0.26	0.45	0.12	0.06	0.09	0.70	99.38
C78	1538.2	68.66	12.91	0.49	6.76	0.17	0.34	0.58	0.42	2.22	0.14	0.02	6.51	99.22
C81	1545.7	66.48	8.94	0.36	2.25	0.17	8.17	0.43	0.39	1.86	0.06	0.10	10.06	99.26

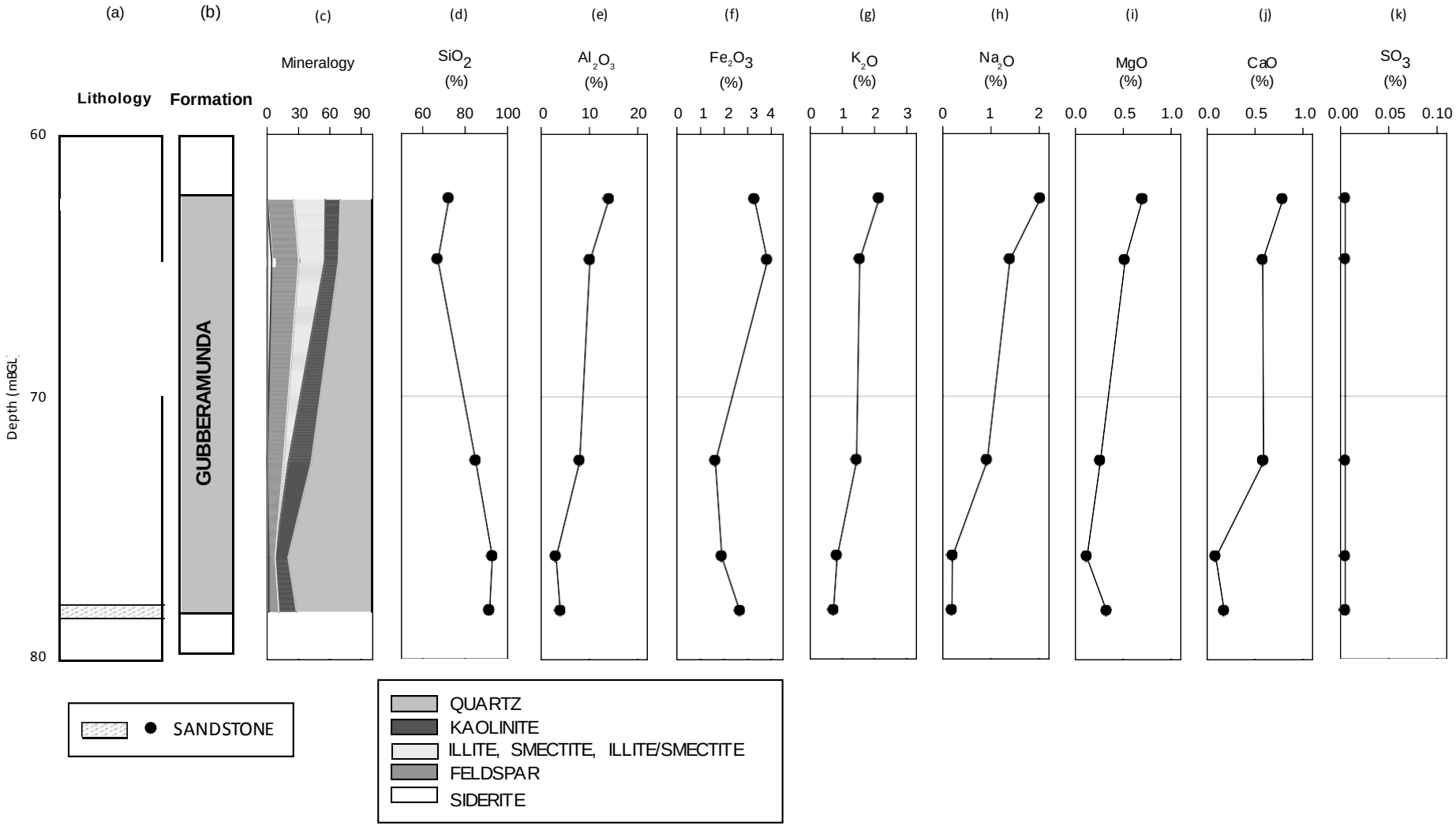

Figure A.7: Depth profile of core Talinga MB9-G showing (a) lithology, (b) stratigraphy, (c) mineralogy, and (d-k) major ions. Depth is reported as metres below ground level (mBGL).

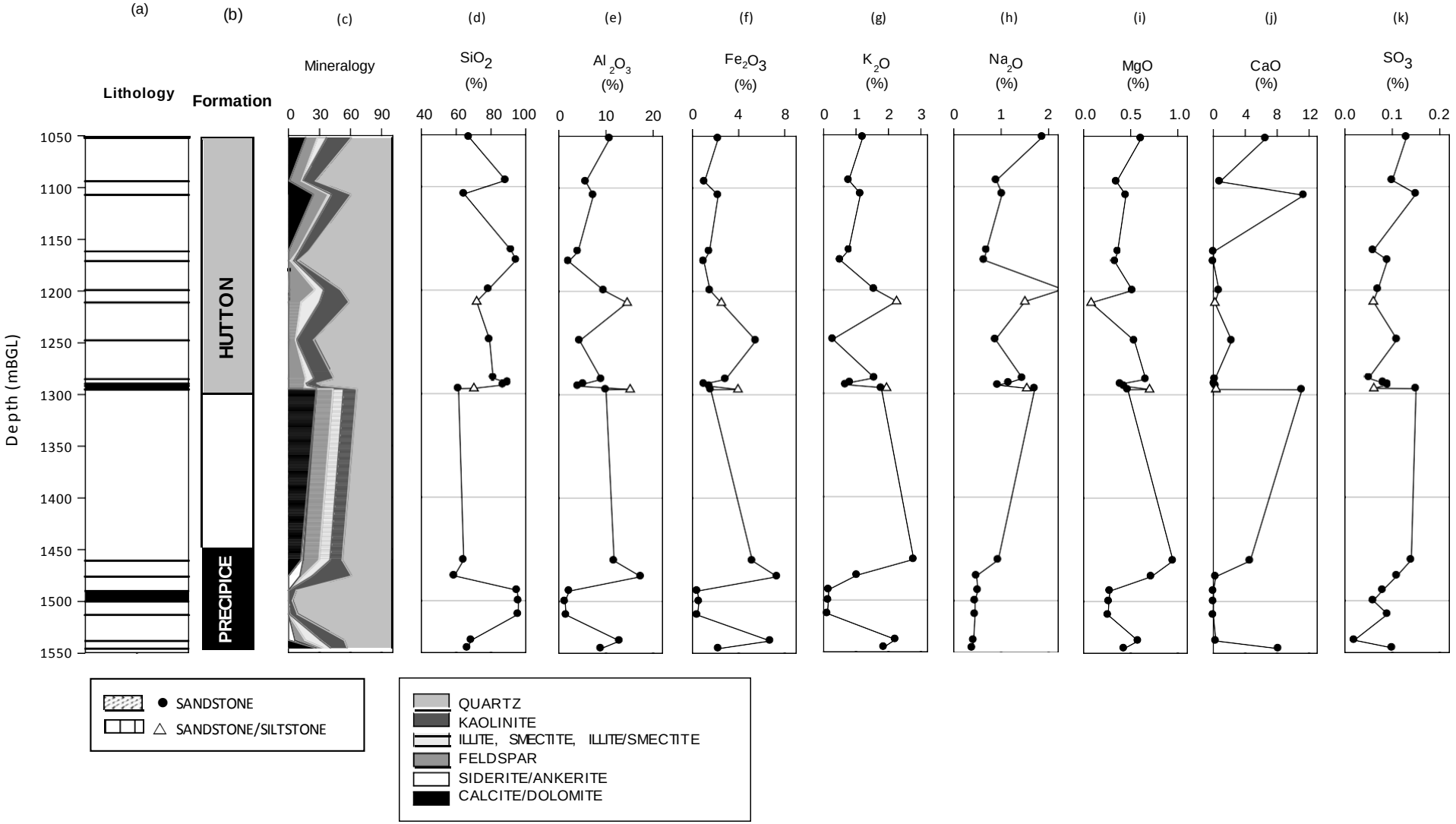

Figure A.8: Depth profile of core Condabri MB9-H showing (a) lithology, (b) stratigraphy, (c) mineralogy, and (d-k) major ions. Depth is reported as metres below ground level (mBGL).

Apx Table A.12: Trace elemental composition (ppm) of Talinga MB9-G (T) and Condabri MB9-H (C) core sub-samples in order of increasing depth.

	Ag	As	Ba	Bi	Br	Cd	Ce	Co	Cr	Cs	Cu	Ga	Ge	Hf	Hg	I	La	Mn	Mo	Nb
TUS#10	nm	6.3	584.2	nm	nm	**1.8**†	38.5	19.2	**203.4**†	nm	23.6	12.7	nm	nm	nm	nm	nm	nm	1.2	1.2
TUS#11	nm	5.1	566.7	nm	nm	**2.2**†	58.7	51.5	**181.3**†	nm	19.0	11.1	nm	nm	nm	nm	nm	nm	2.9	0.8
TUS#12	nm	5.1	472.7	nm	nm	<DL	40.8	24.7	**225.3**†	nm	43.4	8.0	nm	nm	nm	nm	nm	nm	1.3	<DL
TUS#13	nm	3.4	234.8	nm	nm	**1.8**†	31.4	48.9	51.1	nm	**198.6**†	4.9	nm	nm	nm	nm	nm	nm	0.9	<DL
TUS#14	nm	3.7	247.8	nm	nm	<DL	12.2	48.9	**259.3**†	nm	**171.7**†	5.3	nm	nm	nm	nm	nm	nm	1.4	<DL
C3	nm	6.0	416.6	nm	nm	**1.8**†	38.2	5.2	51.6	nm	10.6	11.3	nm	nm	nm	nm	nm	nm	0.6	3.3
C9	nm	6.4	191.6	nm	nm	0.6	24.5	5.8	**110.6**†	nm	8.0	5.7	nm	nm	nm	nm	nm	nm	<DL	<DL
C12	nm	6.6	283.3	nm	nm	<DL	30.8	6.6	46.3	nm	8.7	8.6	nm	nm	nm	nm	nm	nm	<DL	1.6
C24	nm	4.7	206.7	nm	nm	**1.6**†	25.3	3.2	**118.3**†	nm	7.2	4.7	nm	nm	nm	nm	nm	nm	<DL	0.8
C27	nm	3.2	145.0	nm	nm	1.2	20.7	1.8	**175.5**†	nm	6.6	3.2	nm	nm	nm	nm	nm	nm	0.4	<DL
C36	nm	6.3	536.0	nm	nm	**2.7**†	34.7	6.8	47.1	nm	8.5	10.2	nm	nm	nm	nm	nm	nm	1.7	<DL
C39	nm	7.4	633.4	nm	nm	1.5	76.0	11.7	62.2	nm	14.9	15.7	nm	nm	nm	nm	nm	nm	1.3	6.3
C58	nm	6.4	130.0	nm	nm	**2.6**†	34.6	32.5	**129.1**†	nm	7.7	7.2	nm	nm	nm	nm	nm	nm	1.9	2.5
C51	nm	5.9	584.7	nm	nm	1.3	40.2	9.9	56.0	nm	8.2	10.5	nm	nm	nm	nm	nm	nm	0.4	<DL
C54	nm	4.5	289.6	nm	nm	0.8	30.5	3.1	**85.0**†	nm	6.8	5.3	nm	nm	nm	nm	nm	nm	0.8	<DL
C59	nm	5.3	310.3	nm	nm	0.9	49.4	5.1	**439.9**‡	nm	6.4	4.9	nm	nm	nm	nm	nm	nm	2.8	10.4
C42	nm	7.3	632.4	nm	nm	**2.0**†	33.0	16.3	**81.3**†	nm	17.3	17.0	nm	nm	nm	nm	nm	nm	1.4	2.0
C57	nm	6.7	483.5	nm	nm	<DL	37.5	8.5	41.2	nm	8.3	9.9	nm	nm	nm	nm	nm	nm	<DL	0.9
C65	nm	9.9	697.6	nm	nm	**2.3**†	39.2	12.2	46.3	nm	9.1	12.6	nm	nm	nm	nm	nm	nm	0.3	1.8
C82	nm	9.9	216.9	nm	nm	**1.8**†	83.3	23.4	47.7	nm	16.2	20.2	nm	nm	nm	nm	nm	nm	1.4	6.6
C68	nm	4.3	55.3	nm	nm	1.1	17.2	0.2	**143.7**†	nm	6.5	3.4	nm	nm	nm	nm	nm	nm	<DL	<DL
C73	nm	3.5	43.1	nm	nm	**1.7**†	16.2	<DL	**185.8**†	nm	6.9	3.2	nm	nm	nm	nm	nm	nm	0.7	<DL
C83	nm	4.4	25.4	nm	nm	<DL	19.1	<DL	**149.1**†	nm	5.2	3.0	nm	nm	nm	nm	nm	nm	<DL	<DL
C78	nm	5.5	338.8	nm	nm	**2.6**†	34.4	15.8	**90.9**†	nm	16.3	13.7	nm	nm	nm	nm	nm	nm	<DL	<DL
C81	nm	5.4	471.8	nm	nm	<DL	49.3	5.2	73.1	nm	10.6	9.3	nm	nm	nm	nm	nm	nm	<DL	<DL

†Concentration exceeds ANZECC/ARMCANZ (2000) ISQG-low (trigger value) recommended sediment quality guidelines.
‡Concentration exceeds ANZECC/ARMCANZ (2000) ISQG-high recommended sediment quality guidelines.

Table A.12 (continued): Trace elemental composition (ppm) of Talinga MB9-G (T) and Condabri MB9-H (C) core sub-samples in order of increasing depth.

	Nd	Ni	Pb	Rb	Sb	Sc	Se	Sm	Sn	Sr	Ta	Te	Th	Tl	U	V	W	Y	Yb	Zn	Zr
TUS#10	nm	13.5	15.3	56.7	**11.0**†	nm	nm	nm	<DL	153.4	nm	nm	3.3	nm	3.6	117.8	nm	21.8	nm	40.6	130.9
TUS#11	nm	17.0	15.0	45.5	**3.8**†	nm	nm	nm	<DL	119.2	nm	nm	2.7	nm	4.4	197.6	nm	21.3	nm	33.0	144.9
TUS#12	nm	7.8	11.3	40.5	**2.2**†	nm	nm	nm	2.1	63.7	nm	nm	2.2	nm	0.7	91.8	nm	14.2	nm	23.7	102.2
TUS#13	nm	2.5	7.3	26.3	**2.8**†	nm	nm	nm	48.9	36.8	nm	nm	1.0	nm	3.5	37.9	nm	5.8	nm	8.6	61.1
TUS#14	nm	6.4	7.0	24.8	<DL	nm	nm	nm	34.2	34.2	nm	nm	2.4	nm	2.0	81.6	nm	8.9	nm	13.0	111.1
C3	nm	12.0	11.1	40.2	0.1	nm	nm	nm	<DL	167.5	nm	nm	3.6	nm	1.0	80.2	nm	17.4	nm	45.4	170.6
C9	nm	9.2	6.7	25.3	**6.5**†	nm	nm	nm	<DL	80.0	nm	nm	2.3	nm	1.0	40.5	nm	9.9	nm	22.3	78.5
C12	nm	10.7	8.1	36.7	<DL	nm	nm	nm	<DL	203.3	nm	nm	2.3	nm	1.2	64.8	nm	13.0	nm	35.7	112.3
C24	nm	7.9	6.3	25.0	**3.9**†	nm	nm	nm	<DL	30.0	nm	nm	0.7	nm	2.5	36.2	nm	8.6	nm	20.5	78.5
C27	nm	6.9	4.2	16.2	**5.7**†	nm	nm	nm	<DL	21.3	nm	nm	<DL	nm	2.5	24.5	nm	5.3	nm	13.2	50.2
C36	nm	9.9	15.9	50.8	**2.8**†	nm	nm	nm	<DL	106.3	nm	nm	3.4	nm	0.4	47.8	nm	15.6	nm	31.3	216.6
C39	nm	15.6	23.8	86.7	1.4	nm	nm	nm	<DL	109.4	nm	nm	8.0	nm	6.3	82.9	nm	33.2	nm	59.5	287.5
C58	nm	19.6	5.5	8.4	<DL	nm	nm	nm	<DL	86.8	nm	nm	1.8	nm	5.8	53.8	nm	23.6	nm	26.1	107.3
C51	nm	11.6	13.5	52.4	1.1	nm	nm	nm	<DL	75.0	nm	nm	1.7	nm	5.1	51.3	nm	17.3	nm	34.1	148.4
C54	nm	6.6	10.3	25.4	**3.5**†	nm	nm	nm	<DL	41.4	nm	nm	2.3	nm	0.9	38.0	nm	12.6	nm	16.2	182.1
C59	nm	8.8	9.5	23.1	1.6	nm	nm	nm	<DL	42.0	nm	nm	5.4	nm	3.6	110.3	nm	20.4	nm	22.2	458.4
C42	nm	18.2	12.5	66.3	**2.6**†	nm	nm	nm	<DL	156.3	nm	nm	5.3	nm	4.8	161.6	nm	26.2	nm	79.2	313.3
C57	nm	9.4	12.2	57.4	<DL	nm	nm	nm	<DL	152.0	nm	nm	4.0	nm	3.9	61.8	nm	17.5	nm	43.1	127.5
C65	nm	12.3	16.6	81.1	<DL	nm	nm	nm	<DL	119.7	nm	nm	3.2	nm	4.1	62.6	nm	33.6	nm	50.2	162.5
C82	nm	17.5	24.4	46.3	<DL	nm	nm	nm	<DL	76.1	nm	nm	9.2	nm	7.0	103.7	nm	34.6	nm	94.5	272.9
C68	nm	6.2	6.9	7.7	**4.6**†	nm	nm	nm	<DL	20.8	nm	nm	1.4	nm	1.5	22.6	nm	4.3	nm	12.5	54.1
C73	nm	7.2	4.3	5.6	**5.9**†	nm	nm	nm	<DL	18.3	nm	nm	<DL	nm	4.3	21.5	nm	5.1	nm	10.9	55.3
C83	nm	6.5	4.1	7.6	**6.3**†	nm	nm	nm	<DL	16.0	nm	nm	0.8	nm	0.7	16.9	nm	4.2	nm	10.4	59.6
C78	nm	13.9	11.8	93.7	<DL	nm	nm	nm	<DL	55.9	nm	nm	6.8	nm	4.9	84.6	nm	24.1	nm	39.4	122.6
C81	nm	12.1	15.3	65.0	<DL	nm	nm	nm	<DL	76.2	nm	nm	6.6	nm	5.0	57.3	nm	21.2	nm	26.4	104.1

†Concentration exceeds ANZECC/ARMCANZ (2000) ISQG-low (trigger value) recommended sediment quality guidelines.
‡Concentration exceeds ANZECC/ARMCANZ (2000) ISQG-high recommended sediment quality guidelines.

Apx Table A.13: Chromium-reducible S (SCr, %), total organic carbon (TOC, %) and oxalate-extractable Al, Fe and Mn content of Talinga MB9-G core sub-samples in order of increasing depth.

	S_{Cr} (%)	TOC (%)	Al_{OX} (mg/kg)	Fe_{OX} (mg/kg)	Mn_{OX} (mg/kg)
US#10	<0.01	0.18	3527	8221	90
US#11	<0.01	10.68	2693	16026	600
US#12	<0.01	0.12	2263	3900	24
US#13	<0.01	0.07	1777	9263	399
US#14	<0.01	0.11	1928	19863	1314

Apx Table A.14: Chromium-reducible S (SCr, %), total organic carbon (TOC, %) and oxalate-extractable Al, Fe and Mn content of Condabri MB9-H core sub-samples in order of increasing depth.

	S_{Cr} (%)	TOC (%)	Al_{OX} (mg/L)	Fe_{OX} (mg/L)	Mn_{OX} (mg/L)
3	0.02	0.06	4554	8359	1479
9	0.01	0.15	6548	6026	250
12	0.01	0.04	4532	10619	2252
24	0.01	0.06	2907	13029	648
27	0.01	0.04	2094	4068	60
36	0.01	0.10	4631	6691	270
39	0.01	0.50	6130	8098	42
58	0.04	0.05	14221	42752	492
51	0.01	0.08	5109	11425	75
54	0.01	0.04	3171	5301	46
59	0.01	0.05	2833	4838	132
42	0.01	0.42	8894	17893	63
57	0.01	0.04	3171	5807	1757
65	0.04	0.05	5405	35401	847
82	0.03	0.53	5410	73435	932
68	0.01	0.05	1133	1728	34
73	0.01	0.04	1294	2795	50
83	0.02	0.05	1119	1836	51
78	0.01	0.03	3089	39680	1302
81	0.01	0.03	2489	13456	1044

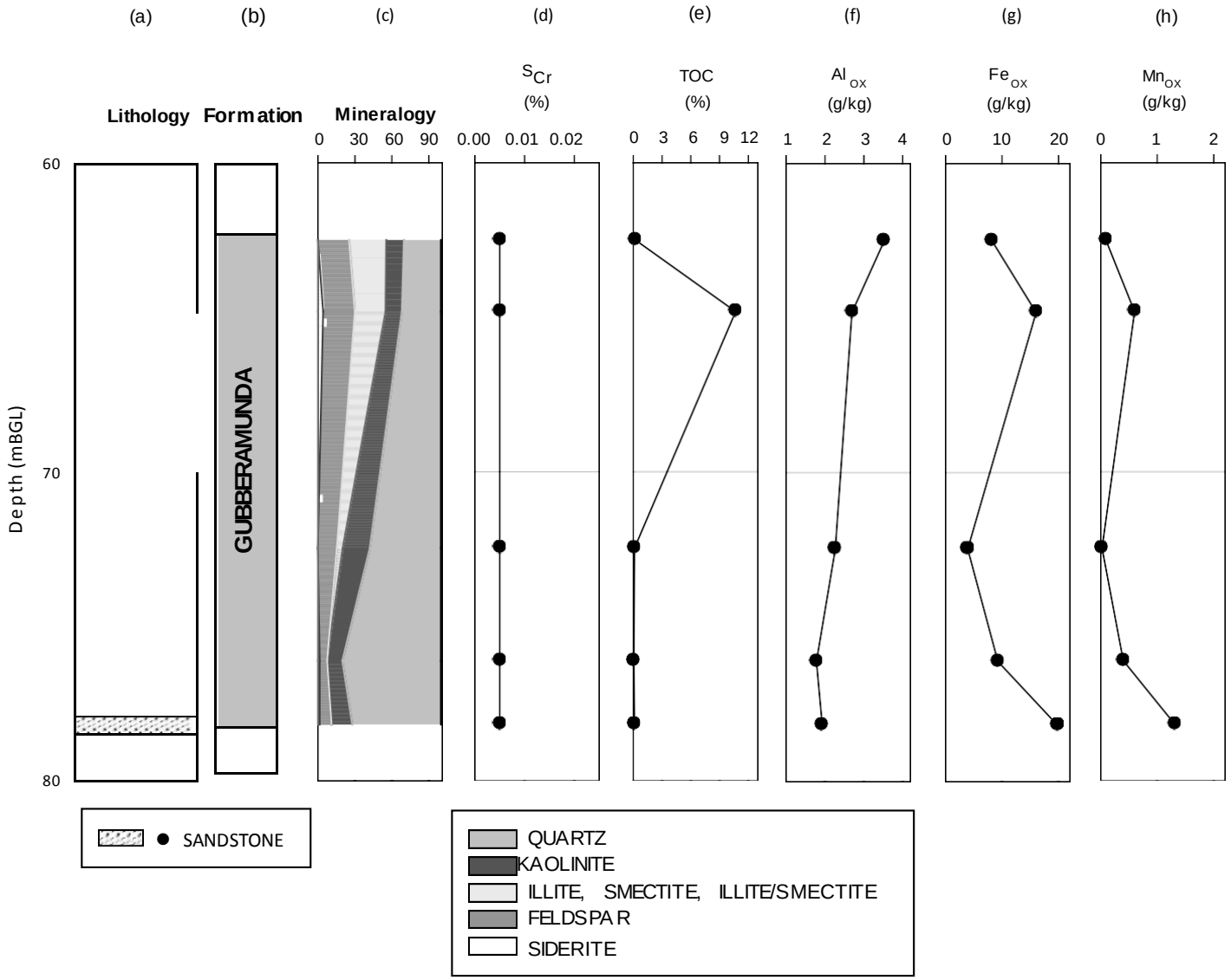

Figure A.9: Depth profile of core Talinga MB9-G showing (a) lithology, (b) stratigraphy, (d) chromium-reducible S (SCr), (e) total organic C (TOC), and oxalate-extractable Al (f), Fe (g) and Mn (h). Depth is reported as metres below ground level (mBGL).

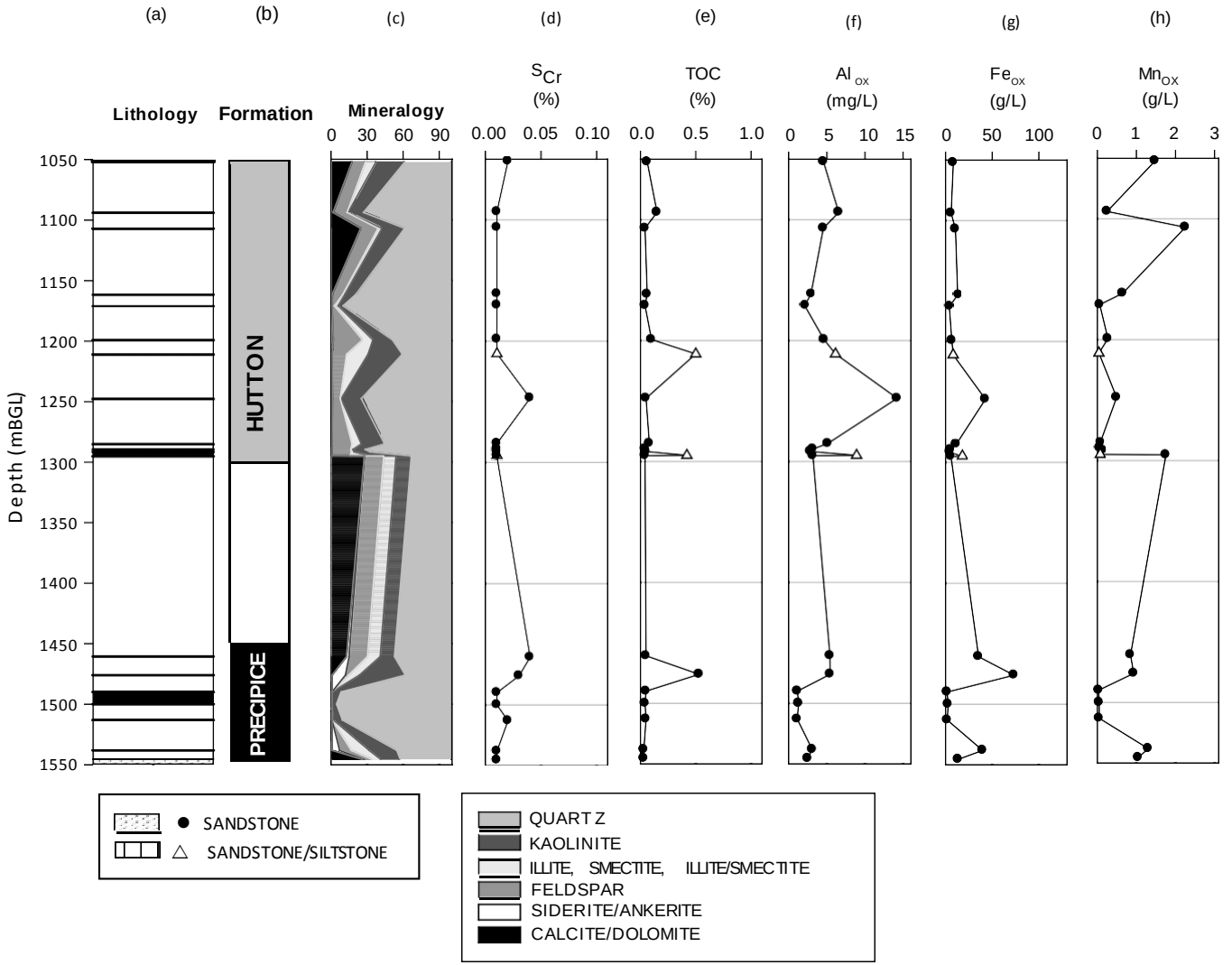

Figure A.10: Depth profile of core Condabri MB9-H showing (a) lithology, (b) stratigraphy, (d) chromium-reducible S (SCr), (e) total organic C (TOC), and oxalate-extractable Al (f), Fe (g) and Mn (h). Depth is reported as metres below ground level (mBGL).

Zirconium was ubiquitous in core samples, most likely as detrital zircon crystals (Hoskin and Ireland, 2000; Pettijohn, 1963). Similarly, Nb and Cr contents of sandstone core samples can likely be attributed to the abundance of rutile and chrome-spinel minerals, respectively (Preston et al., 1998). The Ni content of core samples exhibited moderate correlation (r=0.52) to the total Fe content (as Fe_2O_3). Several trace elements (Ba, Ce, Ga, Ni, Pb, Rb, Sr, and Y) exhibited moderate to strong negative correlation (r=-0.60—0.85) to the quartz content and a concomitant moderate to strong positive correlation (r=0.60-0.94) to the total clay mineral content. The V and Th contents were also moderately (r=0.60-0.63) correlated with total clay contents. Only weak correlations, if any, were observed between trace elements and either total feldspar or total carbonate mineral contents of the core samples. Trace elements which showed no correlation to identified mineral phases included Cr, Co, Cu and Zr, all of which may have been present within minor accessory detrital minerals present in concentrations too low for detection using XRD. Across all core samples, As exhibited no correlation with Fe content (as Fe_2O_3; r=0.05).

Although there are no Australian guidelines concerning the trace element content of aquifer materials, comparison of core sample trace element geochemistry data to Australian and New Zealand Environment and Conservation Council/Agriculture and Resource Management Council of Australia and New Zealand (ANZECC/ARMCANZ) sediment quality guidelines (2000) indicates that certain elements should be carefully evaluated. In particular, Zn and inorganic Hg were frequently present in the core samples analysed at concentrations greater than ANZECC/ARMCANZ (2000) interim sediment quality guideline (ISQG)-high recommended sediment quality guideline values, whilst As, Cd, Cr, Ni and Sb, and occasionally Cu, were detected at concentrations greater than ISQG-low (trigger value) recommended sediment quality guidelines.

A.3 Mineralogical and Geochemical Implications of Aquifer Recharge

Injection of water at a different oxidative-reductive potential (ORP) than existing groundwater has the potential to alter the aquifer's geochemical equilibrium conditions and processes such as dissolution and/or precipitation of minerals (e.g. Fe- and Mn-(hydr)oxides, carbonates, and sulphide minerals), organic matter mineralization, ion exchange and sorption processes. Injection of water containing dissolved oxygen may result in a change from reducing to oxidizing conditions in the injection zone, leading to the oxidation of common reductants such as sedimentary organic matter (SOM) or siderite (FeCO3). Oxidation of reduced Fe minerals and/or SOM has the potential to mobilise elements within the aquifer materials via acidification following depletion of buffering capacity; however, oxidation of aquifer materials can expected to be minimal where injected water is anoxic.

Particular care should be taken to minimise potential oxygenation in zones rich in SOM and/or siderite. Siderite was detected in several core samples from the Gubberamunda sandstone formation, including Condabri MB1-G #3 (381.69-381.80 m) which contained 15.9% siderite, as well as Talinga MB9-G US#11 (64.7-64.93 m) and Condabri MB1-G #4 (394.10-394.59 m) and #5 (402.67-402.86 m) which contained 3.2-4.3% siderite (Table 2, Table 4). Mineralogical analyses of core samples from the Hutton sandstone formation showed some zones with substantial siderite content, including: 20.2% siderite in Talinga MB3-H no. 19 (732.04-732.64 m); 17.3% siderite in Reedy Creek MB3-H no. 003-S (853.45-853.95 m); and up to *ca.* 4% siderite within Reedy Creek MB3-H core samples from 1300.87 to 1322.43 m (Table 2, Table 3). Within Precipice sandstone core samples, Condabri MB9-H samples at 1475.74-1476.25 m (no. 82) and 1537.92-1538.43 m (no. 78) exhibited 11% and 6.2% siderite content, respectively (Table 4). Based on results of quantitative mineralogical analyses and LOI results, core samples likely containing substantial SOM include: Talinga MB9-G US#10 (62.28-62.70 m) and US#11 (64.70-64.93 m); Condabri MB1-G #5 (402.67-402.86 m); Talinga MB3-H no. 43 (837.48-838.00 m) and no. 60 (910.74-911.32 m); and, Reedy Creek MB3-H no. 060-S (1232.40-1232.70 m) and no. 063-S (1250.87-1251.25 m).

Siderite dissolution is possible in zones containing substantial siderite following injection of water with negligible Fe content; however, the rate of siderite dissolution under either oxic or anoxic conditions is extremely slow (Duckworth and Martin, 2004). In most areas, de novo precipitation of iron minerals such as ferric oxides, hydroxides and oxyhydroxides is unlikely to occur due to both the relatively low Fe content of most aquifer materials and slow siderite dissolution kinetics. Alteration of ORP due to injection of oxidised water may also result in calcite dissolution. In addition, dissolution of carbonate mineral phases present within aquifer sediments, namely calcite and dolomite, is likely where injected waters contain substantially lesser quantities of Ca and/or Mg.

Mean major ion composition did not differ greatly between sediment formations at each site (Figure A.11, Figure A.13, Figure A.15). The mean Ca content of the Gubberamunda sediment samples from Reedy Creek was greater than that of the Reedy Creek Hutton or Precipice core samples (Figure 11); however, only two core samples from Gubberamunda sandstone were analysed from the Reedy Creek site. Within the core samples from the Condabri

site, the Fe content was substantially lower in core samples from the Gubberamunda formation compared to those from Hutton or Precipice sandstone (Figure 13), whilst at the Talinga site the S content of Hutton sandstone core samples was more than one standard deviation lower than the mean S content of Gubberamunda formation samples from the same site (Figure 15).

The potential reductive capacity (PRC) of sediment core samples was assessed using a chromium-reducible sulphur test to quantify reduced inorganic sulphur and sulphate minerals, and quantitative XRD to determine siderite content. Across all sites and all sediment types, the PRC could largely be attributed to sedimentary organic matter content, with relatively little contribution from either pyrite or siderite (Figure A.12,Figure A.14, Figure A.16).

With regard to the anticipated Reedy Creek aquifer injection trial per the Reedy Creek Aquifer Injection Trial Execution Plan (Q-4255-95-MP-003), monitoring of bore water hydrogeochemistry will facilitate assessment of potential changes to aquifer chemistry as a result of treated CSG water injection. Although Exon (1972) documented trace iron oxide in Gubberamunda sandstone, no iron oxide minerals were detected in Reedy Creek MB1-G core samples from the Gubberamunda formation examined in this study (Figure 11). The Reedy Creek MB1-G core sample (*ca.* 201 mBGL) contained substantial calcite whilst minor dolomite was detected in RC002 (*ca.* 216 mBGL). Calcite and/or dolomite dissolution due to injection of waters containing low concentrations of Ca and/or Mg may result in release of trace metals selectively accumulated within or adsorbed to the surfaces of these carbonate minerals, particularly Ba, Cd, Co, Pb, Mn, Ni, P, Sr, and Zn (Doner and Grossl, 2002). In addition, the Cr and Sb contents of Reedy Creek MB1-G RC002 (from approximately 216 mBGL) exceeded ANZECC/ARMCANZ (2000) ISQG- low (trigger value) recommended sediment quality guidelines.

Within the Reedy Creek MB3-H core samples from the Hutton sandstone formation, core no. 003-S exhibited substantial siderite, a potential source of acidity upon oxidation. In the absence of oxygen, siderite dissolution generates bicarbonate alkalinity and results in Fe^{2+} release to aqueous solution. Divalent Fe released during siderite dissolution may be oxidised to Fe^{3+} in the presence of oxygen, a process which consumes additional protons. The subsequent hydrolysis of Fe^{3+}, however, results in the release of substantial acidity. Thus, siderite dissolution can neutralise acidity only in anoxic conditions; however, Younger (2004) suggests that even in the absence of oxygen, siderite dissolution provides only localised acid neutralisation.

In addition, the majority of the Reedy Creek MB3-H core samples examined from between approximately 842 and 1251 mBGL contained As in excess of ANZECC/ARMCANZ (2000) ISQG-low (trigger value) recommended sediment quality guidelines and inorganic Hg content was greater than ISQG-high recommended sediment quality guidelines.

Reedy Creek MB3-H core samples from Precipice sandstone exhibited varying mineralogy. A zone of high calcite concentration was identified from *ca.* 1303-1308 mBGL (core samples no. 066-S and 3) and minor/trace siderite and anatase were observed between approximately 1301 and 1343 mBGL (core samples no. 1-12). Trace elements of potential concern in Precipice sandstone core samples from the Reedy Creek MB3-H core (066-S to 078-S, *ca.* 1303-1350 mBGL) included As and Cr, which exceeded ISQG-low (trigger value) recommended sediment quality guidelines, and inorganic Hg, which was higher than ISQG-high guideline values (ANZECC/ARMCANZ, 2000). Zinc was also detected in concentrations greater than ANZECC/ARMCANZ (2000) recommended sediment quality guidelines. Trace element data were not available for Reedy Creek MB3-H core samples 1-15.

In summary, ongoing monitoring of pH, ORP, major cations (Al, Ca, Fe, K, Na, Mg, Mn, and Si) and anions (CO_3^{2-}, HCO_3^-, Cl^-, and SO_4^{2-}), and potentially toxic trace elements (Ag, As, Cd, Cr, Cu, Hg, Ni, Pb, Sb, Se, V, and Zn) during and following injection of treated CSG waters will assist in assessing and interpreting potential changes in aquifer geochemistry during and following aquifer re-injection trials. Additional analysis of Ba, Co, P and Sr may further assist with interpretation of potential carbonate mineral dissolution.

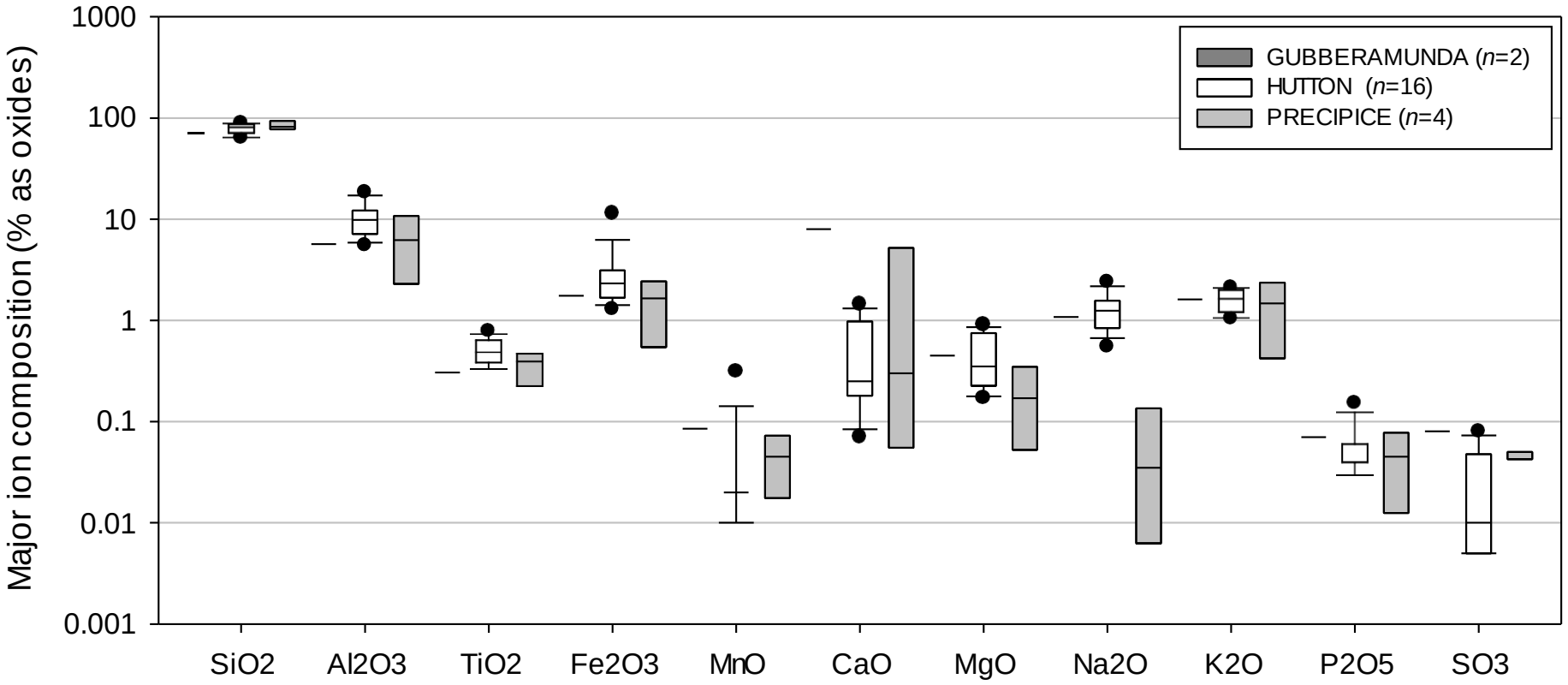

Figure A.11: Comparison of major ion contents (as oxides) in Gubberamunda (ca. 201-216 mBGL), Hutton (ca. 843-1251 mBGL) and Precipice sediment core samples (ca. 1304-1350 mBGL) from Reedy Creek. Dotted lines represent means.

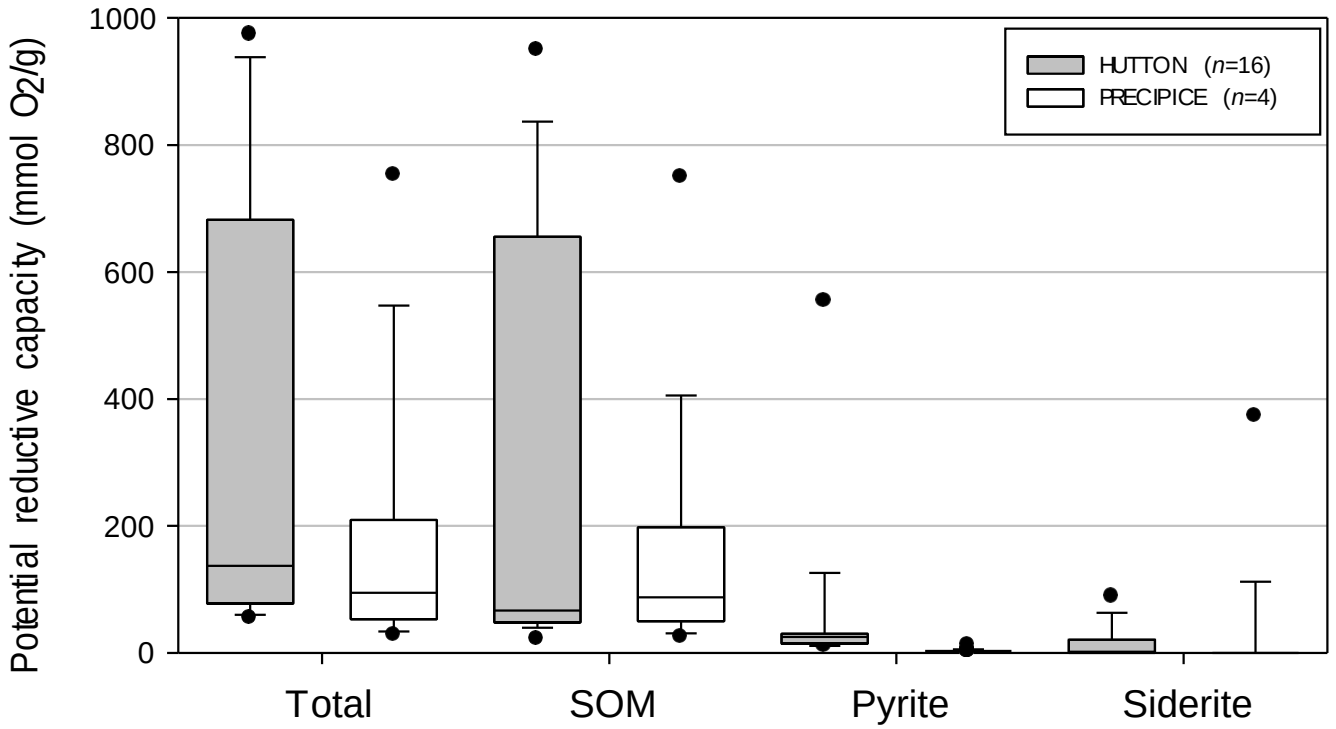

Figure A.12: Comparison of the total potential reductive capacities (in µmol O2/g) and the sedimentary organic matter (SOM), pyrite and siderite components of total PRC, between the Hutton (ca. 843-1251 mBGL) and Precipice sediment core samples (ca. 1304-1350 mBGL) from Reedy Creek. Dotted lines represent means.

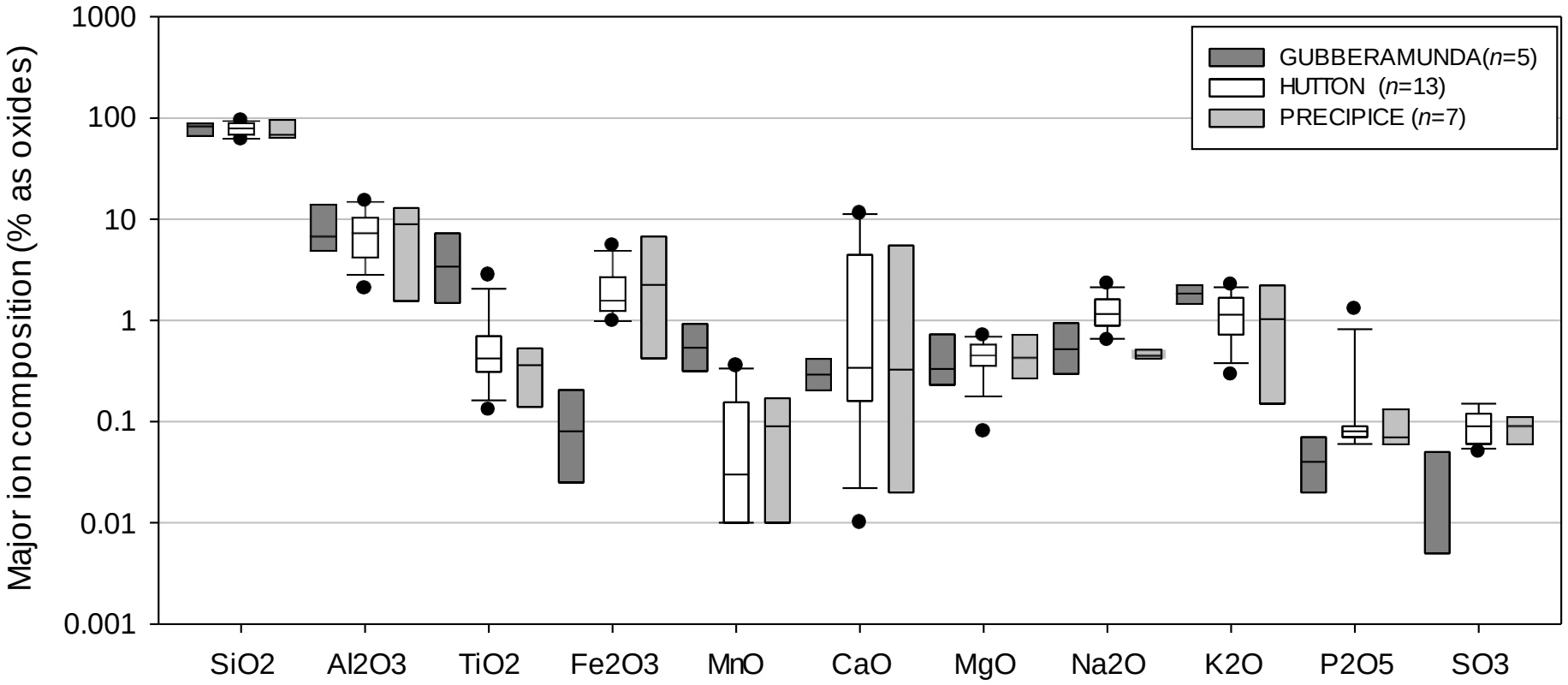

Figure A.13: Comparison of major ion contents (as oxides) in Gubberamunda, Hutton and Precipice formation sandstone core samples from Condabri. Dotted lines represent means.

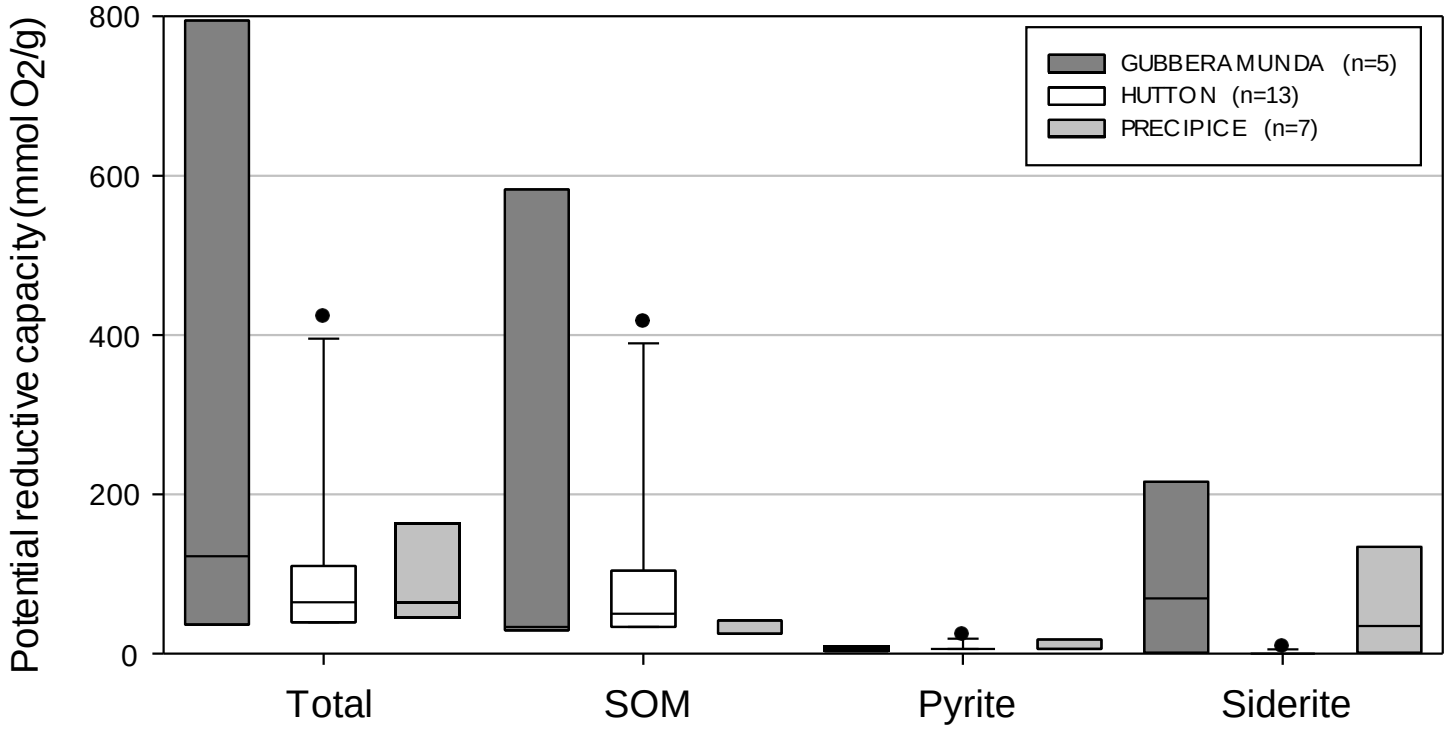

Figure A.14: Comparison of the total potential reductive capacities (in µmol O2/g) and the sedimentary organic matter (SOM), pyrite and siderite components of total PRC, between the Gubberamunda (ca. 62-78 mBGL) and Hutton sediment core samples (ca. 673-937 mBGL) from Condabri. Dotted lines represent means.

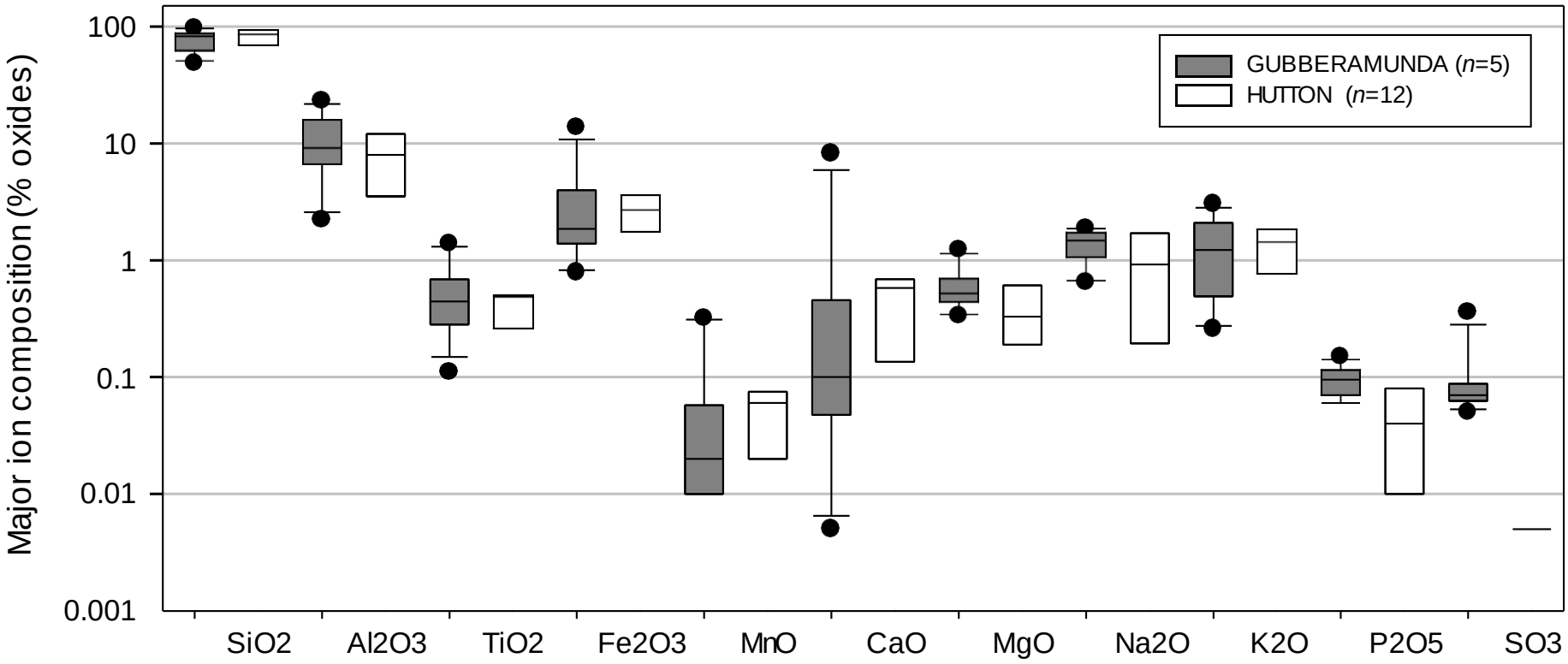

Figure A.15: Comparison of major ion contents (as oxides) in Gubberamunda and Hutton formation sandstone core samples from Talinga. Dotted lines represent means.

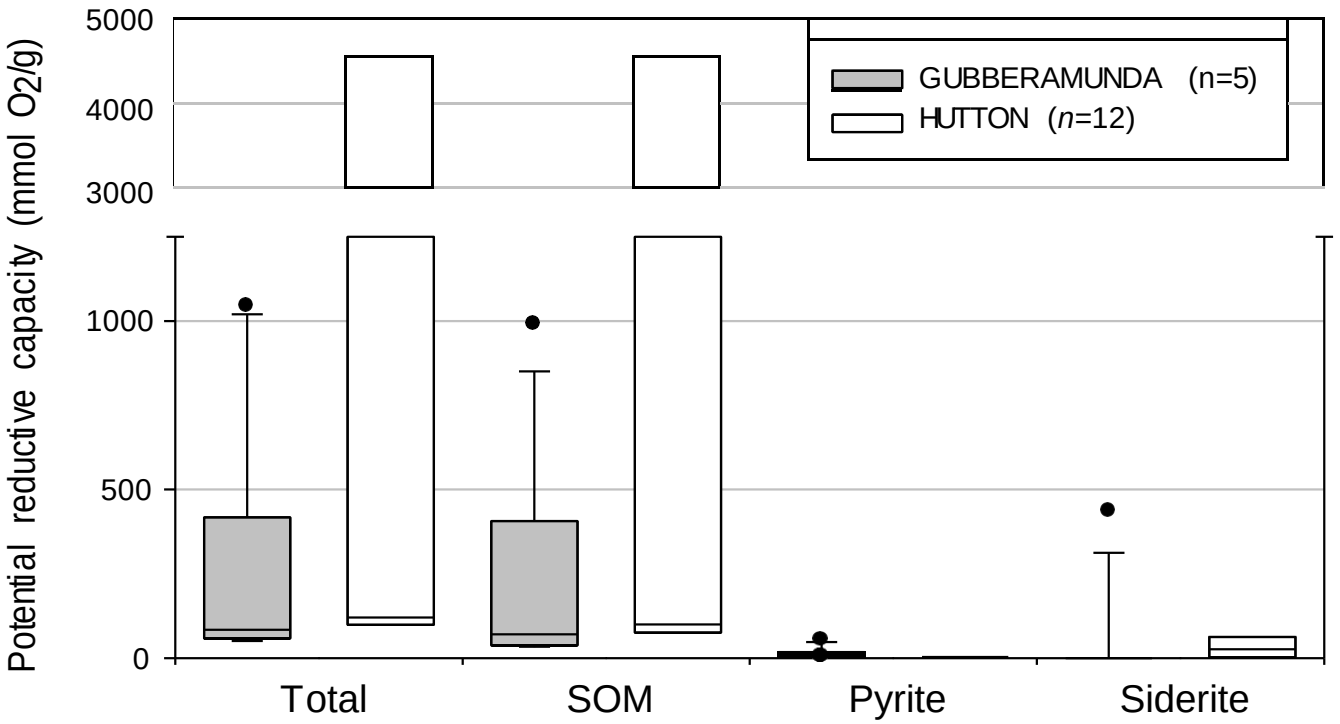

Figure A.16: Comparison of the total potential reductive capacities (in µmol O2/g) and the sedimentary organic matter (SOM), pyrite and siderite components of total PRC, between the Gubberamunda (ca. 62-78 mBGL) and Hutton sediment core samples (ca. 673-937 mBGL) from Talinga. Dotted lines represent means.

A.4 References

Australian and New Zealand Environment and Conservation Council/Agriculture and Resource Management Council of Australia and New Zealand (ANZECC/ARMCANZ). 2000. Australian and New Zealand Guidelines for Fresh and Marine Water Quality. Canberra, ACT, Australia.

Dean, W.E., Jr. 1974. Determination of carbonate and organic matter in calcareous sediments and sedimentary rocks by loss on ignition: Comparison with other methods. *Journal of Sedimentary Petrology* **44**:242–248.

Doner, H.E., Grossl, P.R. 2002. Chapter 6: Carbonated and Evaporites pp. 199-228 in: Dixon, J.B. and Schulze, D.G. 2002. Soil Mineralogy with Environmental Applications. Soil Science Society of America, Inc., Madison.

Duckworth, O.W., Martin. S.T. 2004. Role of molecular oxygen in the dissolution of siderite and rhodochrosite. *Geochimica et Cosmochimica Acta* **68**(3):607-621.

Exon, N.F. 1976. Geology of the Surat Basin in Queensland. Bulletin 166. Department of Natural Resources Bureau of Mineral Resources, Geology and Geophysics. Australian Government Publishing Service, Canberra. 235 pp.

Hoskin, P.W.O., Ireland, T.R. 2000. Rare earth element chemistry of zircon and its use as a provenance indicator. *Geology* **28**:627-630.

Houston, B. R. 1972. Petrology of subsurface samples of Mesozoic arenites of the Bowen and Surat Basins. Appendix 2 pp. 89-98 in: Gray, A.R.G. 1972. Stratigraphic drilling in the Surat and Bowen Basins, 1967-70. Geological Survey of Queensland Report No. 71. S.G. Reid Government Printer, Brisbane.

Morton, A.C., Hallsworth, C.R. 1999. Processes controlling the composition of heavy mineral assemblages in sandstones. *Sedimentary Geology* **124**:3-29.

Norrish, K. and Hutton, J.T. 1969. An accurate X-ray spectroscopic method for the analysis of a wide range of geological samples. *Geochimica et Coscmochimica Acta* **33**(4):431-453.

Pettijohn, F.J. 1963. Chapter S. Chemical composition of sandstones, excluding carbonates and volcanic sands. Geological Survey Professional Paper 440-S, in: Fleischer, M. (Ed.) 1963. Data of Geochemistry, Sixth Ed. United states Government Printing Office, Washington, DC.

Preston, J., Hartley, A., Hole, M., Buck, S., Bond, J., Mange, M., Still, J. 1998. Integrated whole-rock trace element geochemistry and heavy mineral chemistry studies: aids to the correlation of continental reed-bed reservoirs in the Beryl Field, UK North Sea. *Petroleum Geoscience* **4**(1):7-16.

Sutherland, R.A. 1998. Loss-on-ignition estimates of organic matter and relationships to organic carbon in fluvial bed sediments. *Hydrobiologia* **389**:153-167.

Taylor, J.C. 1991. Computer programs for standardless quantitative analysis of minerals using the full powder diffraction profile. *Powder Diffraction* **6**(1):2-9.

Ward, C.L., Taylor, J.C., and Cohen, D.R. 1999. Quantitative mineralogy of sandstones by X-ray diffractometry and normative analysis. *Journal of Sedimentary Research* **69**(5):1050-1062.

Weatherford Laboratories, 2011a. XRD and XRF analysis report of Condabri MB1-G for Origin Energy. 11 August 2011. Weatherford Laboratories (Australia) Pty Ltd, Windsor QLD. 15 pp.

Weatherford Laboratories, 2011b. XRD and XRF analysis report of Condabri MB9-H for Origin Energy. 11 October 2011. Weatherford Laboratories (Australia) Pty Ltd, Windsor QLD. 10 pp.

Weatherford Laboratories, 2011c. XRD and XRF analysis report of Reedy Creek MB3-H for Origin Energy. 24 November 2011. Weatherford Laboratories (Australia) Pty Ltd, Windsor QLD. 17 pp.

Weatherford Laboratories, 2011d. XRD and XRF analysis report of Talinga MB3-H and Reedy Creek MB1-G for Origin Energy. 25 October 2011. Weatherford Laboratories (Australia) Pty Ltd, Windsor QLD. 14 pp.

Weatherford Laboratories, 2012. XRD and XRF analysis report of Talinga MB9-G Origin Energy. 4 April 2012. Weatherford Laboratories (Australia) Pty Ltd, Windsor QLD. 11 pp.

Weatherford Laboratories, 2013. X-ray diffraction analysis of samples of RC-MB3-H for Origin Energy Resources Ltd. XRD analysis report: AB-60772. 2 January 2013. Weatherford Laboratories (Australia) Pty Ltd. Windsor QLD. 25 pp.

Younger, P.L. 2004. Environmental impacts of coal mining and associated wastes: a geochemical perspective. Pp. 169-209 in: Giere, R., Stille, P. (Eds.) 2004. Energy, Waste, and the Environment: a Geochemical Perspective. Special Publication 236. Geological Society, London.

Appendix B Preliminary, pre-trial modelling studies to support the design and monitoring strategy of selected field-scale injection experiments

Understanding and quantifying the geochemical response to reinjection of CSG water permeates, brines and blends

GISERA Project Number W1 1114

Evelien Martens, Henning Prommer

May 2013

Task 6: Preliminary, pre-trial modelling studies to support the design and monitoring strategy of selected field-scale injection experiments

B.1 Overview

A tracer test and subsequent model-based analysis is planned to accompany the injection trial for the Precipice Braided Sand Formation (BSF) aquifer at Reedy Creek. To assist with the design of the test and to maximise the value of the planned data collection, a series of model simulations was carried out. These simulations illustrate the anticipated flow/transport behaviour, including travel distances and tracer dilution and provide insights into how various aquifer parameters affect the anticipated observations. The simulations will therefore support the choice of an appropriate sampling scheme that will allow to identify key aquifer parameters from the collected data.

Modflow (Harbaugh et al., 2000) and MT3DMS (Zheng and Wang, 1999) were employed for the flow and tracer transport simulations, respectively. A local-scale 2D radial model (Wallis et al., 2012) that extends 613 m in radial direction was constructed, based on the conceptual hydrogeological model that was mostly developed from the hydrogeological logs. A variable grid size was used, whereby the column width increases with increasing distance from the well. The Precipice BSF as well as the underlying Moolayember Formation were included in the model. Based on the porosity analysis from wireline logs for the injection bore, it was decided to split the Precipice BSF into 7 different layers. The Moolayember Formation was divided into 4 layers. Assumed thickness, hydraulic conductivity and porosity for each layer are depicted in Apx Table B.1.

Apx Table B.1: Layer properties.

FORMATION	LAYER	DEPTH (M)	THICKNESS (M)	K_H (M/DAY)	H (-)
Precipe BSF	1	1317-1318	1	3	0.05
	2	1318-1325	7	3	0.27
	3	1325-1326	1	3	0.05
	4	1326-1328	2	3	0.22
	5	1328-1336	8	3	0.35
	6	1336-1337	1	3	0.05
	7	1337-1338	1	3	0.32
Moolayember Formation	8	1338-1340	2	0.03	0.005
	9	1340-1342	2	0.03	0.005
	10	1342-1346	4	0.03	0.005
	11	1346-1350	4	0.03	0.005

In the absence of suitable monitoring bores on site, the proposed test will be carried out as push/pull test, i.e., injection and extraction will occur at the same bore. Injection, storage and extraction duration and rates were selected according to the Injection Trial schedule provided by Origin. It is proposed that 30 000 litres of Br tracer solution will be injected over a short time period at a maximum injection rate of Qin = 1600 m3/day ten days before the end of the injection period. A second injection of 30 000 litres is proposed to occur three days before the end of the injection period, just before the proposed second step test. In all model simulations, a concentration of 1 (unity) was assumed; simulated concentrations can subsequently be converted into actual concentrations (note: solubility of NaBr in water is 95g/100ml, solubility of KBr in water is 68g/100ml, both at 25°C).

Besides the analysis of the conservative transport behaviour of Br, temperature will be analysed as a second groundwater tracer. Heat transport will, however, be strongly affected by solution-matrix interactions. The temperature of the inflowing water is expected to be ~27°C, while the temperature in the Precipice BSF is significantly higher (~62°C).

The simulated water fluxes, concentrations and the proposed scheduling of the test are summarized in Apx Table B.2.

B.2 Results of pre-trial simulations

A set of model runs was carried out to investigate the effect of the parameters that were expected to most strongly affect the flow and transport characteristics of the tracer in the BSF formation. This included: (i) dispersivity, (ii) time of tracer injection, and (iii) applying a dual-domain mass-transfer approach to assess the potential impact of fracture flow on tracer transport.

B.2.1 EFFECT OF DISPERSIVITY

The magnitude of hydrodynamic dispersion as created by a heterogeneous hydraulic conductivity distribution is expected to have a strong influence on the shape of the recovered Br peaks. For example, a more homogeneous conductivity distribution will result in shorter and sharper Br peaks which can only be suitably captured by an appropriate high sampling frequency (i.e., the peaks could easily be missed if the sampling events are too widely spaced in time). To explore the effect of dispersion on Br transport, sensitivity runs were performed for the parameter range that was expected to cover the anticipated field-scale behaviour. Simulations were carried out for four different dispersivities (αL = 0.5m, 1 m, 5 m and 25 m).

Apx Table B.2: Overview of the model scenario.

TRIAL PHASE	STRESS PERIOD	DURATION (DAYS)	FLUX[A] (M^3/DAY)	BR CONCENTRATION
Injection	1	1	400	0
	2	1	800	0
	3	21	1600	0
	4	0.0188	1600	1
	5	6.9624	1600	0
	6	0.0188	1600	1
	7	3	1600	0
	8	1	0	0
	9	1	400	0
	10	1	800	0
	11	1	1600	0
Storage	12	39	0	0
Extraction	13	35	-1000	0

[a] A positive flux indicates injection, a negative flux means extraction.

The results of the sensitivity runs are jointly displayed in Figure B.1. The results clearly show how the recovered Br concentrations become lower and how the peak(s) become successively wider for higher dispersivities. For αL ≥ 1 m, the Br peak associated with the first injection becomes very dispersed and therefore no distinction can be made between the peak associated with the first and second tracer amendment, respectively. Closer inspection shows that this effect can be attributed to the injection rates being very high compared to the total volume of the Br-amended solution: the injection of 1.6 ML/day for 10 days amounts to 16 ML of RO water compared to only 0.03 ML of Br per injection. From the recovered Br profiles it is clear that the proposed sampling scheme (indicated on the plots by the vertical green lines) is most likely insufficient to accurately capture the breakthrough behaviour. Especially if the behaviour would be as predicted by the lowest dispersion values, the first peak would be totally missed by the currently planned sampling schedule. Therefore, it is suggested to collect samples daily until concentrations show a decreasing trend (e.g., in at least two consecutive samples). A coarser sampling frequency will be then be sufficient. The bottom plot in Figure B.1 additionally shows the anticipated evolution of the temperature at the injection/extraction well. As temperature transport is more strongly affected by retardation and diffusion, the sampling schedule is less critical.

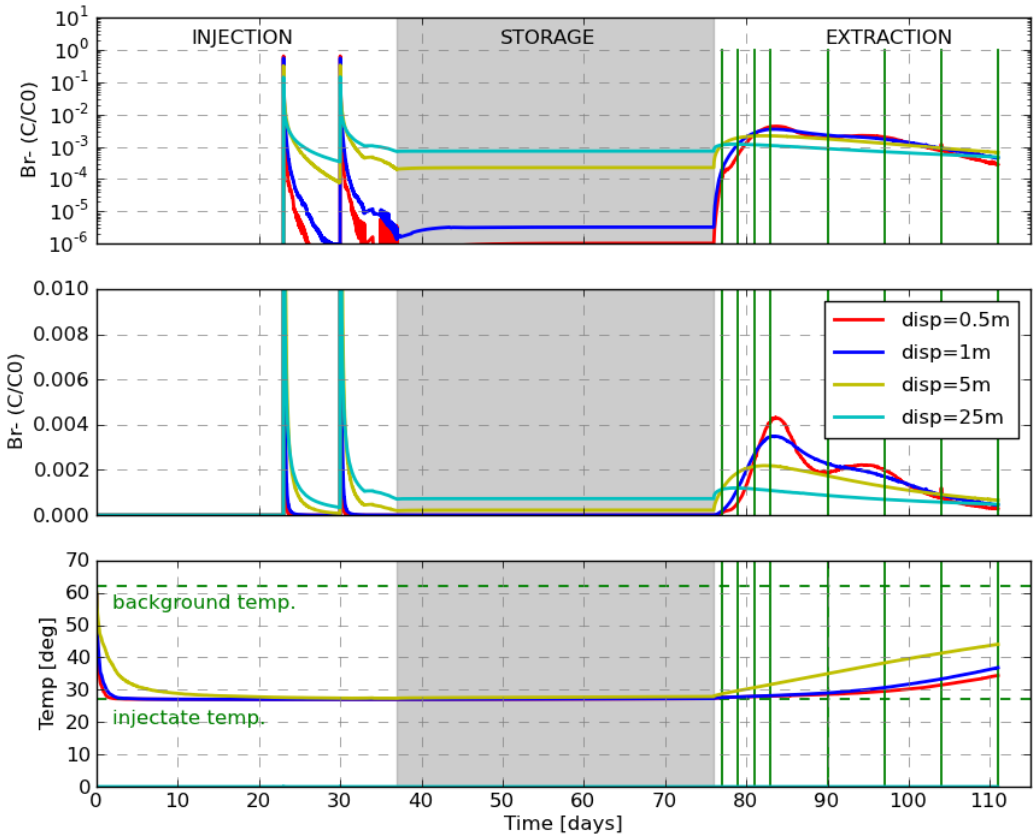

Figure B.1: Model results for different dispersivities, two pulses of Br injection. Br concentration versus time (days), on a logarithmic (top figure) and linear scale (middle figure) and temperature (°C) versus time (days) (bottom figure).

B.2.2 TIME OF TRACER INJECTION

To identify the most suitable time of Br injection, three model variants were investigated. These simulations assess Br amendment for three different times, i.e. after 15, 21 and 28 days after the injection start, respectively. A dispersion value (αL = 0.5 m) at the lower end of the expected parameter range was assumed for these simulations. The results for these simulations are shown in Figure B.2. From these results it may be concluded that a later Br injection is favourable, as this will lead to a more distinct Br peak. However, the later the tracer is injected, the shorter the actual travel distance of the tracer. This implies that the results will express localised aquifer conditions while larger travel distances will provide more representative conditions. This could be an important aspect in the context of using the extracted aquifer parameters in larger-scale predictive models. Figure B.3 shows that the travel distance of the Br plume varies between 50 m for the late injection case up to 108 m for the early injection. A compromise between distinct Br peak and increased representativeness is suggested, i.e., the Br solution may be amended 21 days after the start of the injection.

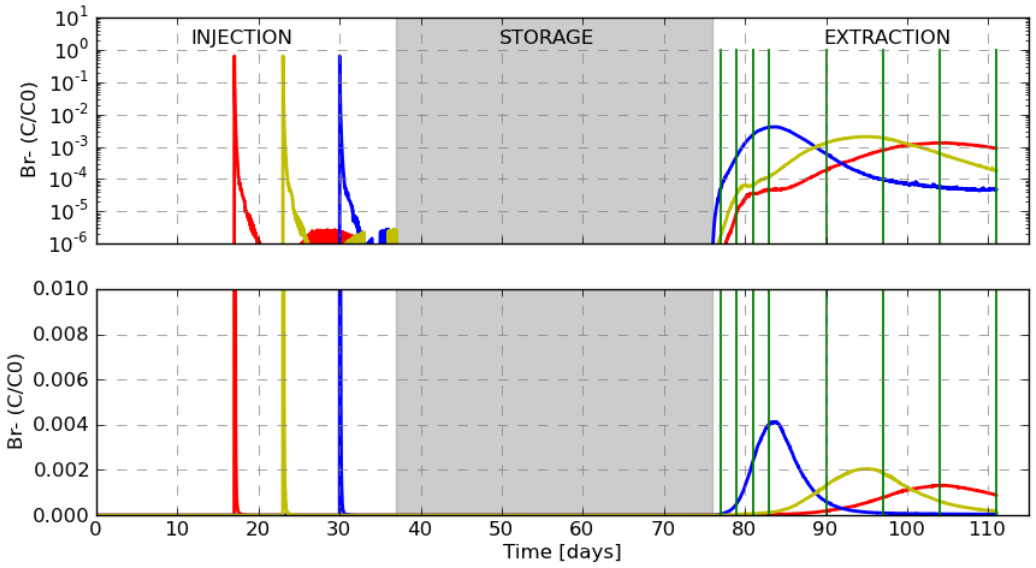

Figure B.2: Effect of time of injection on Br recovery peak: early (red curve), intermediate (yellow curve) and late (blue curve) Br injection. Br concentration versus time (days), on a logarithmic (top figure) and linear scale (bottom figure).

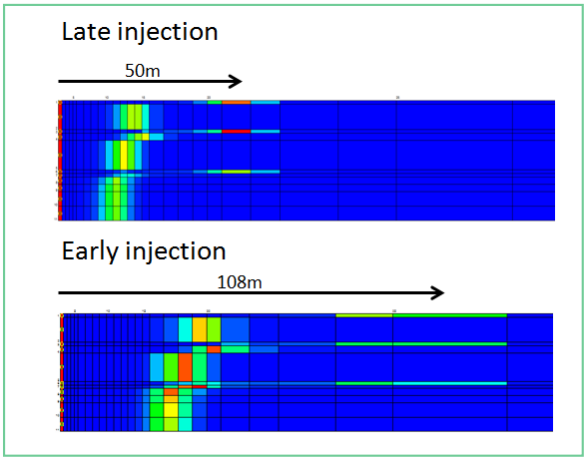

Figure B.3: Travel distance of Br plume for a late injection (top figure) and an early injection (bottom figure). The red cells on the left side indicate the well position. Note that only a part of the model grid is shown (model extends up to 613m to the right side).

B.2.3 EFFECT OF FRACTURED FLOW

Given that the BSF aquifer at Reedy Creek may be, at least partially, composed of fractured rock, the effect of fractures on Br transport was assessed. The simulations were performed by invoking the dual domain capabilities of the solute transport simulator MT3DMS. The dual-domain approach is a commonly used approach to mimic the typical transport behaviour of fracture rocks, which involves early peaks and an extended tailing phase. The approach distinguishes the water-filled pore space into a mobile and an immobile fraction. In the underlying conceptual model the latter represent the pore space occupied by the rock matrix, whereas the former represents the pore space occupied by the fractures. Water and solute exchange between the two fractions is typically simulated through a first-order mass-transfer that is driven by the concentration differences between mobile and immobile pore-space. The mobile porosity was set to estimated values of 2% for the BSF and 0.2% for the Moolayember Formation (see Apx Table B.3 for an overview of all porosity values). A low hydrodynamic dispersivity ($\alpha_L = 0.05$ m) was assumed. The mass transfer coefficient, ω, was varied between 0 (no mass transfer between mobile and immobile zone) and

1×10^{-2} day^{-1} (fast mass transfer). The results are displayed in Figure B.4, showing that the mass transfer coefficient has a critical influence on the results.

Apx Table B.3: Layer properties for the dual domain model.

FORMATION	LAYER	DEPTH (M)	THICKNESS (M)	K_H (M/DAY)	H_MOBILE (-)	H_IMOBILE (-)
Precipe BSF	1	1317-1318	1	3	0.02	0.03
	2	1318-1325	7	3	0.02	0.25
	3	1325-1326	1	3	0.02	0.03
	4	1326-1328	2	3	0.02	0.20
	5	1328-1336	8	3	0.02	0.33
	6	1336-1337	1	3	0.02	0.03
	7	1337-1338	1	3	0.02	0.30
Moolayember Formation	8	1338-1340	2	0.03	0.002	0.003
	9	1340-1342	2	0.03	0.002	0.003
	10	1342-1346	4	0.03	0.002	0.003
	11	1346-1350	4	0.03	0.002	0.003

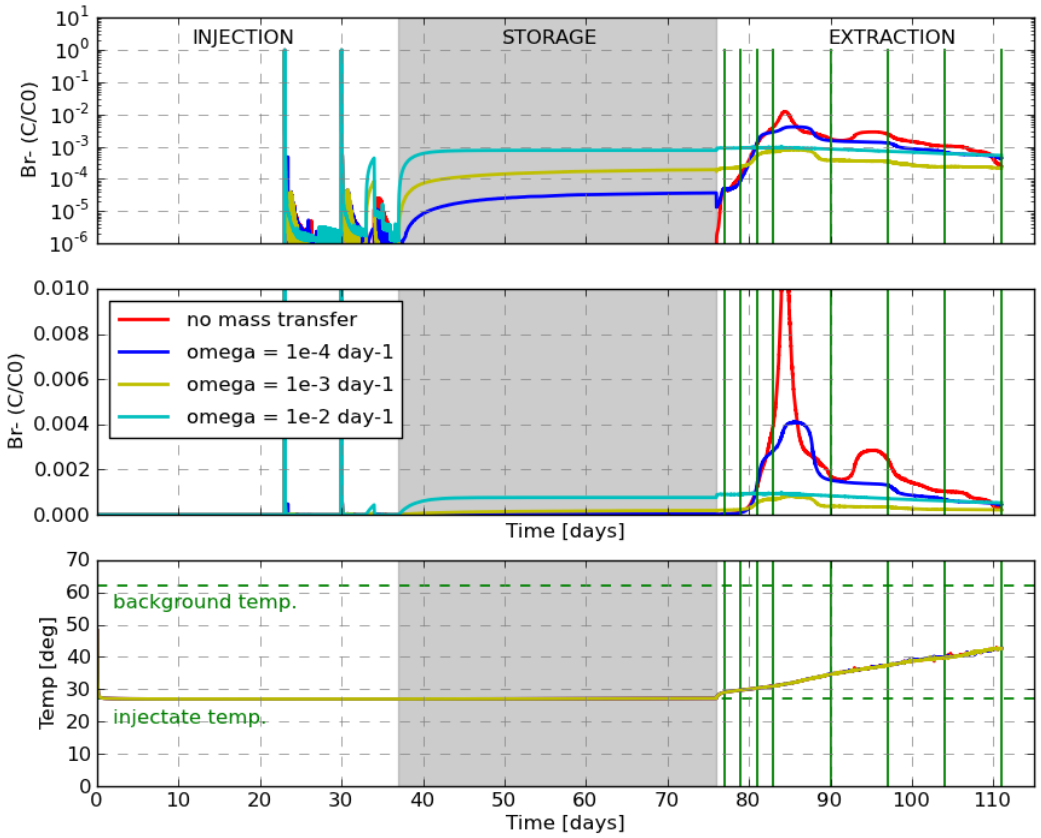

Figure B.4: Model results for Scenario 2 (with dual domain mode invoked): Br injection at the beginning and at the end of the injection period. Br concentration versus time (days), on a logarithmic (top figure) and linear scale (middle figure) and temperature (°C) as a function of time (days) (bottom figure), for different values of the mass transfer coefficient. The grey area indicates the storage period.

B.3 Summary and recommendations for the design of the tracer test

- The small volume of Br amended water causes a strong dilution and Br concentrations in the recovered water will be several orders of magnitude below the injectant concentration.
- Late injection of Br helps to recover higher concentrations but travel distances of the tracer would be shorter and less representative, i.e., insufficient averaging of aquifer properties may occur.
- A relatively high sampling frequency will be required to capture distinct peaks and to minimise uncertainties from incomplete recovery of the shape of the breakthrough curve.

B.4 References

Harbaugh, A.W., Banta, E.R., Hill, M.C., McDonald, M.G., 2000. MODFLOW-2000, the U.S. Geological Survey modular ground-water model—user guide to modularization concepts and the ground-water flow process. USGS Open-File Report 00-92. U.S. Geological Survey, Reston, Virginia, US.

Wallis, I.; Prommer, H.; Post, V.; Vandenbohede, A.; Simmons, C. T. Simulating MODFLOW-Based Reactive Transport Under Radially Symmetric Flow Conditions. *Ground water* **2012**, *281*.

Zheng, C., Wang, P.P., 1999. MT3DMS, A modular three-dimensional multispecies transport model for simulation of advection, dispersion and chemical reactions of contaminants in groundwater systems; documentation and user's guide. U.S. Army Eng. Res. Dev. Cent. Contr. Rep. SERDP-99-1, Vicksburg, Miss.

CONTACT US

t 1300 363 400
+61 3 9545 2176
e enquiries@csiro.au
w www.csiro.au

YOUR CSIRO

Australia is founding its future on science and innovation. Its national science agency, CSIRO, is a powerhouse of ideas, technologies and skills for building prosperity, growth, health and sustainability. It serves governments, industries, business and communities across the nation.